NAVAL POSTGRADUATE SCHOOL
Monterey, California

THESIS

THE CIRCULATION AND VARIABILITY IN THE WESTERN ARCTIC OCEAN - MODEL RESULTS

by

Jeffrey S. Dixon

September 2003

Thesis Advisor: Wieslaw Maslowski
Second Reader: Stephen Okkonen

THIS PAGE INTENTIONALLY LEFT BLANK

REPORT DOCUMENTATION PAGE	*Form Approved OMB No. 0704-0188*

1. AGENCY USE ONLY ***(Leave blank)***	**2. REPORT DATE** September 2003	**3. REPORT TYPE AND DATES COVERED** Master's Thesis

4. TITLE AND SUBTITLE: The Circulation and Variability in the Western Arctic Ocean - Model Results	**5. FUNDING NUMBERS**
6. AUTHOR(S) Jeffrey S. Dixon	
7. PERFORMING ORGANIZATION NAME(S) AND ADDRESS(ES) Naval Postgraduate School Monterey, CA 93943-5000	**8. PERFORMING ORGANIZATION REPORT NUMBER**
9. SPONSORING /MONITORING AGENCY NAME(S) AND ADDRESS(ES) N/A	**10. SPONSORING/MONITORING AGENCY REPORT NUMBER**

11. SUPPLEMENTARY NOTES The views expressed in this thesis are those of the author and do not reflect the official policy or position of the Department of Defense or the U.S. Government.

12a. DISTRIBUTION / AVAILABILITY STATEMENT Approved for public release; distribution unlimited	**12b. DISTRIBUTION CODE** A

13. ABSTRACT ***(maximum 200 words)***

Circulation in the western Arctic Ocean is not well understood. To address some of its outstanding questions, volume transport and property fluxes are investigated using a coupled ice-ocean model of the pan-Arctic region configured at a 1/12-degree and 45-level grid. Results for analyses are from the last 23 years of a 70-year integration forced with realistic 1979-2001 atmospheric data. Velocity at three depth intervals, mean transports and fluxes are investigated to identify the main current pathways and directions. Variability is determined by comparison of results a decade apart.

Mean velocity fields describe a climatological circulation pattern that is cyclonic in nature with increased intensity during the late 1980s and early 1990s. The meander through the Chukchi Borderland Pass is the main pathway for boundary flow across the Chukchi Plateau. The northern Chukchi Plateau is modeled as a region of major volume, heat and freshwater transport into the Canada Basin interior. It also appears to be an area of net upward heat transport, which may be available for melting ice. Northward flow along the eastern side of the Northwind Ridge is identified as a mechanism for advection of freshwater from the Chukchi shelves into the interior.

14. SUBJECT TERMS Arctic Ocean, Oceanography, Modeling	**15. NUMBER OF PAGES** 129
	16. PRICE CODE

17. SECURITY CLASSIFICATION OF REPORT	**18. SECURITY CLASSIFICATION OF THIS PAGE**	**19. SECURITY CLASSIFICATION OF ABSTRACT**	**20. LIMITATION OF ABSTRACT**
Unclassified	Unclassified	Unclassified	UL

NSN 7540-01-280-5500 Standard Form 298 (Rev. 2-89)
Prescribed by ANSI Std. 239-18

THIS PAGE INTENTIONALLY LEFT BLANK

Approved for public release; distribution is unlimited

THE CIRCULATION AND VARIABILITY IN THE WESTERN ARCTIC OCEAN - MODEL RESULTS

Jeffrey S. Dixon
Lieutenant, United States Navy
B.S., State University of New York, College at Oswego, 1991

Submitted in partial fulfillment of the
requirements for the degree of

MASTER OF SCIENCE IN METEOROLOGY AND PHYSICAL OCEANOGRAPHY

from the

NAVAL POSTGRADUATE SCHOOL
September 2003

Author: Jeffrey S. Dixon

Approved by: Wieslaw Maslowski
Thesis Advisor

Stephen Okkonen
Second Reader

Mary L. Batteen
Chairman, Department of Oceanography

THIS PAGE INTENTIONALLY LEFT BLANK

ABSTRACT

Circulation in the western Arctic Ocean is not well understood. To address some of its outstanding questions, volume transport and property fluxes are investigated using a coupled ice-ocean model of the pan-Arctic region configured at a 1/12-degree and 45-level grid. Results for analyses are from the last 23 years of a 70-year integration forced with realistic 1979-2001 atmospheric data. Velocity at three depth intervals, mean transports and fluxes are investigated to identify the main current pathways and directions. Variability is determined by comparison of results a decade apart.

Mean velocity fields describe a climatological circulation pattern that is cyclonic in nature with increased intensity during the late 1980s and early 1990s. The meander through the Chukchi Borderland Pass is the main pathway for boundary flow across the Chukchi Plateau. The northern Chukchi Plateau is modeled as a region of major volume, heat and freshwater transport into the Canada Basin interior. It also appears to be an area of net upward heat transport, which may be available for melting ice. Northward flow along the eastern side of the Northwind Ridge is identified as a mechanism for advection of freshwater from the Chukchi shelves into the interior.

THIS PAGE INTENTIONALLY LEFT BLANK

TABLE OF CONTENTS

THIS PAGE INTENTIONALLY LEFT BLANK

LIST OF FIGURES

LIST OF TABLES

THIS PAGE INTENTIONALLY LEFT BLANK

ACKNOWLEDGMENTS

I would like to thank my thesis advisor, Dr. Wieslaw Maslowski, for his constant patience and guidance. I thank my second reader, Dr. Steve Okkonen, for his assistance and the unique field experience opportunity. I would also like to thank Jaclyn Clement and Dr. Jaromir Jakakci of the Arctic Modeling Effort group at the Naval Postgraduate School, Dr. Waldemar Walczowski of the Institute of Oceanology at the Polish Academy of Sciences and Dr. Don Stark and Mike Cook from the Department of Oceanography at the Naval Postgraduate School. The wide range of assistance that these people provided was invaluable.

The National Science Foundation and Office of Naval Research provided funding support. Computer resources have been provided by the Arctic Region Supercomputing Center through the Department of Defense High Performance Computer Modernization Program.

I would like to dedicate this to my parents, Don and Terry Dixon who have given me the opportunity and support to do whatever I want.

THIS PAGE INTENTIONALLY LEFT BLANK

I. INTRODUCTION

A. BACKGROUND OF RESEARCH IN THE ARCTIC

Research effort in the Arctic region has historically lagged efforts in other oceanic basins. As a result the body of scientific knowledge that exists for the Arctic is less than that of other more accessible oceans. However, understanding of the Arctic Ocean circulation and its interaction with the surrounding environment and adjacent ocean basins is crucial.

The remote geography and harsh environment of the Arctic region has inhibited field exploration resulting in limited observational data. However, a number of recent research projects such as the Arctic Ice Dynamics Joint Experiment (AIDJEX) in the mid-1970's, the U.S. Navy Submarine Scientific Ice Experiments (SCICEX) and the Surface Heat Budget of the Arctic Ocean (SHEBA) experiment in the 1990's have provided a windfall of information. Additionally, the current Study of Environmental Arctic Change (SEARCH) and Western Arctic Shelf-Basin Interactions (SBI) projects have provided momentum in Arctic field research that must be sustained.

The jointly sponsored Office of Naval Research (ONR) and National Science Foundation (NSF) SBI program is intended to contribute toward the NSF Arctic System Science (ARCSS) program goal of understanding the role of the Arctic Ocean in the global climate system (Grebmeier et al., 1998). The SBI program is a three-phase project intended to understand major processes involved in shelf water volume modification, exchange with the Arctic Ocean's interior, and biological structure and function of Arctic

shelf and slope ecosystems in the Chukchi and Beaufort Seas. The SBI science plan identifies four recommendations for research it considers necessary to accomplish these goals. Two of these four recommendations specifically solicit modeling efforts in the western Arctic region. Phase two calls for the development of a Pan-Arctic modeling component in support of the project goals (Grebmeier et al., 1998).

The prohibitive environmental conditions of the Arctic region that have limited research in the past have often forced researchers to base conclusions regarding complex circulation pathways in the Arctic on data collected from a limited number of sites and over a limited time. The relatively small numbers of observation stations that have been employed to analyze circulation in the entire Artic Ocean emphasize the increased need for accurate and comprehensive modeling of the region to supplement limited observational data.

The recent upgrade of the ocean and sea ice modeling components as part of the Naval Postgraduate School (NPS) Arctic Modeling Effort include the increase of model resolution from 18 km to the 9 km, the domain expansion into the North Pacific and are consistent with the SBI program goals. This advancement of the ocean and sea ice model aligned with the ongoing multi- and inter-disciplinary SBI initiative presents a valuable opportunity to provide insight to the circulation in the region of the Chukchi Plateau and Canada Basin.

B. IMPORTANCE OF THE ARCTIC REGION

The Arctic region is an integral part of global climate. It is an important link between the Pacific and Atlantic Oceans for freshwater transport (Wijffels, et al., 1992), and it influences control over global thermohaline circulation (Aagaard and Carmack, 1994). Sea ice plays an important role in insulating the water below from colder air temperatures, thereby reducing heat flux from the ocean into the atmosphere and, as a consequence, is an important factor in overall heat exchange at high latitudes (Maykut, 1978). Understanding Arctic Ocean circulation patterns and property exchanges between the shelves, basin and with adjacent oceans is necessary for understanding how the Arctic Ocean interacts with the global thermohaline circulation and climate. This is a main focus of this project.

The Polar Regions are a primary source of deep water for the global ocean basins (Pfirman et al., 1994). Aagaard and Carmack (1994) indicate that convective cells drive global thermohaline circulation. These convective cells are conditioned by freshwater export from the Arctic Ocean. Rapid freshening of water volumes in the Greenland, Iceland and Labrador Seas by increased freshwater export from the Arctic can result in the reduction or discontinuation of meridional overturning circulation that is crucial to the ventilation of the deeper water masses as well as to northward transport of warm surface waters and heat from the tropics.

Overflow of cold dense water from the Arctic via the Nordic seas through the sills of the Denmark Strait and Faroe-Shetland Channel, combined with dense water formation

further south in the Labrador Sea, is a primary mechanism for ventilation of the North Atlantic. Flows through these channels are important factors of the water column structure in the Labrador Sea and are important contributors to global thermohaline circulation (Dickson et al., 2002).

The effects of environmental perturbations in the Arctic region can extend well beyond its geographic boundaries. The Labrador Sea water column has sustained cooling and freshening during the previous three decades (Dickson et al., 2002). Cooling ceased in the late 1990s and the effects of freshening were noted as deep as 3300 meters. These depths are beyond the depth of convection, which supported the hypothesis that the primary source of the freshening is dense outflow from the Nordic Seas, which are in turn fed by export from the Arctic Ocean. The potential slowdown of the production of North Atlantic Deep Water and meridional overturning circulation are possible outcomes of this freshening of the Labrador Sea and North Atlantic (Dickson et al., 2002).

Dickson et al. (1988) estimated the salt deficits in the upper North Atlantic Ocean in order to determine whether enough fresh water passed along the West Greenland Banks and Labrador coast in the early 1970's to account for the freshening that was observed in the Atlantic over the following years during the Great Salinity Anomaly. The salt deficit budget that Dickson et al. (1988) determined for different regions of the northeast Atlantic indicates that fresh water brought south by the Labrador Current is the source of the freshening observed in the northeast Atlantic. Based on the influence that the Arctic region

has on the formation of dense water in the Labrador Sea (Dickson et al., 2002) it can be inferred that the Arctic Ocean has a strong influence on the Atlantic Ocean structure. These examples illustrate the extensive influence that the Arctic Ocean maintains on climate and global thermohaline circulation and are a testimony to the demand for understanding the Arctic Ocean circulation, which can only be met by continued research.

Evidence suggests that the Arctic environment had been in a state of transition during the late 1980's and 1990's (Maslowski et al., 2001, McPhee et al., 1998, Proshutinsky and Johnson, 1997, Steele and Boyd, 1998). Smith (1998) used the length of the sea ice summer surface melt season as a proxy indicator of Arctic warming. His analysis of sea ice coverage derived from passive microwave data from 1979 to 1996 reveals an 8% increase in the number of melt days per summer per decade. High Arctic Oscillation (AO) index values occurred during all but one month between 1968 and 1997 (Thompson et al., 2000). A high AO index is typically associated with anomalously warm temperatures for much of the northern hemisphere and often indicative of atmospheric regime shifts, a weakening of the Beaufort Gyre, changes in sea ice drift patterns and thickness reductions. Atlantic layer temperature increases in three basins of the Arctic Ocean, as summarized by McLaughlin et al. (2002), indicate that changes first observed in the atmosphere have extended into the Arctic Ocean water column as well.

An analysis of the upper ocean salinity and ice thickness in the central Beaufort Gyre during the October 1997 phase of the SHEBA experiment afforded researchers a

unique opportunity to compare conditions in the region to those measured during the AIDJEX experiment of 1975. Mean ice thickness observed during the initial SHEBA transit were expected to range between 2 and 3 meters but rarely exceeded 1.8 m (McPhee et al., 1998). Rothrock et al. (1999) compared historical ice draft data against ice thickness data obtained in the U.S. Navy Scientific Ice Expedition (SCICEX) cruises between 1993 and 1997. Their research documented an average 1.3 m reduction in the ice draft at the end of the melt season in the 1990's in most overlapping deep-water portions of the Arctic Ocean as compared to historical ice thickness data acquired between 1958 and 1976. A more comprehensive analysis of digitally recorded ice draft data from eight submarine cruises spanning the years 1987 to 1997 by Rothrock et al. (2003) indicates a decrease of about 1 m over the eleven year time frame. A comparison of data between SHEBA and AIDJEX by McPhee et al. (1998) indicated that the surface layer was warmer and fresher during the SHEBA as compared to AIDJEX.

A definitive identification of the causes of these observed changes in the Arctic will require a prolonged research campaign. The documented changes in the Arctic provide irrefutable evidence of climate variability. The Arctic region influences global climate and thermohaline circulation. These facts, combined with the general acceptance that the Arctic region is undergoing climatic changes emphasize that continued research is necessary.

C. OCEAN CIRCULATION IN THE WESTERN ARCTIC

An early framework of the Arctic Ocean intermediate depth circulation presented by Aagaard (1989) and Rudels et

al. (1994) included distinct circulation gyres in the Nansen, Amundsen, Makarov and Canada Basins with major exchanges to other basins via the Fram Strait, Barents Sea, Canadian Archipelago and the Bering Strait (Figure 1.1). According to Rudels et al. (1994) general circulation in the western Arctic and Canada Basin consists of a roughly cyclonic gyre with the Atlantic water inflow adjacent to the Barents Sea across the Lomonosov Ridge and the Pacific inflow through the Bering Strait. Primary outflow is across the opposite side of the Lomonosov Ridge into the Eurasian Basin and then Fram Strait in addition to export via the Canadian Archipelago.

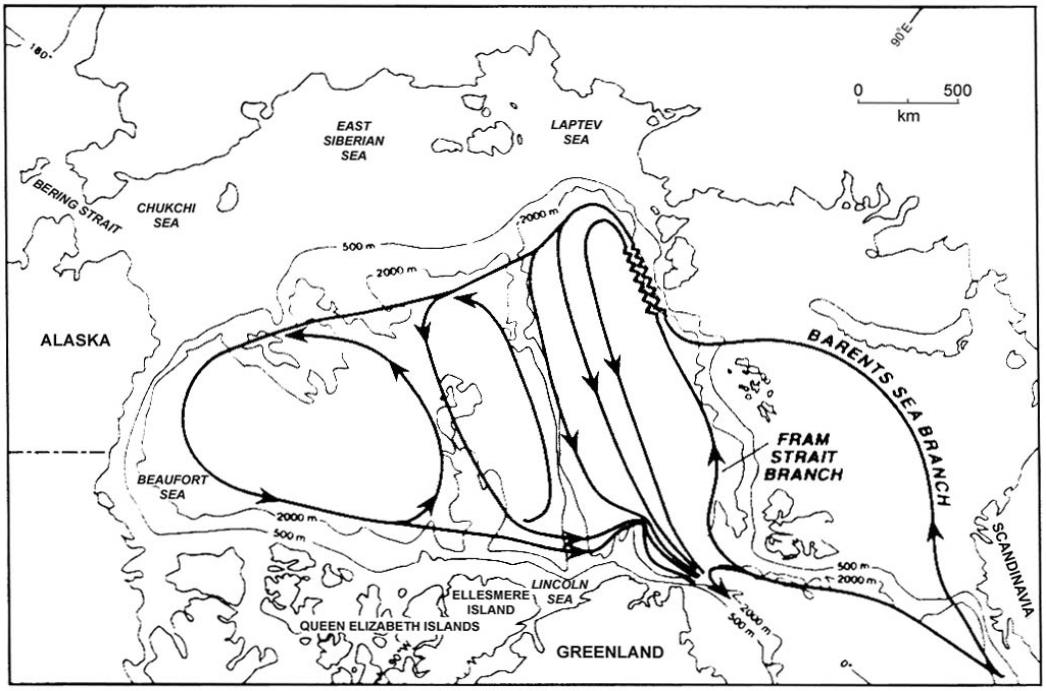

Figure 1.1 Schematic diagram showing the inferred circulation in the Arctic Ocean of the Atlantic layer and intermediate depth waters, between 200m and 1700 m (from Rudels et al., 1994).

SCICEX 96 data analyzed by Smethie et al. (2000) illustrates a circulation pattern consisting of a single

Atlantic Water flow fed from both the Fram Strait and Barents Sea that splits into two branches, one flowing along the Eurasian side of the Lomonosov Ridge and the second entering the Makarov Basin (Figure 1.2). This flow geometry of the Atlantic water in vicinity of the junction of the Lomonosov Ridge and Eurasian continent was supported and quantified by Woodgate et al. (2001). The Canada basin branch continues along the shelf slope following topography into the region of the Chukchi Plateau, portions of which break off from the main flow and are transported into the Canada Basin interior. Mooring data collected from 1995-1996 at three slope sites spanning the junction of the Lomonosov Ridge with the Eurasian continent supports the consensus that the majority of volume transport is via topographic following boundary currents in the Atlantic layer (Woodgate et al., 2001). The Atlantic water is a primary source of heat and salinity for the western Arctic.

Well-ventilated Atlantic water in the center of the Canada Basin observed in the SCICEX 96 cruise indicates renewal times are of the order of 1-2 decades, much shorter that previously thought. This suggests a pattern of recirculating gyres that ventilate the interior as opposed to the single large gyre pattern proposed in the past by Rudels et al. (1994). The ventilated Atlantic water observed in the Canada Basin by Smethie et al. (2000) supports the idea that the spreading of the boundary current provides a mechanism for the propagation of shelf and slope properties to the basin interior in the vicinity of the Chukchi-Mendeleyev boundary as proposed by Swift et al. (1997). However, observational data supporting this hypothesis is still lacking.

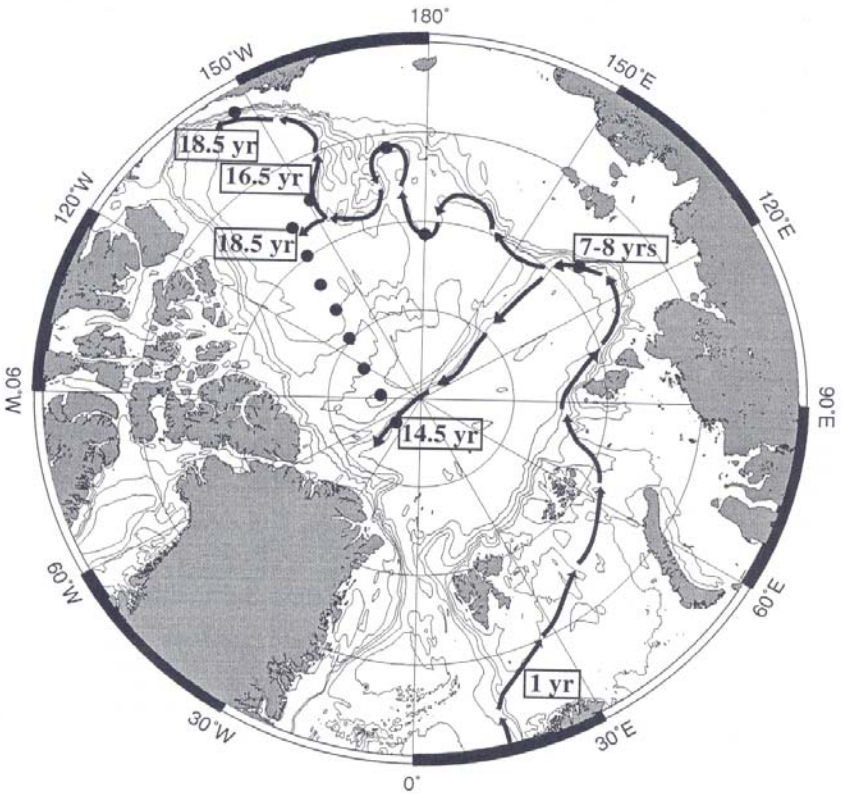

Figure 1.2 Circulation pathway of Barents Sea Branch Water with tritium^{3}/He ages (from Smethie et al., 2000).

The western Arctic receives Pacific water through the Bering Strait. Pacific water inflow is a source of fresh water but is highly variable (Coachman and Aagaard, 1988; Roach et al., 1995). The Pacific water inflow divides into three main branches after passing through the Bering Strait (Figure 1.3) (Pickart, 2003). Two branches flow northward into the Chukchi Sea between Herald and Hanna shoals and merge with a larger scale eastward boundary flow proceeding towards the Beaufort Sea. The third and smallest branch flows between Hanna Shoal and the Alaskan coast towards Barrow Canyon merging with the eastward boundary flow. In summer the majority of incoming Pacific water continues northward into the Chukchi Sea as the Alaskan Coastal Current (Pickart, 2003).

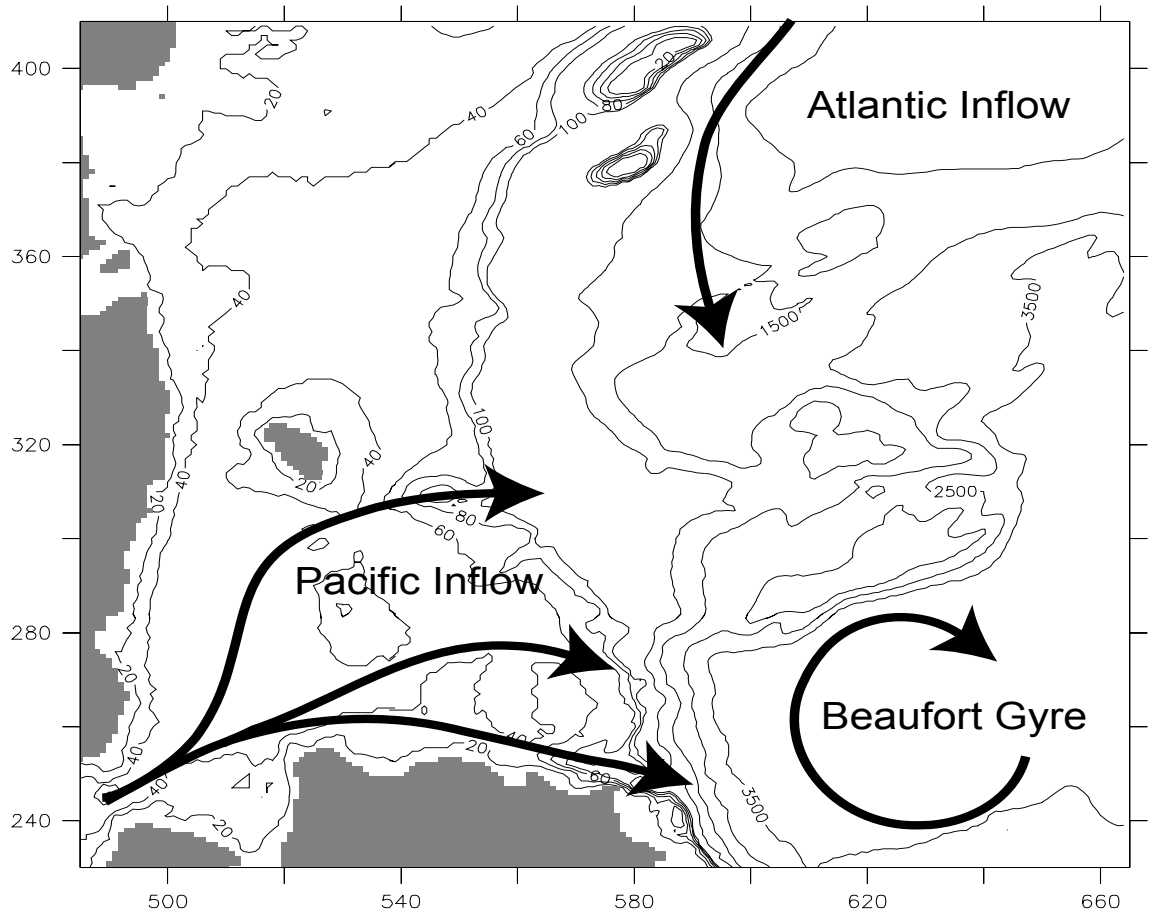

Figure 1.3 General circulation in the western Artic region includes boundary flow from the Eurasian Basin, three branches of Pacific water inflow and the Beaufort Gyre.

Reduced ice thickness concurrent with increased temperature and freshening in the surface layer of the Canada Basin as discussed by McPhee et al. (1998) may lead to the assumption that a primary source of the excess fresh water in the SHEBA study region is the melted ice. McPhee et al. (1998) indicate that oceanic heat flux was much greater during 1997 than in the mid-1970's, which suggests a mechanism to melt ice. Shimada et al. (2001) state that summertime temperature maxima of shallow waters of the Chukchi and Beaufort Seas carry enough heat in the upper layers of the ocean to affect ice coverage. However, this seems contrary to the expectation that vertical exchange

will be inhibited by the strong seasonal halocline that would be expected to form due to ice melt during this period.

McPhee et al. (1998) indicated that the source of freshwater found in the SHEBA study region is unclear. Ice melt alone cannot account for the increased freshwater that was observed. Suggestions of additional sources of fresh water include runoff and imbalance in precipitation and evaporation. However, little evidence exists to support a shift in precipitation during this period nor a complete shift in the entire Mackenzie River discharge would account for the freshening either. It is suggested that an additional mechanism is the advection of ice, previously formed elsewhere, into this region.

Macdonald et al. (2002) verified that a significant amount of fresh water in the SHEBA study region is meteoric including some originating from the Mackenzie River. They also confirmed that a surplus of ice meltwater was present in the central Canada Basin while a deficit existed in the shelf regions supporting the possibility that a meltwater source of ice formed elsewhere which was then advected into the region. This will be discussed further in Chapter IV.

D. SCIENCE GOALS

The Chukchi Plateau is a region of complex bathymetry and a confluence of Atlantic-derived boundary current flow from the west, Pacific water inflow from the Bering Strait and eastward flow driven by the Beaufort gyre (Figure 1.3). Despite the progress of research, some conclusions regarding circulation in the western Arctic region are inconsistent. The interaction of the Atlantic layer flow

with Pacific water outflow from the Bering Strait in the vicinity of the Chukchi Plateau, the fate of these currents beyond the Chukchi Plateau in the Canada Basin and their subsequent interactions in the central Canada Basin is inadequately understood.

The inferred circulation of the Atlantic layer boundary flow across the Chukchi Plateau as indicated by Rudels et al. (1994) (Figure 1.1) differs from the propagation pathway proposed by Smethie et al. (2000) who indicate that the Atlantic layer flows around the slope of the Chukchi Plateau (Figure 1.2). The question regarding whether the Atlantic Water boundary current crosses the Chukchi Rise as it approaches from the northwest, flows along the topography of the rise or breaks into a number of pathways remains unanswered.

The western Arctic and Canada Basin circulation warrant further research. The Chukchi Plateau region is a confluence of boundary flow from the Eurasian Basin, Bering Strait and Beaufort Gyre while also an area of complex bathymetry. This unique combination of issues presents many challenges to understanding the circulation in the western Arctic. The disparity between the inferred pathway of the boundary flow across the Chukchi Plateau as portrayed by Rudels et al. (1994) and as portrayed by Smethie et al. (2000) (Figures 1.1 and 1.2) is an example of a discrepancy within the oceanographic community that requires resolution. Additionally, the Chukchi Plateau region is the upstream source area of transport into the SBI study region. Understanding of circulation and property transport in the Chukchi Plateau is crucial to understand these same issues in the SBI study region, as

well as to successfully meet the goals of the SBI initiative.

The primary scientific goal of this project is to improve understanding of the circulation and property transport in the western Arctic and in the vicinity of the Chukchi Plateau in particular through the use of a high resolution coupled ice-ocean model forced with realistic atmospheric data. Comprehensive modeling can provide a tool to supplement limited observational data and to improve our knowledge of the regional circulation. The NPS Pan-Arctic sea ice and ocean model, developed in part for the SBI program, provides valuable insights into the circulation of the region.

This project will attempt to answer some questions that exist regarding circulation and property transport in the western Arctic by qualitatively describing and quantitatively assessing the oceanic circulation pathway of the Atlantic layer boundary flow in the region of the Chukchi Plateau. Ultimately these comparisons will be utilized to determine requirements for the realistic representation of ocean and sea ice circulation and water volume properties in regional and global ocean and climate models based on the example of the western Arctic region.

E. SIGNIFICANCE TO NAVAL OPERATIONS

Few in the military community predicted the dramatic shift from the anti-Soviet blue water naval operations characteristic of the cold war in the nineteen-seventies and early nineteen-eighties to the focus on littoral warfare just over a decade ago, climaxing in the 1991 Gulf War. As a result of this rapid shift in the battlespace

environment, the Navy has been forced to overcome great challenges. Although the Arctic region is not currently a common operating area nor expected to be so in the near future, defense strategists must ensure that a rapid shift towards operations in the Arctic does not find the Navy unprepared. The recent warming trends in the Arctic and reduced ice coverage warrants a sustained research program to ensure the US Navy is prepared for the contingency of increased commercial and tactical operations in the Arctic environment in the near future.

A symposium held in July of 2000 by the Oceanographer of the Navy and the National Ice Center brought together representatives from these two organizations as well as from the Office of Naval Research (ONR), the Arctic Research Commission, the U.S. Coast Guard and recognized experts in climate change. This unique collaboration of military and scientific leadership framed national and strategic issues surrounding operations in an ice-free, or ice-diminished Arctic. The results of this symposium presented a plausible scenario of the Arctic region with greatly reduced ice coverage in fifty years (Brass, 2002). This meeting indicated that many historically ice-covered areas would be ice free for part or all of the year. The Sea of Okhotsk and Sea of Japan would remain ice-free year round while the entire Russian coast and Northwest Passage through the Canadian Arctic Archipelago would be ice free during the summer months and navigable by non-icebreaking vessels. Diminished sea ice coverage in the Arctic poses tangible implications that must be considered, such as the opening of Russia's Northern Sea Route, sonar performance for anti-submarine warfare operations as well as socio-

economic issues (Brass, 2002). Long-term changes in the Arctic environment present significant implications for the architects of United States Naval operations. Prudence demands that Navy leaders foster the investigation of complex environmental changes today, which can affect ice coverage trends in the Arctic tomorrow. Preparation for increased operations in an environment as harsh as the Arctic requires formulation of a strategic framework, grounded in good science.

THIS PAGE INTENTIONALLY LEFT BLANK

II. MODELING DESCRIPTION

A. THE OCEAN MODEL

The model domain covers all Northern Hemisphere ice-covered waters including the Arctic Ocean, the Sea of Japan, the Sea of Okhotsk, the sub-polar North Pacific and North Atlantic Oceans, the Canadian Arctic Archipelago (CAA), the Bering Sea and the Nordic Seas and all major inflow and outflow pathways of the Arctic Ocean (Figure 2.1).

The model horizontal grid contains 1280 x 720 points and is configured at $1/12^{\circ}$, or approximately 9.26 kilometers, and has been rotated off the pole to eliminate the convergence of meridians at the North Pole (see Figure 2.1). The model consists of forty-five levels in the vertical (Table 2.1). The large domain allows investigation of the most important processes in the Arctic Ocean and facilitates realistic exchanges between the Arctic Ocean and adjacent basins, which fosters realistic thermohaline forcing in the Arctic Ocean. The model is not eddy resolving but can be considered eddy permitting, by resolving mesoscale features down to ~37 km (four grid points).

This regional ocean model is based on the Los Alamos National Laboratory (LANL) Parallel Ocean Program (POP) model (Dukowicz and Smith, 1994), which evolved from the Semtner and Chervin (1992) global ocean model. The free surface approach (Killworth et al., 1991; Semtner, 1995), allows for the use of unsmoothed, high-resolution bathymetry. The model assumes hydrostatic balance and uses

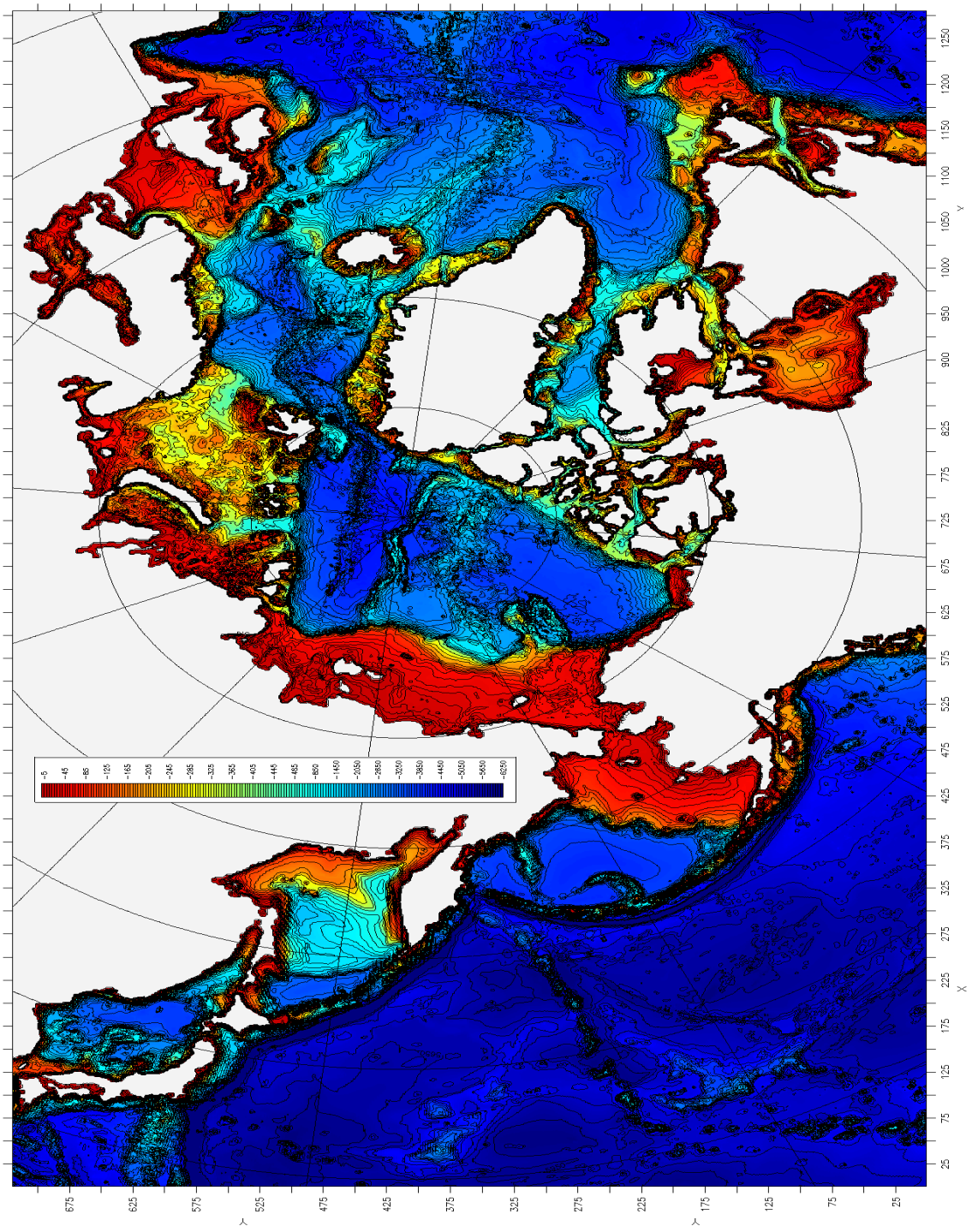

Figure 2.1 Model domain and combined IBCAO and ETOPO5 based bathymetry(m) (from Marble, 2001).

the Bousinessq approximation. The finite difference scheme uses an Arakawa B-grid (Mesinger and Arakawa, 1976) and integrates the primitive equations in spherical coordinates. The ocean model time step is 480 seconds (8 minutes).

The model lateral boundaries, including those for river runoff, are closed and do not allow volume or momentum transfer across them. An 18-grid point wide (~162 km), 500 m deep U-shaped channel through North America, south of Hudson Bay was created to balance the flow of the Pacific Ocean water into the Arctic Ocean and provide a return path for the net flow of water from the Pacific Ocean, through the Arctic Ocean, to the Atlantic Ocean. A westward wind forcing of 1.75 dyne cm^{-2} is prescribed over the channel. The result of net average northward volume transport into the Arctic Ocean across the Bering Strait ranges from 0.5 to 0.8 Sv (McClean et al., 2001), which approximates observed mean flow of 0.83 Sv (Roach et al., 1995). A no-slip boundary condition is imposed at the lateral walls. No flux of heat or salt is allowed through the boundary. At the bottom, flow is required to follow the slope of the bathymetry and no fluxes are allowed through the bottom.

B. SPIN UP AND FORCING

The ocean was started from rest and initialized using three dimensional temperature and salinity fields from the University of Washington Polar Science Center Hydrographic Climatology 1.0 (PHC) (Steele et al., 2000) interpolated on to the model grid. The PHC is a combination of the 1998 version of the World Ocean Atlas (Antonov et al., 1998;

Layer	Thickness	Lower depth	Midpoint
1	5.0	5.0	2.5
2	5.0	10.0	7.5
3	5.0	15.0	12.5
4	5.0	20.0	17.5
5	6.0	26.0	23.0
6	7.3	33.3	29.7
7	8.8	42.1	37.7
8	10.6	52.7	47.4
9	12.8	65.4	59.1
10	15.4	80.8	73.1
11	18.6	99.4	90.1
12	22.4	121.8	110.6
13	27.0	148.9	135.4
14	32.6	181.5	165.2
15	39.3	220.8	201.2
16	47.5	268.3	244.6
17	57.3	325.5	296.9
18	69.1	394.6	360.1
19	83.3	477.9	436.3
20	100.5	578.4	528.2
21	121.6	700.0	639.2
22	150.0	850.0	775.0
23	200.0	1050.0	950.0
24	200.0	1250.0	1150.0
25	200.0	1450.0	1350.0
26	200.0	1650.0	1550.0
27	200.0	1850.0	1750.0
28	200.0	2050.0	1950.0
29	200.0	2250.0	2150.0
30	200.0	2450.0	2350.0
31	200.0	2650.0	2550.0
32	200.0	2850.0	2750.0
33	200.0	3050.0	2950.0
34	200.0	3250.0	3150.0
35	250.0	3500.0	3375.0
36	250.0	3750.0	3625.0
37	250.0	4000.0	3875.0
38	250.0	4250.0	4125.0
39	250.0	4500.0	4375.0
40	250.0	4750.0	4625.0
41	300.0	5050.0	4900.0
42	300.0	5350.0	5200.0
43	300.0	5650.0	5500.0
44	300.0	5950.0	5800.0
45	300.0	6250.0	6100.0

Table 2.1. Vertical distribution of model levels.

Boyer et al., 1998) with the regional Arctic Ocean Atlas (Environmental Working Group, 1997; 1998).

The model has been integrated for ~ 70 years using European Centre for Medium-Range Weather Forecasts (ECMWF) realistic forcing. During the 27-year model spin-up, the model was forced using a 15-year mean annual cycle of daily-averaged atmospheric forcing derived from the ECMWF 1979-1993 reanalyzed data (Gibson et al., 1999). Deep acceleration was used through the second decade of this integration. This numerical method is applied to temperature and salinity diffusion calculations at depth, where property change is much slower, in order to save computation time. The timestep in the top sixteen layers (0-220m) remains at 8 minutes. However, the timestep applied to the equations governing temperature and salinity diffusion below 220m is increased gradually by a factor of one to ten through level 33 (3050m). Below 3050 m the deep ocean evolves ten times faster than the upper 220 m, as a result the deep ocean has been essentially integrated for 100 years at the end of ten years of model integration.

Deep-acceleration was discontinued during the remaining seven years of initial spinup and then followed by a 6-year run forced with the repeated 1979 daily-averaged ECMWF reanalyzed data. During that time and the subsequent 15-year integration with the repeated 1979-1981 daily-averaged ECMWF data the model was forced towards conditions of the late 1970s / early 1980s, in order to begin the 1979-2001 interannual simulation. Beginning in year 42 of spinup, river runoff forcing was prescribed through restoring to temperature and salinity as a function of daily-averaged annual cycle of each river discharge,

including Russian (Dvina, Pechora, Ob, Yenisey, Kotuy, Lena, Indigirka, and Kolyma), Mackenzie and Yukon rivers.

Forcing fields include 10 m elevation east-west (u) and north-south (v) wind velocity components, surface pressure, temperature and dewpoint, and long-wave and short wave radiation. The atmospheric forcing of 1979-2001 includes years dominated by both anticyclonic and cyclonic regimes. Comparison of the two-year mean 0-50 m Arctic Ocean circulation pattern with representative ocean surface circulation patterns for each regime (Proshutinsky and Johnson, 1997; Maslowski et al., 2000 and 2001) shows a flow in between the two extremes, with a medium-sized Beaufort Gyre and a Transpolar Drift Stream aligned along the Mendeleyev Ridge. Long model integration through this choice of forcing can have a significant impact on sea ice and ocean properties.

In considering ocean temperature and salinity climatology bias, the time span of the merged ocean climatology datasets (Steele et al., 2000) shows the 1946 to 1994 data were collected during periods of anticyclonic and cyclonic atmospheric forcing regimes (Proshutinsky and Johnson, 1997; Johnson et al., 1999). Thus, it is felt there is no strong ocean climatology bias toward either regime.

The model results in this analysis consist of 276 monthly averaged ocean data sets from the 1979-2001 run, 365 daily ocean data sets from year 1987 and 365 daily ice sets files from year 1987. For an additional description of the model readers are referred to Marble (2001), Preller et al. (2002), Maslowski et al. (2003).

C. ANALYSIS METHODS

In order to investigate the circulation in the western Arctic, the monthly mean velocity fields are analyzed from 1979-2001. Depth-averaged model velocities were computed for the upper ocean (0-26 m), at the halocline (54-149 m) and the Atlantic layer (268-850 m) in order to investigate circulation in each of these distinct layers. Cross-sections of temperature and salinity in the Canada Basin were analyzed to determine depths of the model-defined halocline and Atlantic layer (Figures 2.2 - 2.4).

Twenty-three year (1979-2001) mean climatological velocity fields were computed to determine the mean state circulation in the upper ocean, halocline and Atlantic layer. Decadal variability in the western Arctic Ocean is investigated by comparing two-year mean velocities in the upper ocean, halocline and Atlantic layer from the early 1980s, 1990s and 2000s.

Volume transport and the flux of heat and freshwater are calculated across twenty-two cross-sections (Figure 2.5) in the model domain of the western Arctic from 1979 - 2001. Net volume transport, heat and freshwater fluxes are calculated in the upper ocean (0-220 m) and the Atlantic layer (268-850 m) to identify the pathways and directions of greatest property transport.

Heat flux is referenced to $-0.1^{\circ}C$ and freshwater flux is referenced to a salinity value of 34.70 ppt (i.e. parts per thousand). The flux is defined as the product between the mean volume transport in the positive or negative direction and the difference between the reference value and the mean value of the temperature or salinity. A

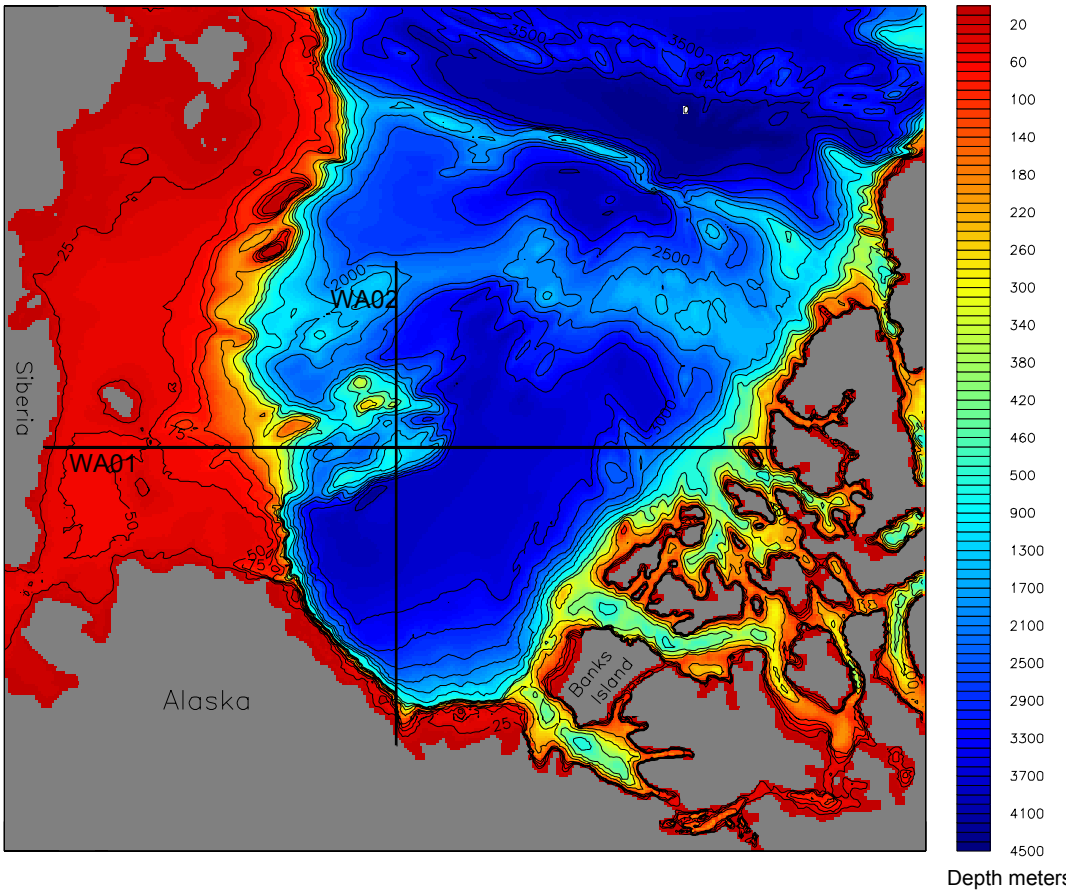

Figure 2.2 Western Arctic region of study. Cross-sections WA01 and WA02 were used in determination of the halocline and Atlantic layer.

negative flux can result from two possibilities, first when the mean volume transport is in the positive direction and the mean temperature or salinity difference has a negative value. The second case can be when the mean volume transport is in the negative direction and the mean temperature or salinity difference has a positive value. In the case of a volume flux through a vertical section the total flux in the positive / negative direction is a sum of fluxes through model vertical grid cells.

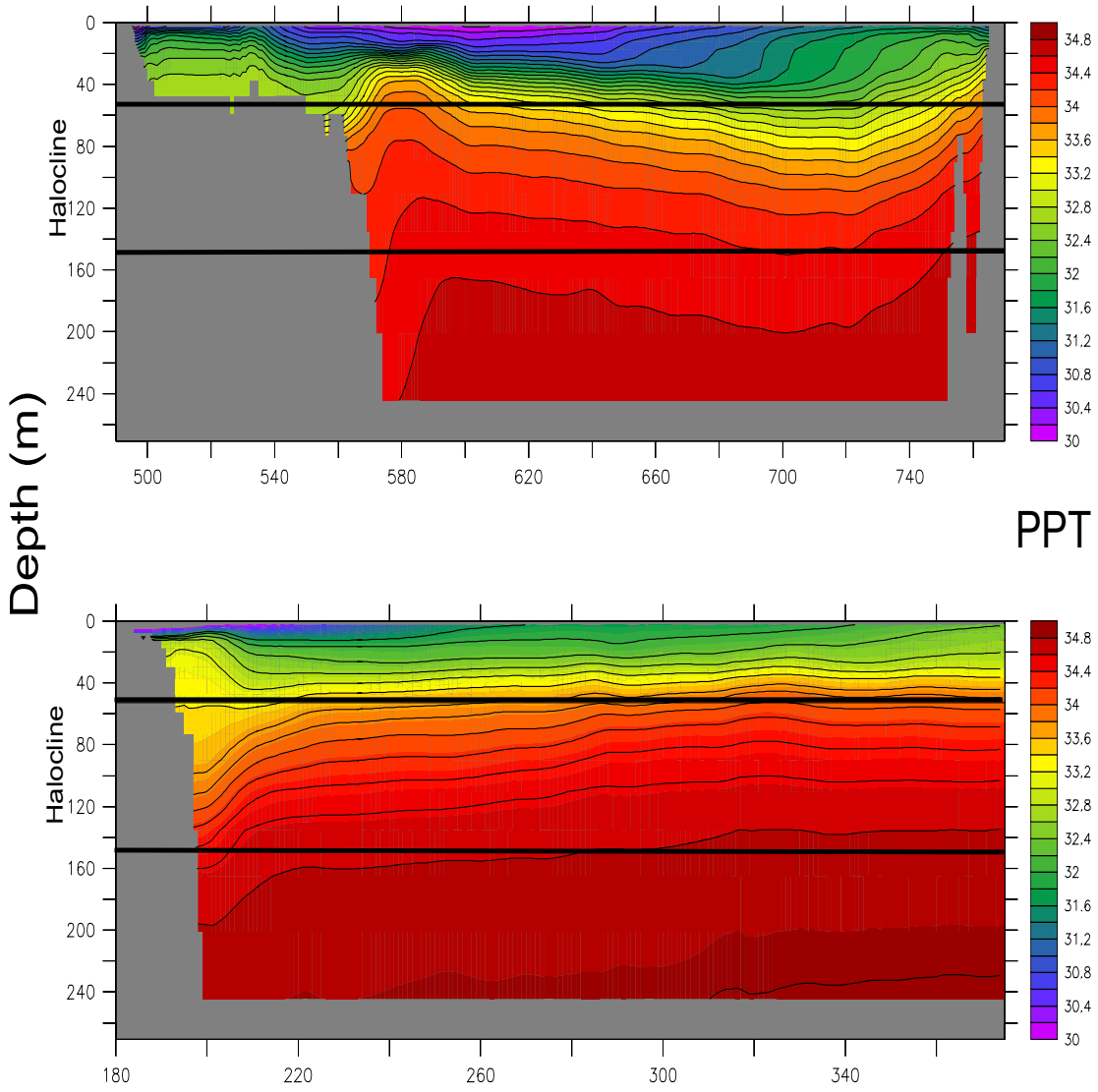

Figure 2.3 Salinity cross-section indicating the model-defined halocline across section WA01 (top) and WA02 (bottom).

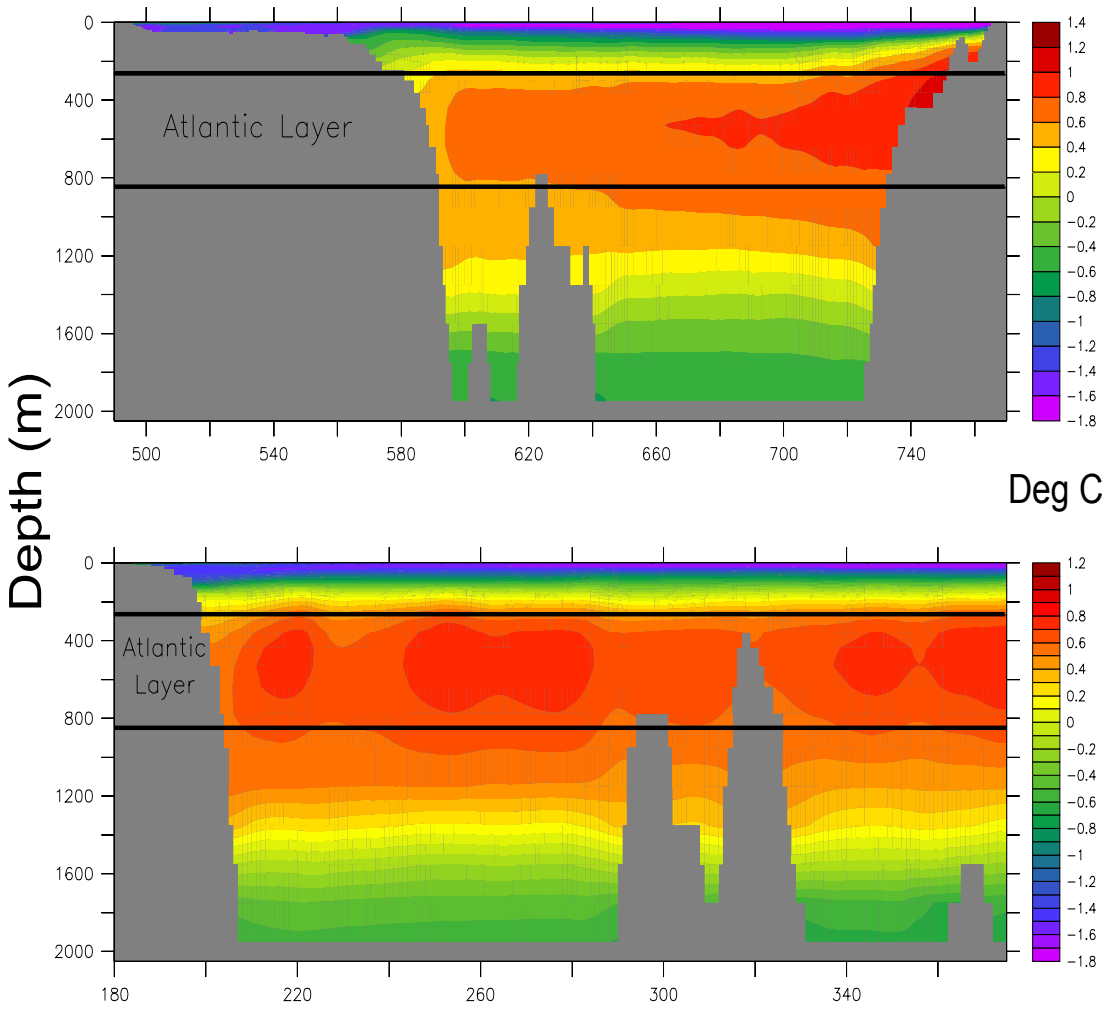

Figure 2.4 Temperature cross-section indicating the model-defined Atlantic layer across section WA01 (top) and WA02 (bottom).

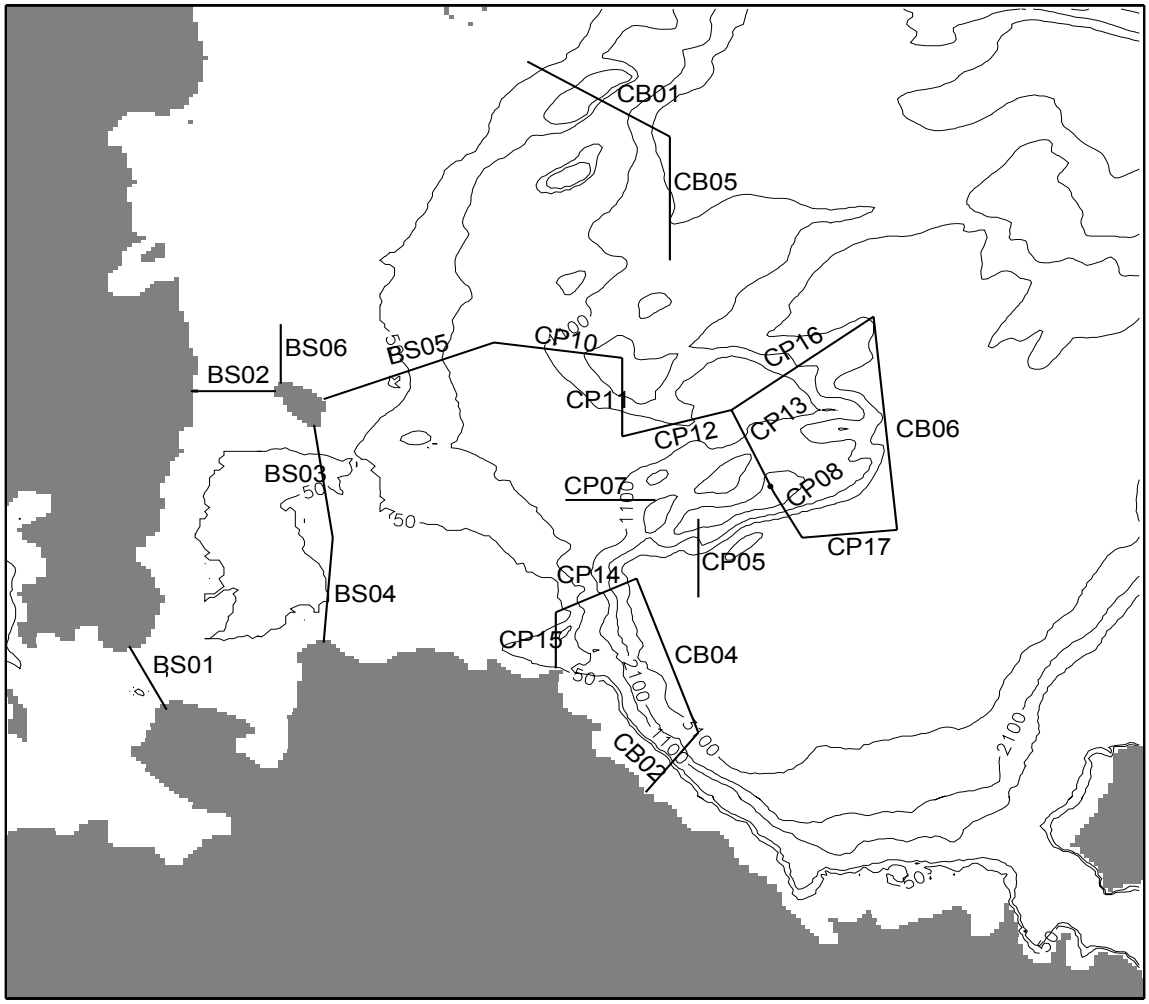

Figure 2.5 Cross sections used in study region for analysis of volume transport and property flux.

THIS PAGE INTENTIONALLY LEFT BLANK

III. RESULTS

A. CANADA BASIN

1. Volume Transport

Twenty-three year (1979-2001) mean climatological velocity fields are calculated from the monthly mean velocity fields. Bathymetric features of the study area are labeled in Figure 3.1. Depth-averaged transport in the model-defined upper ocean (0-26 m) (Figure 3.2), halocline depth (54-149 m) (Figure 3.3) and Atlantic layer (268 - 850 m) (Figure 3.4) are analyzed. .

The general circulation of the Canada Basin is cyclonic in nature. Atlantic water enters the Canada Basin from the Eurasian Basin at the junction of the Lomonosov Ridge with the Eurasian continent. This Atlantic inflow contributes to a cyclonic boundary flow that is evident at all three analyzed depth levels throughout the Canada Basin. Boundary flow is generally confined above the slope over the depth range roughly between 200 to 1100 m.

The upper ocean boundary flow upstream of the Chukchi Plateau is characterized by two distinct branches that extend along the upper and lower slope from the junction of the Lomonosov Ridge and the Eurasian continent to Mendeleyev Ridge (Figure 3.2). Northwest of Wrangel Island in the vicinity of 73° N, 170° E the upper slope branch merges with Pacific Water outflow that originates from the Bering Strait. This merged upper ocean flow continues eastward towards the Beaufort Sea.

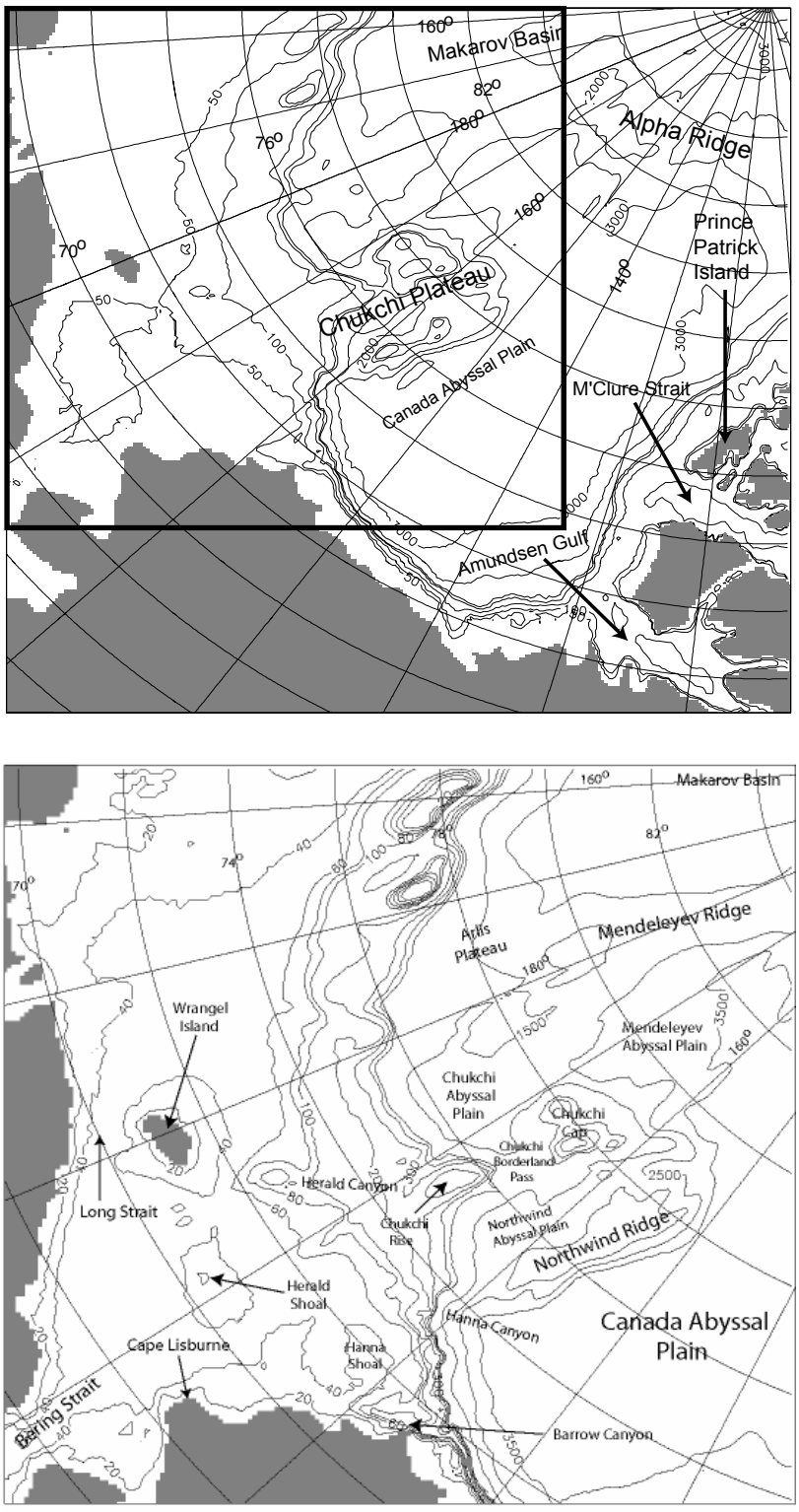

Figure 3.1 Common features of the Canada Basin (top) and Chukchi Plateau (bottom). The region identified as the Chukchi Borderland Pass refers to the sill between the 500m isobaths south of the Chukchi Cap and north of the Chukchi Rise.

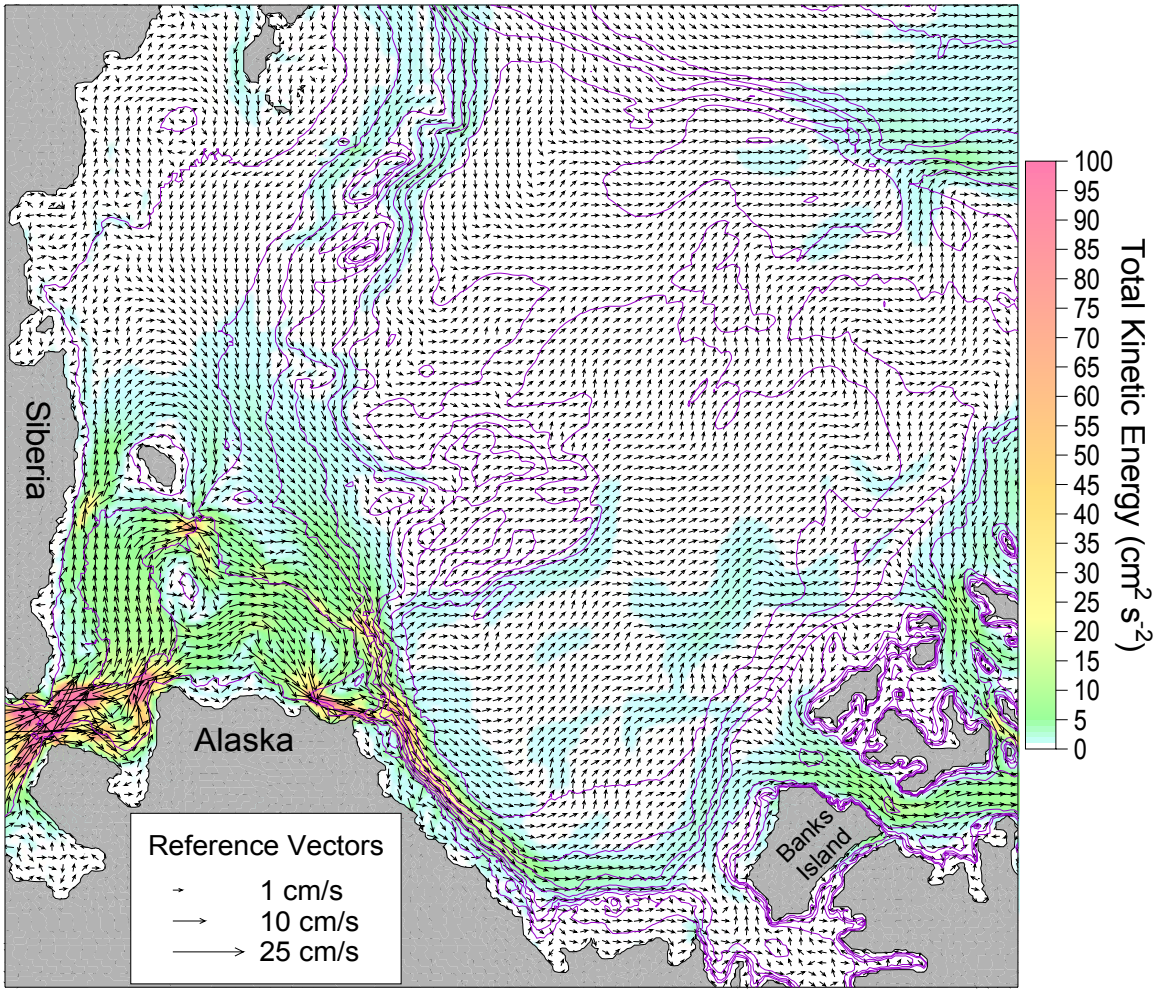

Figure 3.2 Vertically averaged velocity over the upper ocean layer (0-26m) averaged over 1979-2001. Every third vector in each direction is shown. Velocity vectors greater than 7cm/sec were truncated and the rest are shown using the square root function. Color shading represents total kinetic energy (cm^2/s^2) at every grid point. Total kinetic energy values between 0 and 1 cm^2/s^2 are not shaded.

Circulation through the Bering Strait into the Chukchi Sea is more energetic relative to the majority of upper ocean circulation in the Canada Basin (Figure 3.2). Pacific Water flow divides into three main branches as it enters the Chukchi Shelf through the Bering Strait. Two branches flow northward into the Chukchi Sea: one between Herald and Hanna shoals and the other along the eastward boundary flow proceeding towards the Beaufort Sea. The

third branch forms the basis of the Alaska Coastal Current. This branch flows along the Alaskan coast, between Hanna Shoal and the Alaskan coast towards Barrow Canyon and merges with boundary flow out of the west (see Figure 1.3). An additional westward flow is along the Siberian coast between the coast and Wrangel Island.

The majority of Pacific water merges with the eastward boundary flow that follows the slope parallel to the north Alaskan coast. This current continues along the slopes of the northern Canada after turning north in the southeast Beaufort Sea (Figure 3.2). Comparatively little water enters the Amundsen Gulf but model results suggest some recirculation occurs here. The majority of the boundary current passes along Banks Island and enters the CAA via the M'Clure Strait with the remainder continuing northeastward towards the Alpha Ridge.

The twenty-three year mean boundary flow along the continental slope at depths 54-149 m, corresponding to the model-designated halocline, maintains a generally cyclonic structure throughout the western Arctic (Figure 3.3). A strong signature (~25 cm^2/s^2 total kinetic energy (TKE) or greater) of the current within the halocline is evident after it enters the Canada Basin across the Lomonosov Ridge at its junction with the Eurasian continent. This elevated TKE is sustained across the Makarov Basin, Chukchi Plateau and into the Beaufort Sea. The majority of boundary current at this depth is observed to pass across the Chukchi Abyssal Plain, south of the Chukchi Cap, through the Chukchi Borderland Pass, across the Northwind Abyssal Plain and then crossing the Northwind Ridge just north of the Hanna Canyon. A northward flow within the halocline

parallels the eastern flank of the Northwind Ridge to its northern end. The strength of the boundary current diminishes in the southeastern Beaufort Sea with a portion recirculating in the Amundsen Gulf and an additional portion entering the M'Clure Strait. Boundary flow remains organized over the slope towards the Alpha Ridge and is enhanced by three distinct branches with TKE greater than 2 cm^2/s^2, that originate from the basin interior.

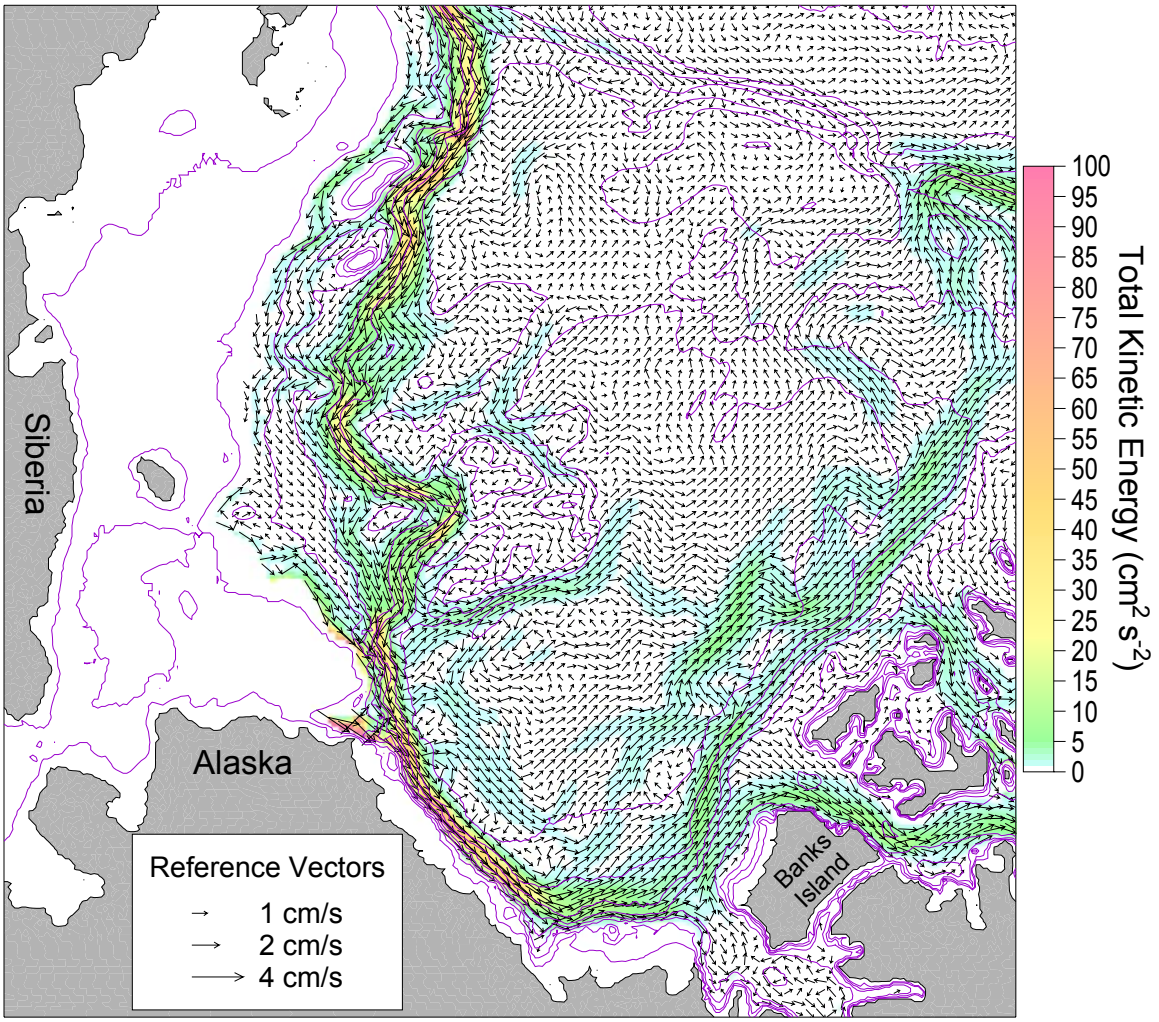

Figure 3.3 Vertically averaged velocity over the halocline layer (54-149m) averaged over 1979-2001. Every third vector in each direction is shown. Velocity vectors greater than 7cm/sec were truncated and the rest are shown using the square root function. Color shading represents total kinetic energy (cm^2/s^2) at every grid point. Total kinetic energy values between 0 and 1 cm^2/s^2 are not shaded.

Boundary flow along the slope within the model-designated Atlantic layer maintains a generally cyclonic structure throughout the western Arctic as well but is weaker, less organized, and more variable as compared to flow in the halocline layer (Figure 3.4). Organized Atlantic layer circulation is evident along the continental slope from the Makarov Basin through the Chukchi Plateau via the Chukchi Borderland Pass but diminishes beyond the Northwind Ridge of the Chukchi Plateau. Organization of the boundary current along the slope is reestablished near the Alpha Ridge and evident from the Alpha Ridge towards the Lomonosov Ridge. Some weak (~1 cm^2/s^2 TKE) but still organized broad eastward flow exists in the deep Beaufort Sea originating east of the Northwind Ridge. A similar circulation pattern is evident from the northeastern flank of the Northwind Ridge across the basin interior to where it merges with the boundary flow towards the Alpha Ridge.

2. Interdecadal Comparisons

Two-year means from monthly velocity fields averaged at the three separate depth intervals are calculated at the beginning of each decade to determine decadal variability in the circulation of the Canada Basin. The resulting fields for the time periods 1981-1982, 1991-1992 and 2000-2001 for the upper ocean, halocline and Atlantic layer depth intervals are shown in Figures 3.5 through 3.13, respectively.

The upper ocean circulation during the three time periods is similar to the twenty-three year mean climatological circulation (Figures 3.5 - 3.7). The general flow in most regions of the western Arctic appears

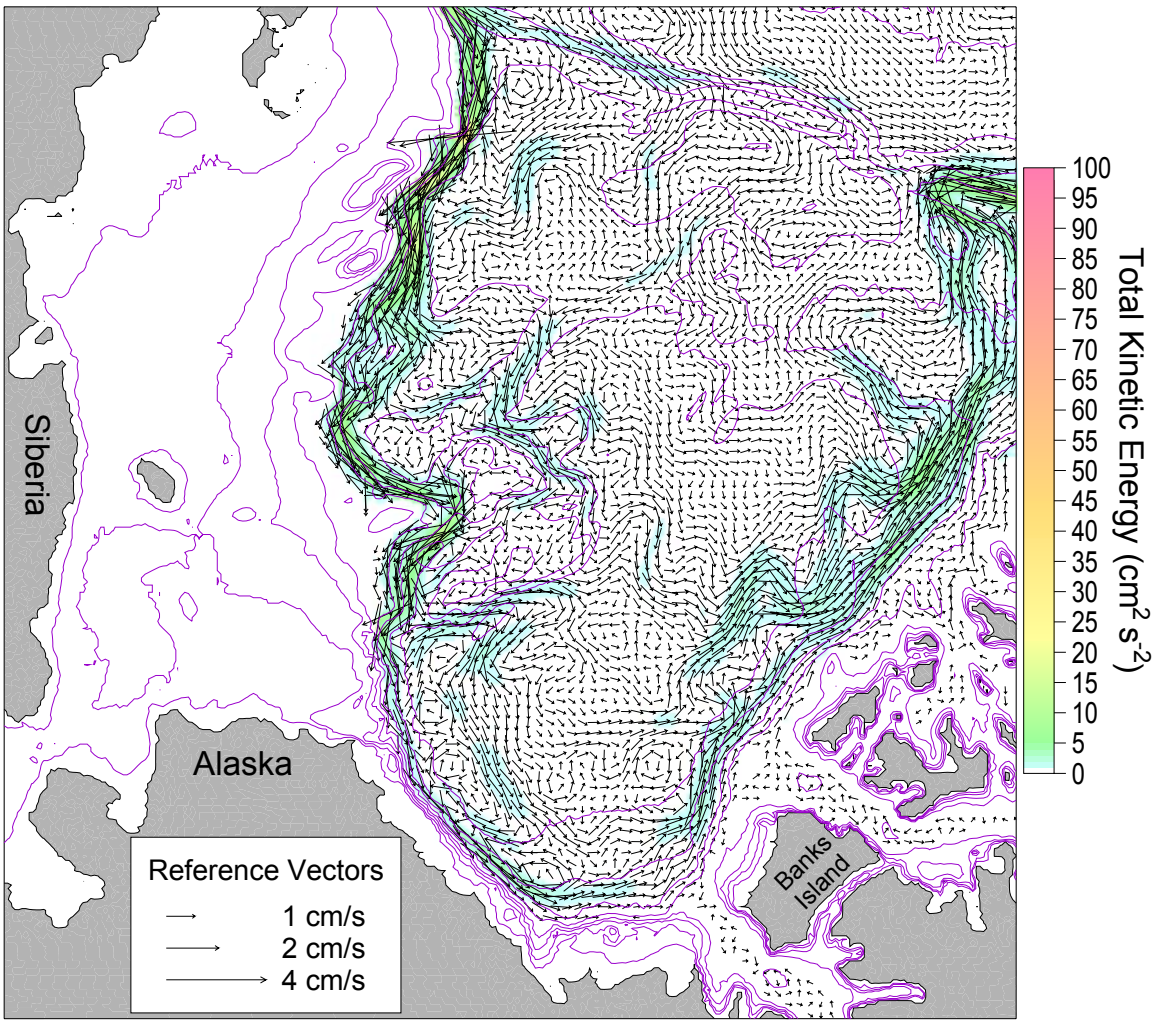

Figure 3.4 Vertically averaged velocity over the Atlantic layer (268-850m) averaged over 1979-2001. Every third vector in each direction is shown. Color shading represents total kinetic energy (cm^2/s^2) at every grid point. Total kinetic energy values between 0 and 1 cm^2/s^2 are not shaded.

stronger during the 1991-1992 period, where TKE values frequently exceeded 50 cm^2/s^2, as compared to 1981-1982 and 2000-2001. Upper ocean boundary flow TKE in much of the Beaufort Sea is over 20 times stronger during the 1991-1992 time period as compared to the 1981-1982 period. The two-branch structure of the boundary current in the upper ocean of the Makarov Basin and extending towards the Chukchi Plateau is evident in each two-year mean field. It is strongest and most organized beyond the Mendeleyev Ridge

during the 1991-1992 period and weakest during the 2000-2001 period losing organized structure in the Makarov Basin. The southeastward flow over the East Siberian slope and adjacent slope is strongest during the 1991-1992-time period. Two organized northward flows, one weaker in the vicinity of the Chukchi Cap and Mendeleyev Abyssal Plain, and the second relatively stronger east of and parallel to the Northwind Ridge are evident in the 1981-1982 time period but they are weaker of absent in the subsequent time periods. The upper ocean circulation in the Beaufort Sea in the 1981-1982 mean includes an anticyclonic flow of a semi-enclosed Beaufort Gyre (Figure 3.5).

Some northward flow over the Northwind Ridge exists in all three-time periods except over the northern end where it becomes more eastward in the 2000-2001-time period (Figure 3.7). Eastward flow from Barrow Canyon along the northern Alaskan Coast is evident in all three-time periods but is notably weaker and less organized during 1981-1982. The Beaufort Gyre exhibits a shift to more cyclonic circulation between the 1981-1982 and 1991-1992 time periods (Figures 3.5 and 3.6).

The circulation in the northern Beaufort Sea and adjacent to the entrances of the CAA displays variable organization among the three decadal time periods in the upper ocean (Figures 3.5, 3.6, 3.7). Common to each of the three time periods is an organized boundary circulation along the slope from the southeastern Beaufort Sea northward with a distinct branch entering the M'Clure Strait. However, this pattern is very weak in the Beaufort Sea during the 1981-1982-time period. Recirculation in the

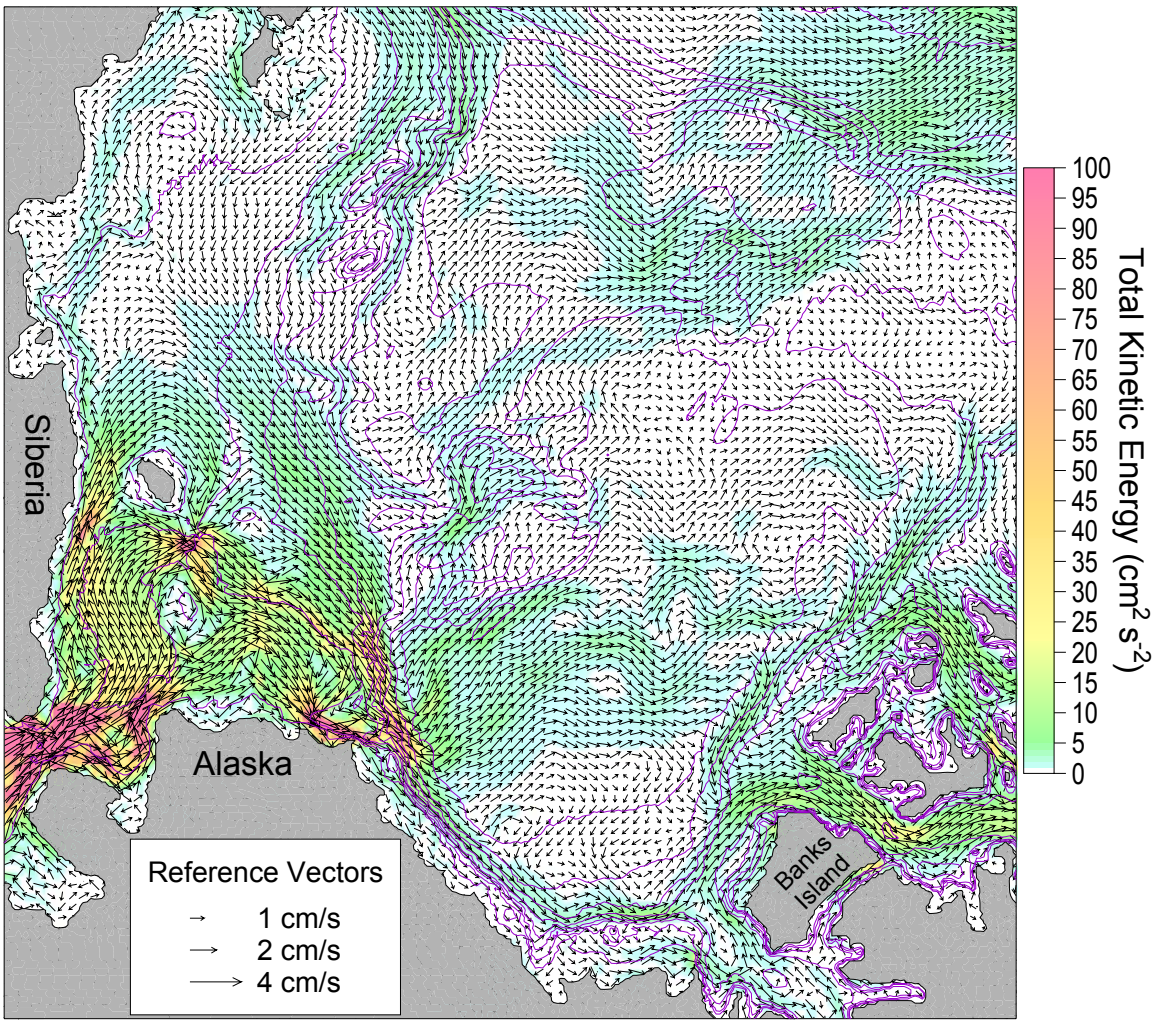

Figure 3.5 Vertically averaged velocity over the upper ocean layer (0-26m) averaged over 1981-1982. Every third vector in each direction is shown. Velocity vectors greater than 7cm/sec were truncated and the rest are shown using the square root function. Color shading represents total kinetic energy (cm^2/s^2) at every grid point. Total kinetic energy values between 0 and 1 cm^2/s^2 are not shaded.

Amundsen Gulf is evident in the 1981-1982 and 2000-2001 time periods but absent during the 1991-1992 time period. Broad meanders moderately of various horizontal scales are present across the southern Canada Basin. These eddy-like features are numerous and strongest in the 1991-1992 time period. An organized, narrow southwestward current,

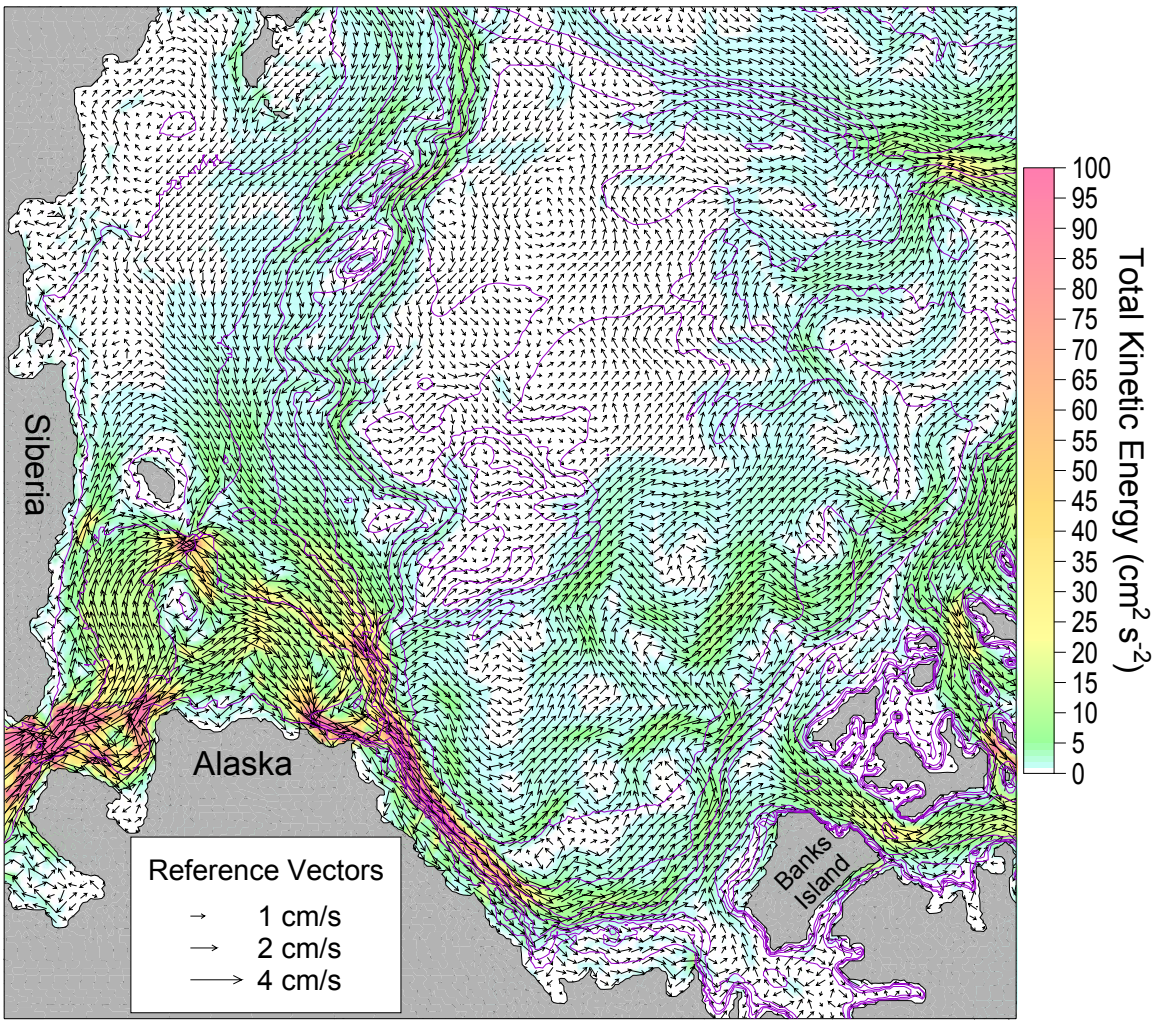

Figure 3.6 Vertically averaged velocity over the upper ocean layer (0-26m) averaged over 1991-1992. Every third vector in each direction is shown. Velocity vectors greater than 7cm/sec were truncated and the rest are shown using the square root function. Color shading represents total kinetic energy (cm^2/s^2) at every grid point. Total kinetic energy values between 0 and 1 cm^2/s^2 are not shaded.

seaward of the entrances to the CAA in the 1981-1982 time period is reversed in the subsequent time periods.

As was the case for the upper ocean, the circulation pattern of the model-defined halocline layer for each of the three time-averaged periods resembles the twenty-three year mean cyclonic pattern with the 1991-1992 period exhibiting higher TKE levels in all regions of the western

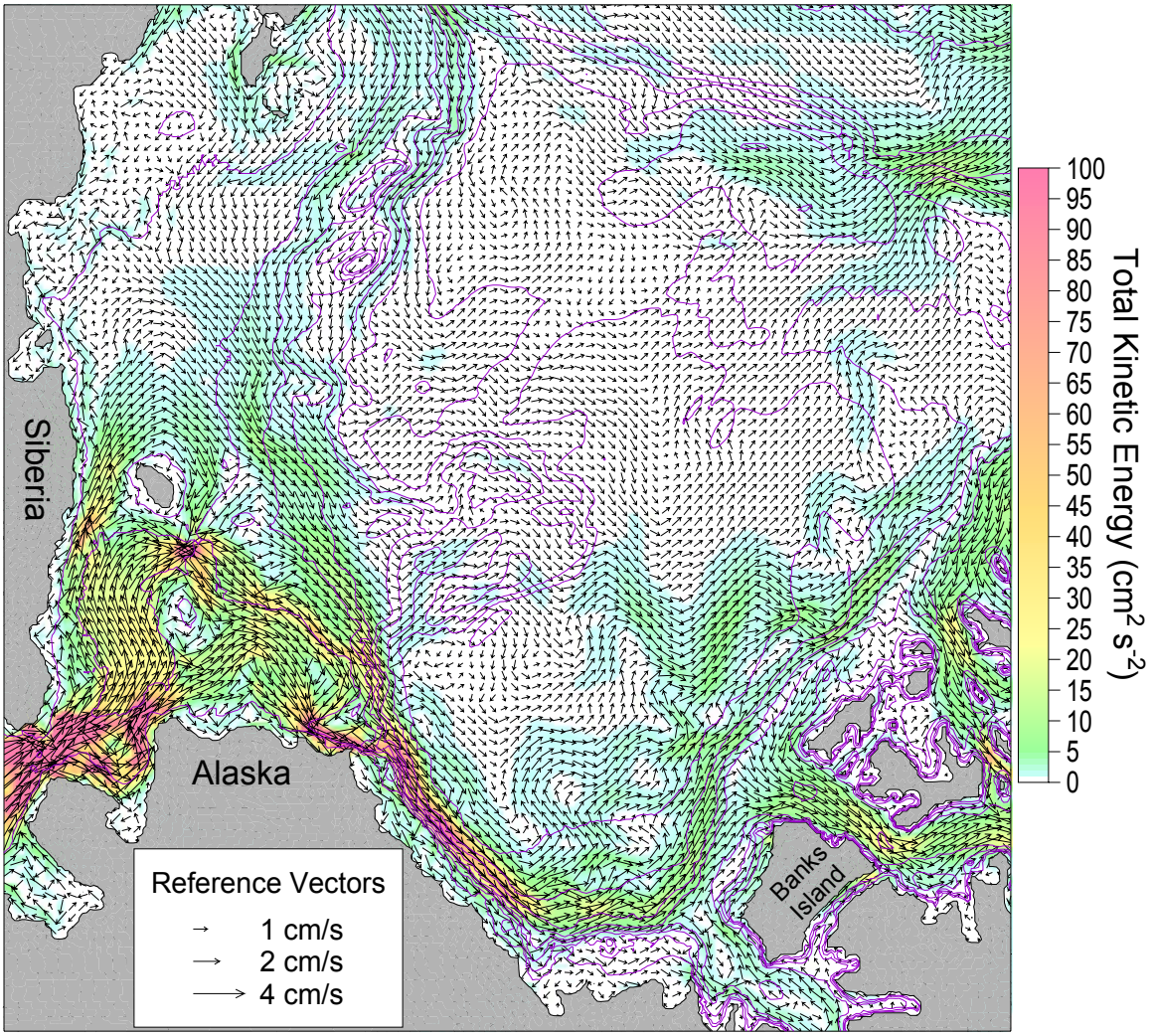

Figure 3.7 Vertically averaged velocity over the upper ocean layer (0-26m) averaged over 2000-2001. Every third vector in each direction is shown. Velocity vectors greater than 7cm/sec were truncated and the rest are shown using the square root function. Color shading represents total kinetic energy (cm^2/s^2) at every grid point. Total kinetic energy values between 0 and 1 cm^2/s^2 are not shaded.

Arctic (Figures 3.8 - 3.10). The organized structure and strength of the boundary current is greatest in the 1991-1992-time period and is sustained along the entire western Arctic perimeter. The boundary flow is maintained from the Makarov Basin to Beaufort Sea but diminishes in the eastern Beaufort Sea in the 1981-1982-time period. In the 2000-2001 time period a portion of the boundary current continues northeastward along the western flank of the

Chukchi Cap but diminishes in strength as it separates to the east of the northern end of the Chukchi Plateau. This pattern does not occur in previous time periods. The boundary current along the north slope of Alaska and the CAA towards the Alpha Ridge is strong (in excess of ~80 cm^2/s^2) and well organized in the 1991-1992 and 2000-2001 time periods. At this depth every time period shows a consistent flow into the M'Clure Strait and a weak cyclonic recirculation in the Amundsen Gulf.

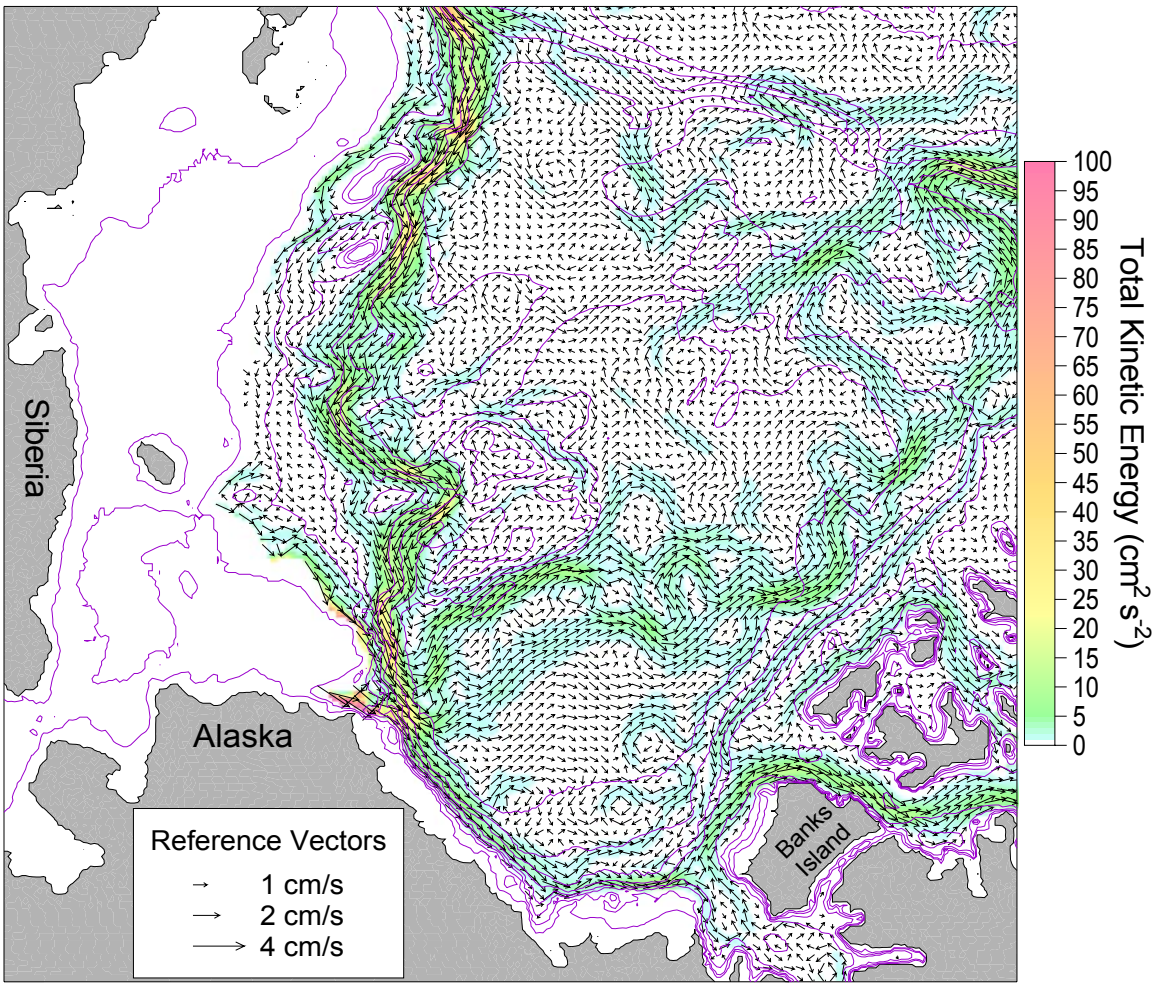

Figure 3.8 Vertically averaged velocity within the halocline layer (54-149m) averaged over 1981-1982. Every third vector in each direction is shown. Velocity vectors greater than 7cm/sec were truncated and the rest are shown using the square root function. Color shading represents total kinetic energy (cm^2/s^2) at every grid point. Total kinetic energy values between 0 and 1 cm^2/s^2 are not shaded.

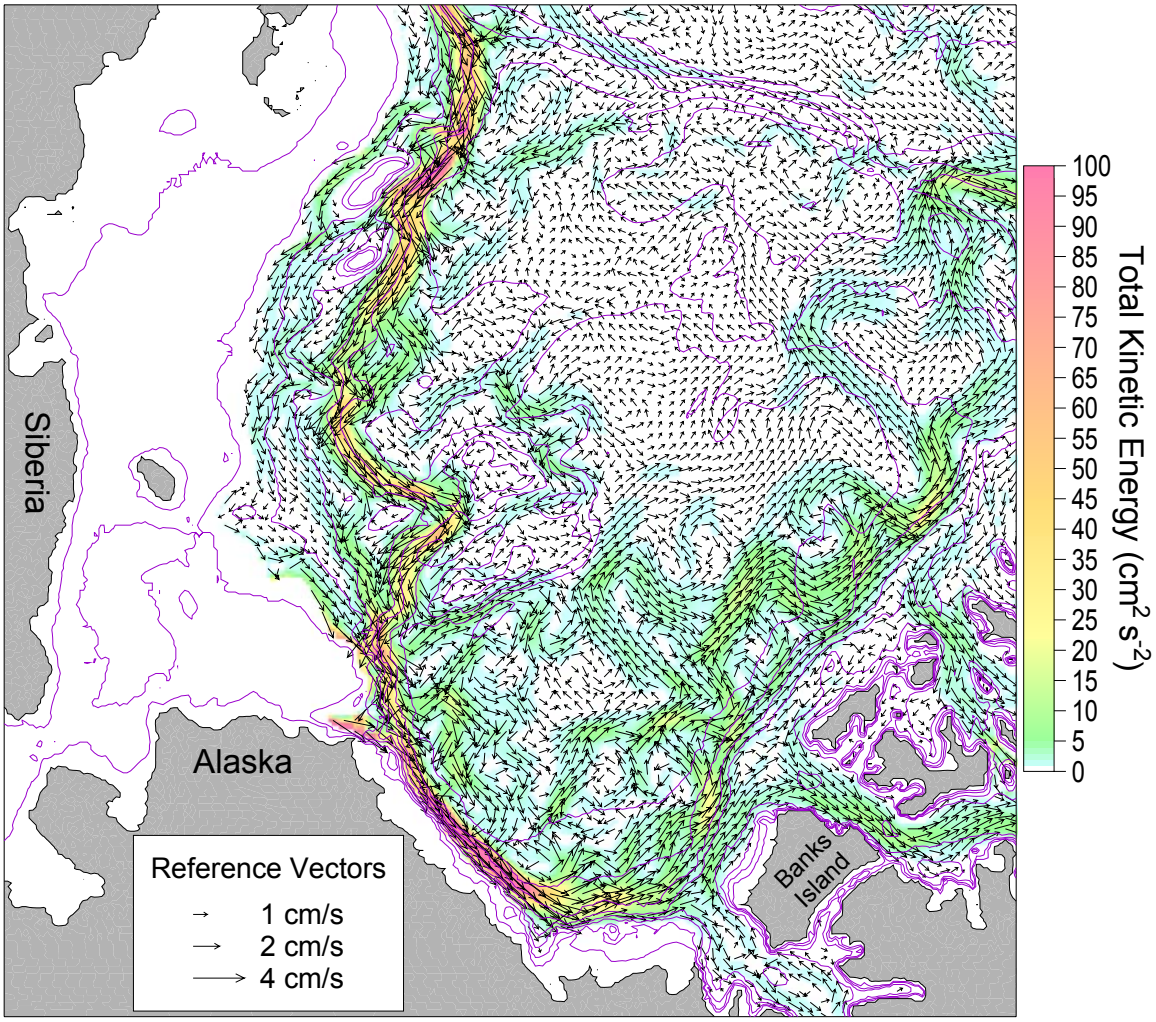

Figure 3.9 Vertically averaged velocity within the halocline layer (54-149m) averaged over 1991-1992. Every third vector in each direction is shown. Velocity vectors greater than 7cm/sec were truncated and the rest are shown using the square root function. Color shading represents total kinetic energy (cm^2/s^2) at every grid point. Total kinetic energy values between 0 and 1 cm^2/s^2 are not shaded.

Flow patterns adjacent to the entrances of the CAA display variability among the three decadal periods in the halocline layer. Each two-year period displays a narrow flow into the M'Clure strait of up to ~25 cm^2/s^2 TKE. However, a stronger branch with TKE up to ~25 cm^2/s^2 that continued along the slope pass the M'Clure Strait towards the Alpha Ridge that is evident in 1991-1992 and 2000-2001 is absent in the 1981-1982 time period. A narrow (~50 km)

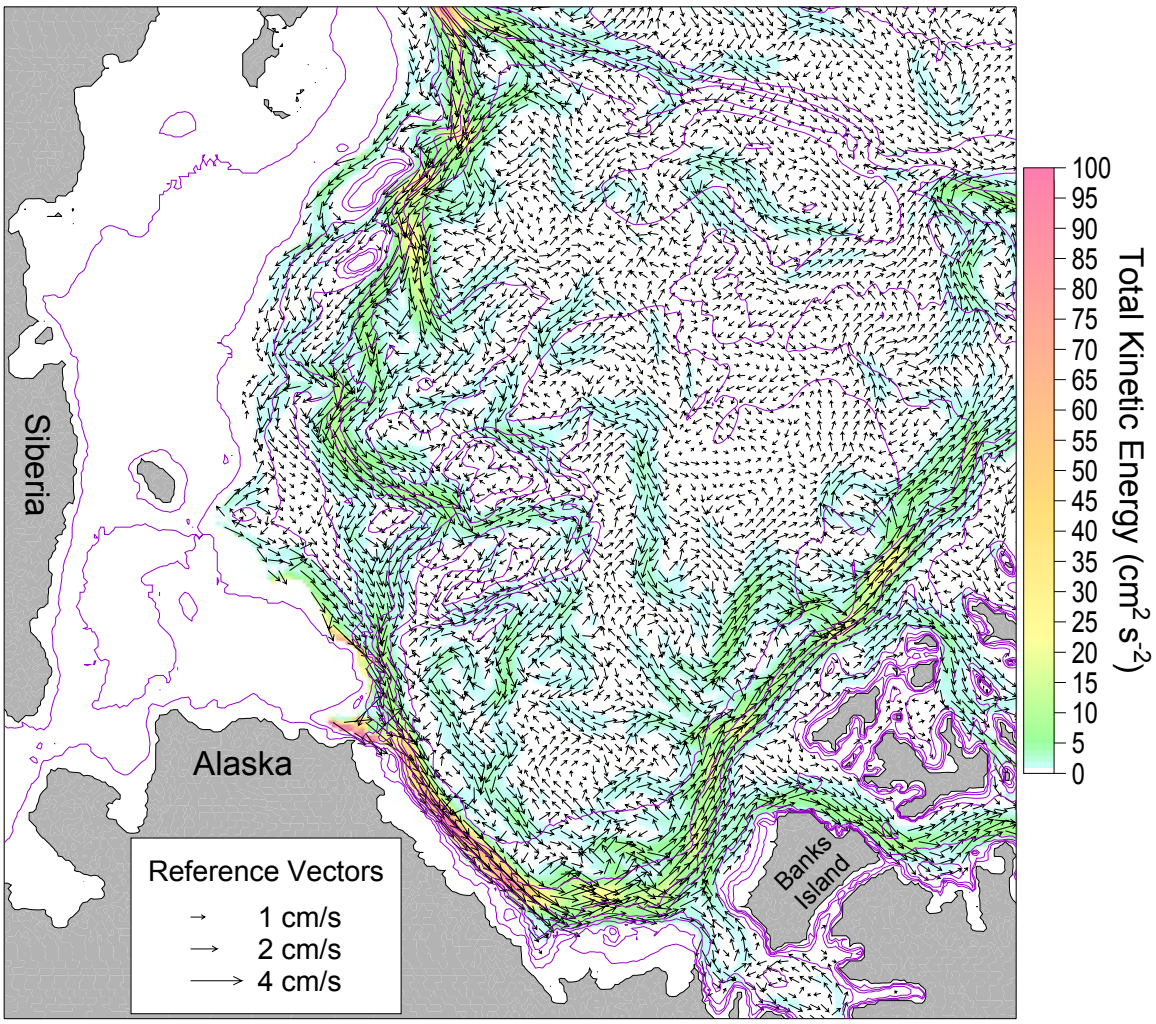

Figure 3.10 Vertically averaged velocity within the halocline layer (54-149m) averaged over 2000-2001. Every third vector in each direction is shown. Velocity vectors greater than 7cm/sec were truncated and the rest are shown using the square root function. Color shading represents total kinetic energy (cm^2/s^2) at every grid point. Total kinetic energy values between 0 and 1 cm^2/s^2 are not shaded.

organized countercurrent (~1-3 cm^2/s^2 TKE) roughly follows the 1000 m isobath in the 1981-1982 time period between two flows propagating towards the Alpha Ridge (Figure 3.8). A weak southwestward current is present in the 1991-1992-time period along the shelves and upper slopes of the CAA. In contrast to the 1981-1982 case a strong meandering northeastward flow (~ 30 cm^2/s^2 TKE) exists over depths greater that 500 m in the 1991-1992 time period (Figure

3.9). No countercurrent is present in the vicinity of the CAA in the 2000-2001 time-period (Figure 3.10). A strong northeastward boundary flow exceeding ~50 cm^2/s^2 TKE off the coast of Alaska, is present during the 2000-2001 time-period.

In addition to boundary flow other circulation features exist in the model-defined halocline layer at different time periods. A meandering northeastward flow from the Hanna Canyon, parallel to the Northwind Ridge across the Canada Basin interior to the Alpha Ridge is evident in the 1981-1982-time period. A similar flow regime, although less organized and exhibiting more meandering, exists in the 1991-1992 period but is absent in the 2000-2001-time period. The 1991-1992-time period is also characterized by a stronger, semi-cyclonic meandering flow across the entire western Arctic as compared to the other time periods.

Significant differences exist in the circulation patterns of the model-defined Atlantic layer among the three time periods (Figures 3.11 - 3.13). Circulation in the Atlantic layer is dominated by a cyclonic boundary current along the slope regions throughout the Canada Basin with much weaker and meandering flow in the basin interior. A distinct boundary current signature is maintained throughout the entire Canada Basin only during the 1991-1992-time period. This flow is particularly strong (TKE in excess of 80 cm^2/s^2) in the Makarov Basin approaching the Mendeleyev Ridge and along the slopes north of the CAA with frequent meanders. The boundary current is weaker and less organized in both the 1981-1982 and 2000-2001 time periods.

A boundary current signature is not evident in the Atlantic layer of the Beaufort Sea during the 1981-1982 time-period.

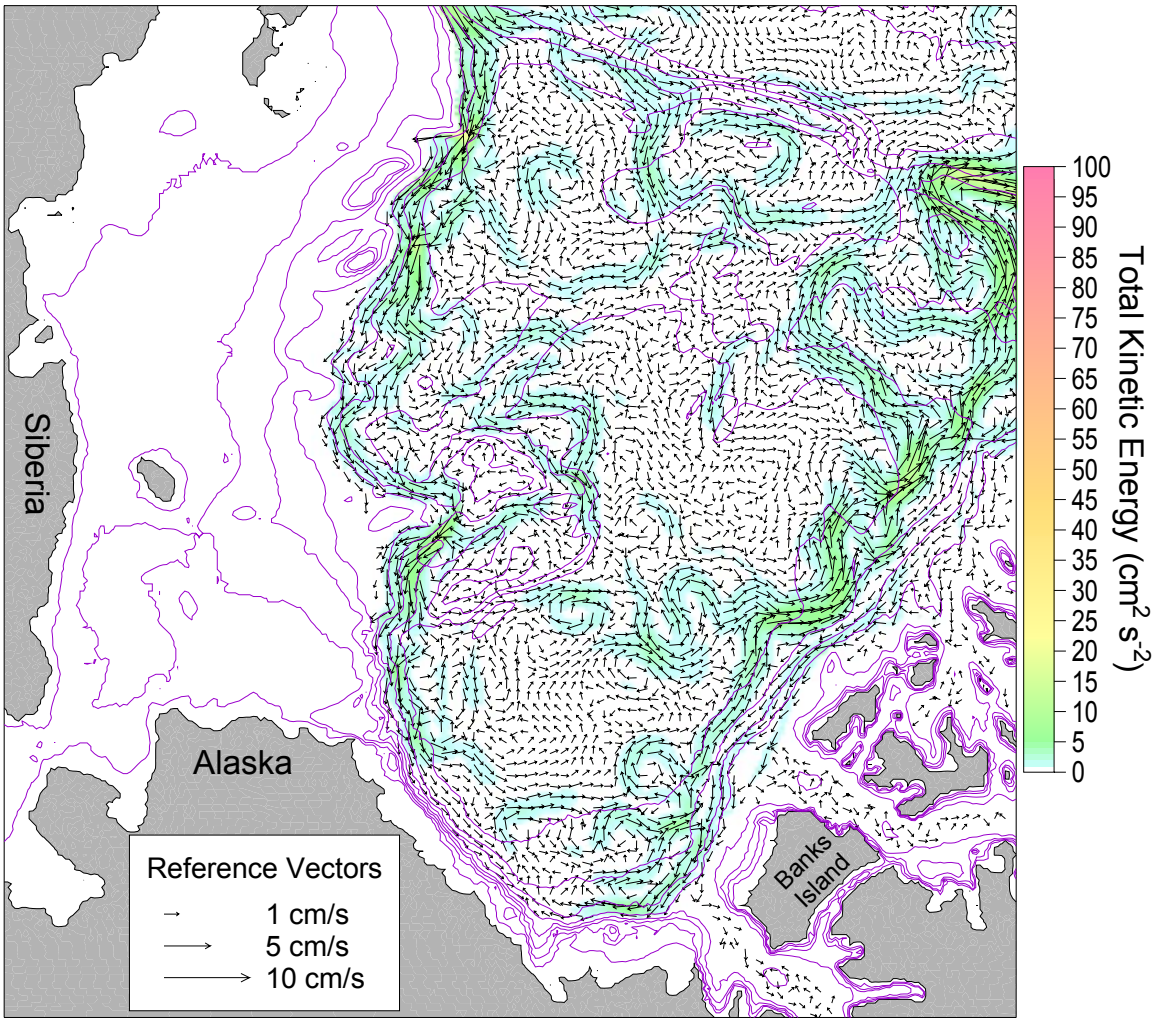

Figure 3.11 Vertically averaged velocity within the Atlantic layer (268-850m) for the period 1981-1982. Every third vector in each direction is shown. Color shading represents total kinetic energy (cm^2/s^2) at every grid point. Total kinetic energy values between 0 and 1 cm^2/s^2 are not shaded.

3. Inter-Decadal Variability

Differences between two-year means velocities in the upper ocean, halocline and Atlantic layer for years 1981-1982, 1991-1992 and 2000-2001 are plotted in Figures 3.14 through 3.22 respectively. Existence of organized difference vectors denotes disparities between the

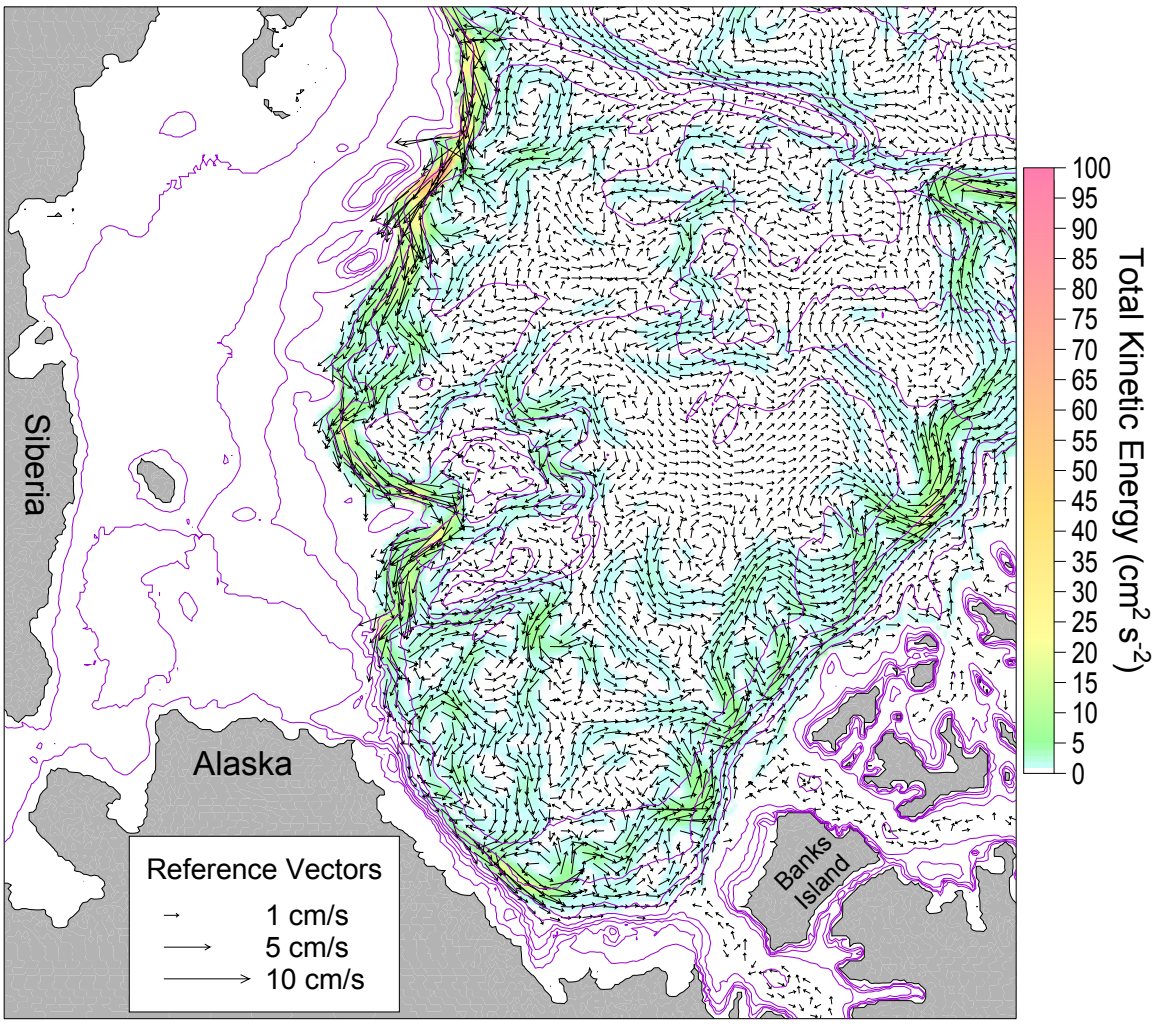

Figure 3.12 Vertically averaged velocity within the Atlantic layer (268-850m) for the period 1991-1992. Every third vector in each direction is shown. Color shading represents total kinetic energy (cm^2/s^2) at every grid point. Total kinetic energy values between 0 and 1 cm^2/s^2 are not shaded.

circulation of the two time periods compared. However, analysis of the two-year means (Figures 3.5 - 3.13) is required concurrently to determine the cause of velocity differences. The difference between the 1991-1992 and 1981-1982 upper ocean velocity means (Figure 3.14) is indicative of strong boundary flows observed in the 1991-1992 period where TKE exceeded 75 cm^2/s^2 in some areas (see Figure 3.6). This cyclonic pattern suggests that a stronger cyclonic flow along the slope regions off the

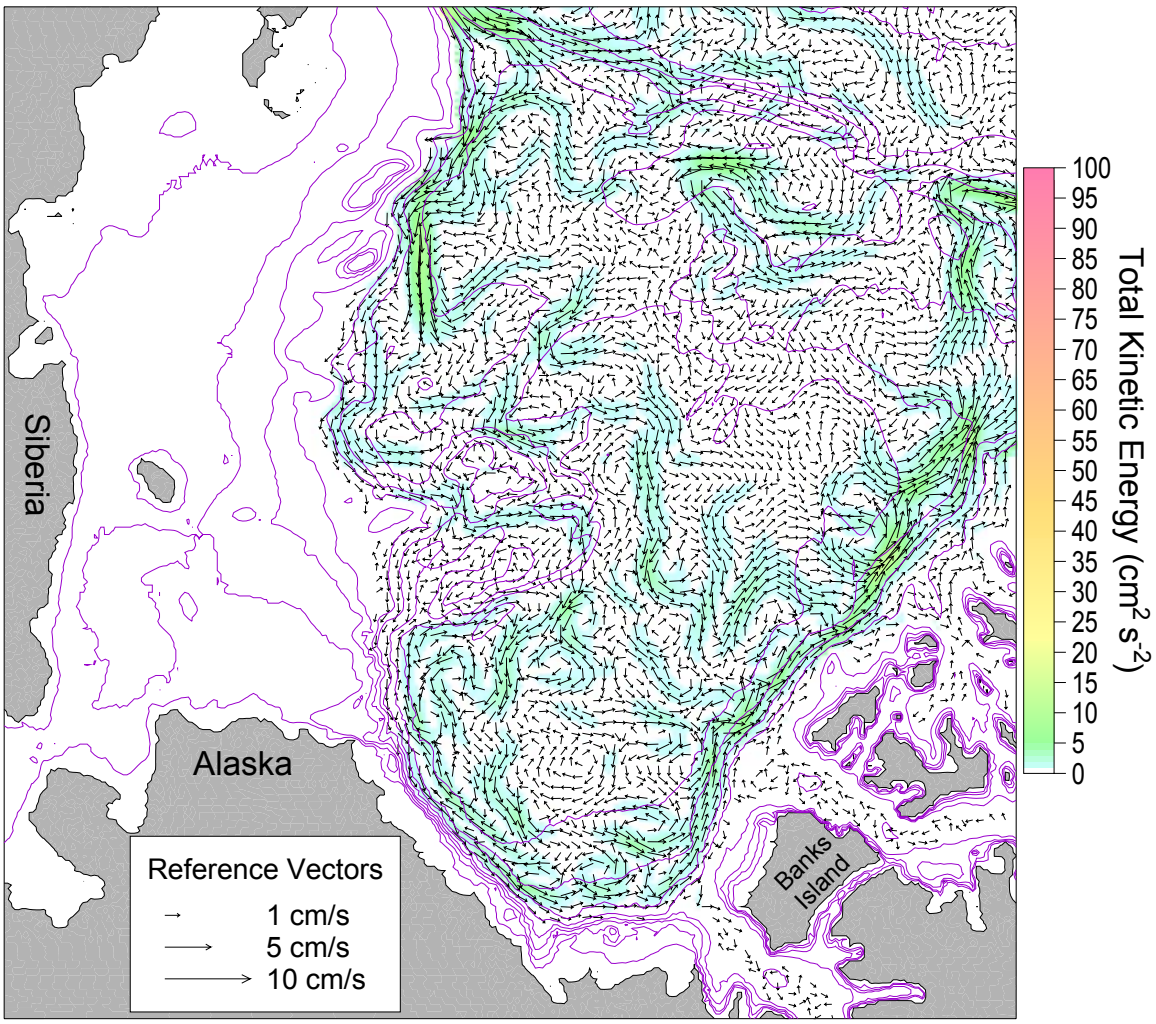

Figure 3.13 Vertically averaged velocity with the Atlantic layer (268-850m) for the period 2000-2001. Every third vector in each direction is shown. Color shading represents total kinetic energy (cm^2/s^2) at every grid point. Total kinetic energy values between 0 and 1 cm^2/s^2 are not indicated.

north Alaskan coast existed in the upper ocean in this region during the 1991-1992 period (see Figure 3.6) as compared to the 1981-1982 average (see Figure 3.5) or that the strength of the anticyclonic Beaufort Gyre was greater in 1981-1982 as compared to 1991-1992 or both.

Three areas of difference vectors oriented in a southeastward direction are noted in Figure 3.14. The first residing along the Siberian Coast from Wrangel Island to the Bering Strait, indicates that northwestward flow

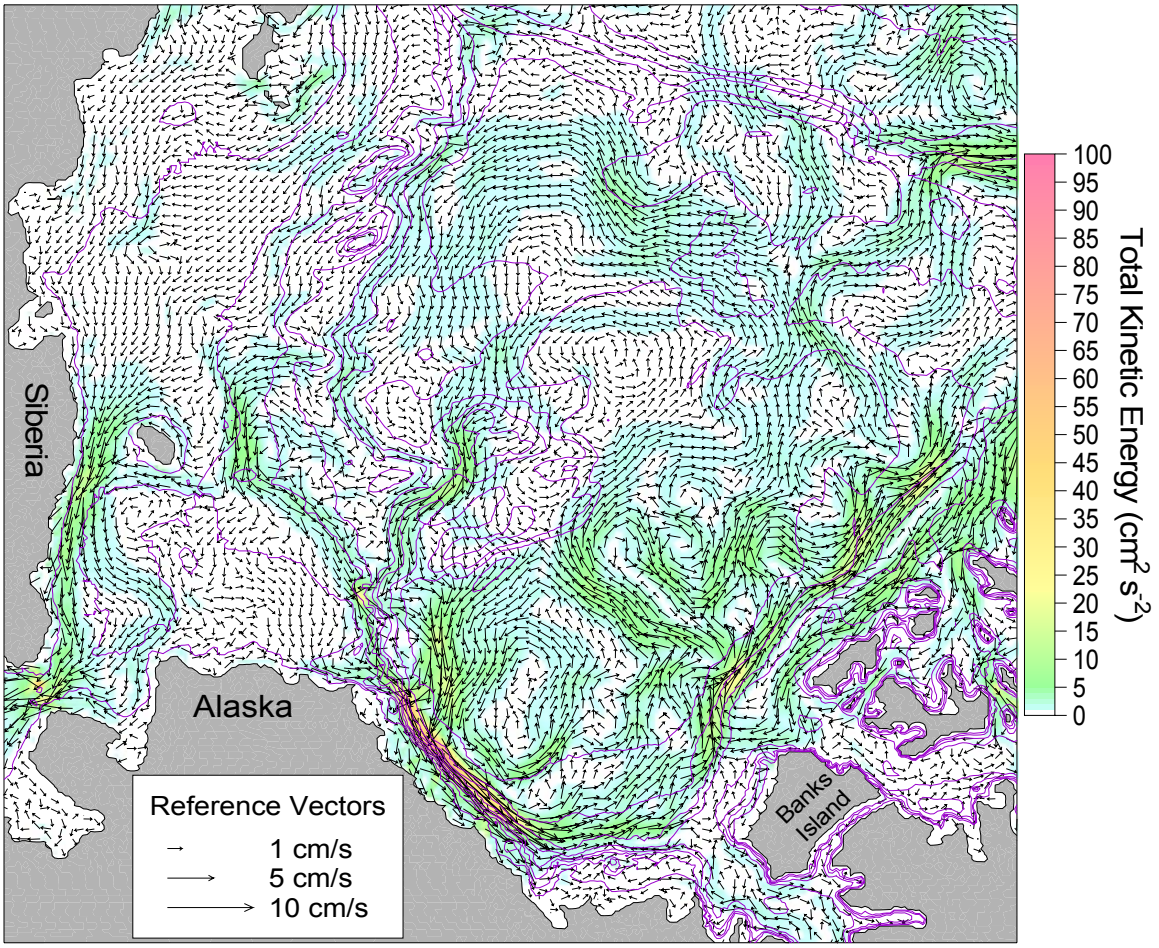

Figure 3.14 Decadal velocity difference between 1991-1992 and 1981-1982 in the upper ocean (0-26m). Every third vector in each direction is shown. Color shading represents total kinetic energy (cm^2/s^2) at every grid point. Total kinetic energy values between 0 and 1 cm^2/s^2 are not shaded.

along this branch of Pacific Water flowing from the Bering Strait to Wrangel Island was weaker, or opposite in 1991-1992 as compared to the 1981-1982 averaging period. The second area extends from north of Wrangel Island eastward to the north of Hanna Shoal with a minor branch along the Barrow Canyon. A third region from the Chukchi Abyssal Plain southeast to Hanna Canyon indicates eastward-directed flow. This suggests they were both stronger in the 1991-1992 time period as compared to the 1981-1982 time period.

Two parallel and oppositely oriented difference vectors present along the entrances of the CAA from the

Alpha Ridge to M'Clure Strait indicate complex changes of circulation between 1991-1992 and 1981-1982. The southwestward series of strong difference vectors (~25 $cm^2/^2$) immediately adjacent to the entrances to the CAA indicate southwestward flow here in the 1991-1992 time period as compared to northeastward flow during the 1981-1982 time period. The second series of difference vectors is seaward and parallel but oriented northeastward which indicates that there was boundary flow in 1991-1992 as compared to a weaker but southwestward flow here in the upper ocean in 1981-1982.

Larger northward vectors in the Bering Strait indicate Pacific water inflow through the Bering Strait was stronger during the 2000-2001 time period compared to 1991-1992 (Figure 3.15). Similarly, westward vectors along the Siberian Coast west from the Bering Strait to Wrangel Island indicate stronger flow in this direction during 2000-2001 than during 1991-1992. An organized series of difference vectors along the slope from the Beaufort Sea into the Chukchi Sea and the Northwind Abyssal Plain, as well as along the slope region in the Makarov Basin, illustrate stronger cyclonic boundary flow in the upper ocean along these regions in the 1991-1992 time period as compared to 2000-2001. The southeastward oriented difference vectors originating from the Canada Basin interior to the northeast flank of the Chukchi Plateau implies that a stronger northwestward current flowed from the slope into the Canada Basin interior in 2000-2001 in this region as compared to the 1991-1992 period. A region of difference vectors from the Beaufort Sea northeast to

the Alpha Ridge indicates unorganized but relatively strong changes between the 2000-2001 and 1991-1992 time periods.

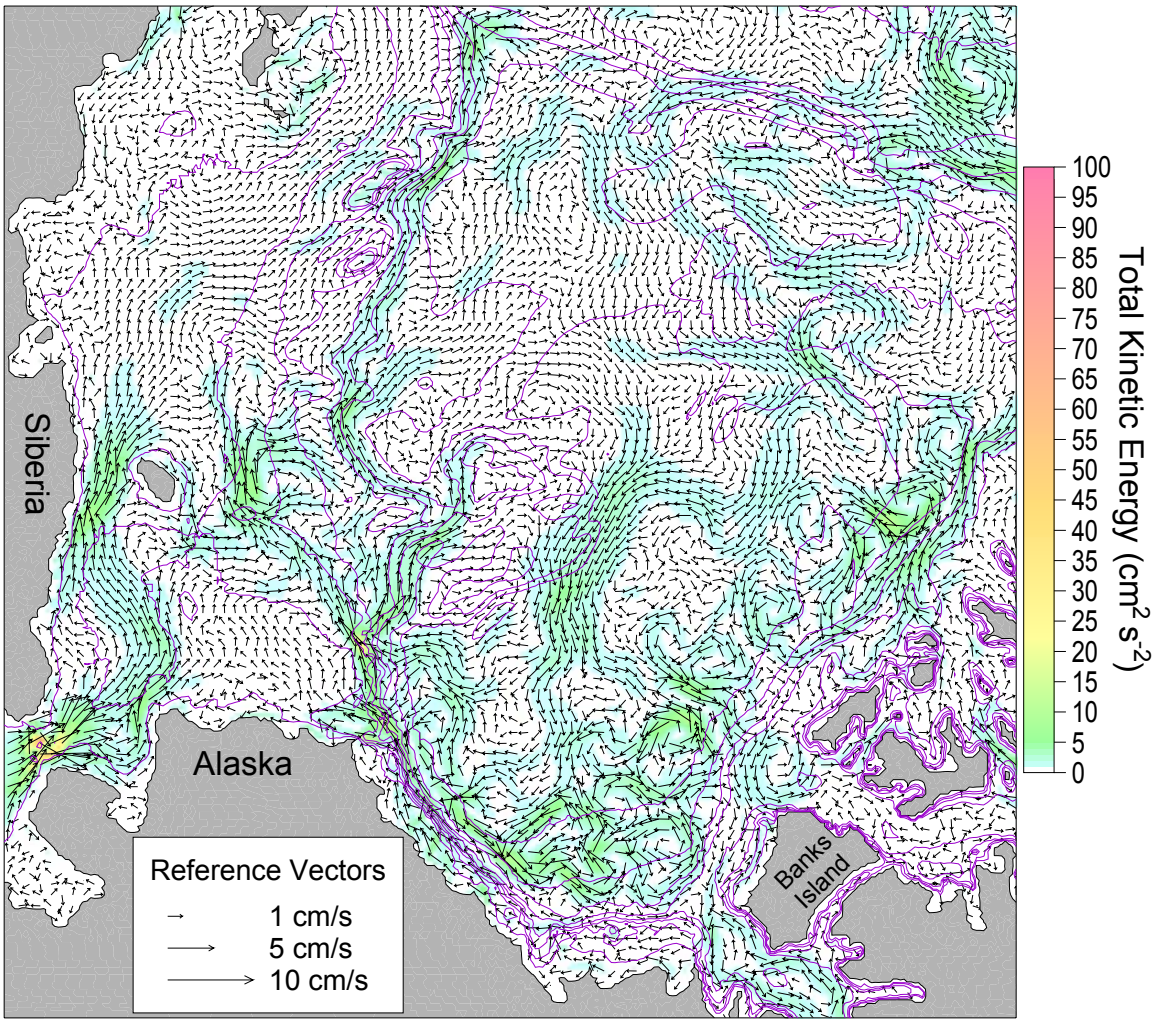

Figure 3.15 Decadal velocity difference between 2000-2001 and 1991-1992 in the upper ocean (0-26m). Every third vector in each direction is shown. Color shading represents total kinetic energy (cm^2/s^2) at every grid point. Total kinetic energy values between 0 and 1 cm^2/s^2 are not shaded.

Inspection of the 2000-2001 and 1981-1982 difference figure in the upper ocean reveals a distinct cyclonic organization of difference vectors in the Beaufort Sea region (Figure 3.16). This difference implies that the strength of the cyclonic boundary flow along the shelf break of the western Arctic was greater during the 2000-

2001 period as compared to the 1981-1982 period or that the anticyclonic Beaufort Gyre was stronger in 1981-1982 as compared to 2000-2001. Organization of difference vectors along the shelves and slopes to the north of the CAA between the Amundsen Gulf and the Alpha Ridge (Figure 3.16) is similar to the 1991-1992 and 1981-1982 mean difference figure (see Figure 3.14) in this region. Relatively few weak differences exist in the rest of the Canada Basin to the west of the Northwind Ridge between 2000-2001 and 1981-1982.

Velocity differences between the two-year periods of 1991-1992 and 1981-1982, 2000-2001 and 1991-1992 as well as 2000-2001 and 1981-1982 in the model defined halocline depth region are presented in Figures 3.17 - 3.19. Most differences between two-year averages are concentrated along the boundary current and in the Beaufort Gyre. Cyclonically oriented difference vectors are organized along the slope regions of the entire western Arctic and Beaufort Gyre in the halocline level of the 1991-1992 and 1981-1982 difference plot (Figure 3.17). As was the case of the upper ocean, this indicates that the strength of the cyclonic boundary current was greater in 1991-1992 as compared to 1981-1982 or that the strength of the anticyclonic Beaufort Gyre was less during the 1991-1992 period as compared to the 1981-1982 average in the halocline layer. A number of relatively strong meanders of order of 200 km are present in the Canada Basin interior between the northern Northwind Ridge and the Alpha Ridge.

A generally anticyclonic sense of changes along the boundary current and the Beaufort Sea between the 2000-2001

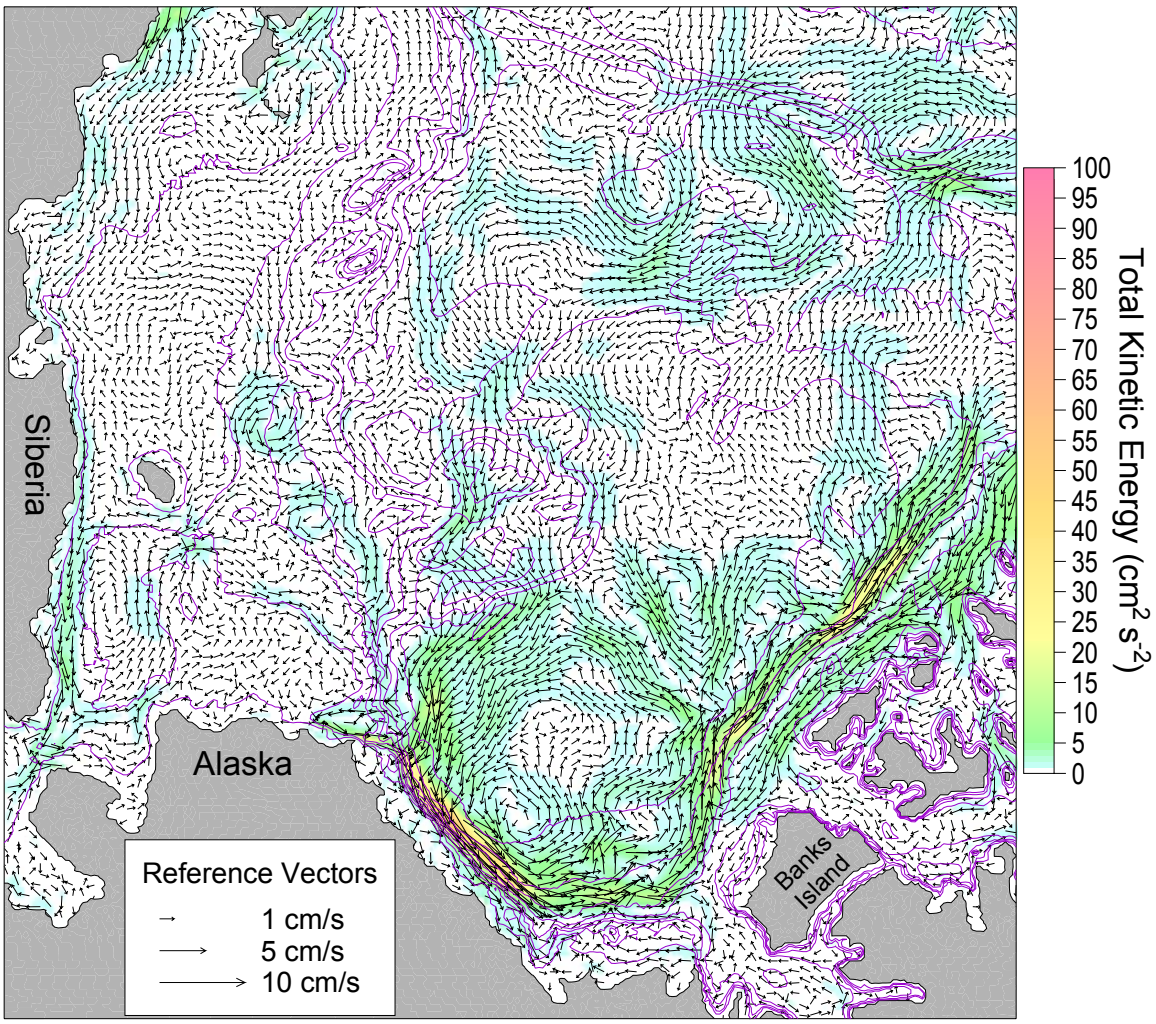

Figure 3.16 Decadal velocity difference between 2000-2001 and 1981-1982 in the upper ocean (0-26m). Every third vector in each direction is shown. Color shading represents total kinetic energy (cm^2/s^2) at every grid point. Total kinetic energy values between 0 and 1 cm^2/s^2 are not shaded.

and 1991-1992 time periods is in contrast to the differences between 1991-1992 and 1981-1982 (Figure 3.18). Weakly organized velocity vectors oriented in the northwestward direction along the slope from Hanna Canyon to the junction of the Lomonosov Ridge and Eurasian continent are consistent with other indications that cyclonic boundary flow was stronger in the 1991-1992-time

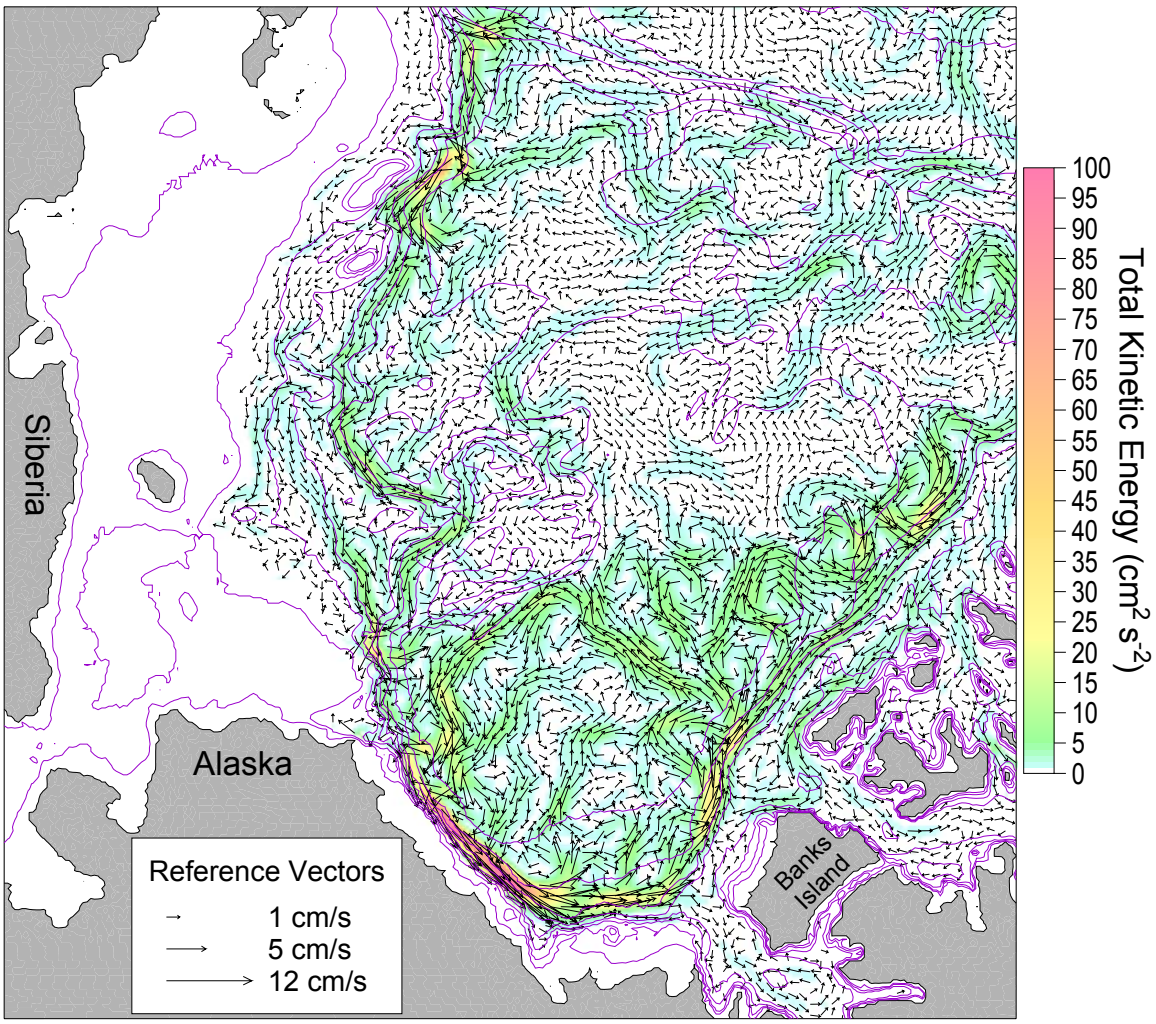

Figure 3.17 Decadal velocity difference between 1991-1992 and 1981-1982 in the halocline (54-149m). Every third vector in each direction is shown. Color shading represents total kinetic energy (cm^2/s^2) at every grid point. Total kinetic energy values between 0 and 1 cm^2/s^2 are not shaded.

period than during the 2000-2001 time period. A concentration of eddy-like features from the Beaufort Sea to Alpha Ridge suggests that this region of the halocline is energetic and highly variable.

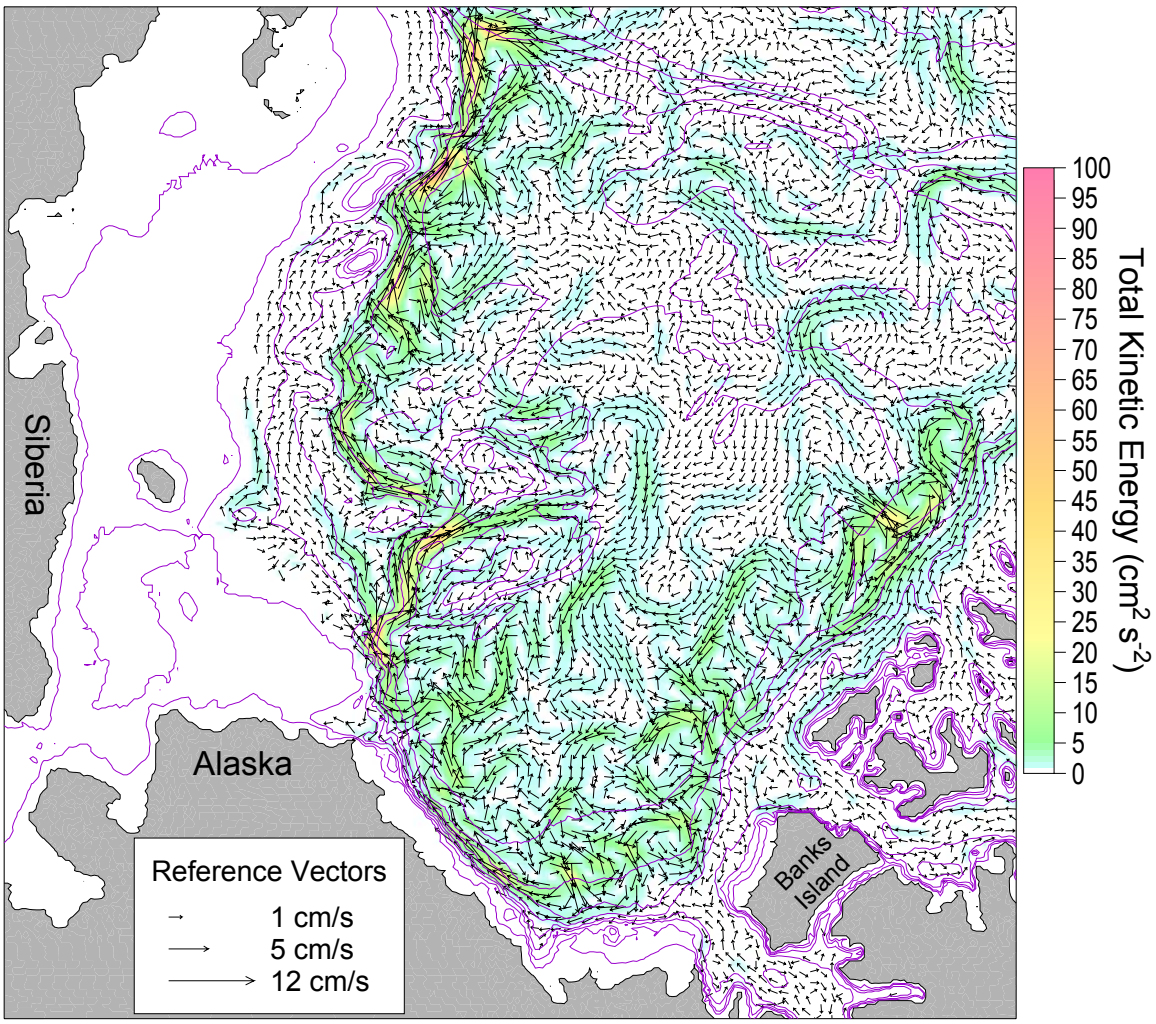

Figure 3.18 Decadal velocity difference between 2000-2001 and 1991-1992 in the halocline (54-149m). Every third vector in each direction is shown. Color shading represents total kinetic energy (cm^2/s^2) at every grid point. Total kinetic energy values between 0 and 1 cm^2/s^2 are not shaded.

Differences between 2000-2001 and 1981-1982 velocity means within the halocline are dominated by a series of cyclonically oriented difference vectors in the Beaufort Gyre region. These differences indicate that the strength of the anticyclonic Beaufort Gyre was higher in the 1981-1982-time period as compared to 2000-2001 or that the strength of the eastward boundary flow along the north slope of Alaska was greater in 2000-2001 as compared to the 1981-1982-time period, or both (Figure 3.19).

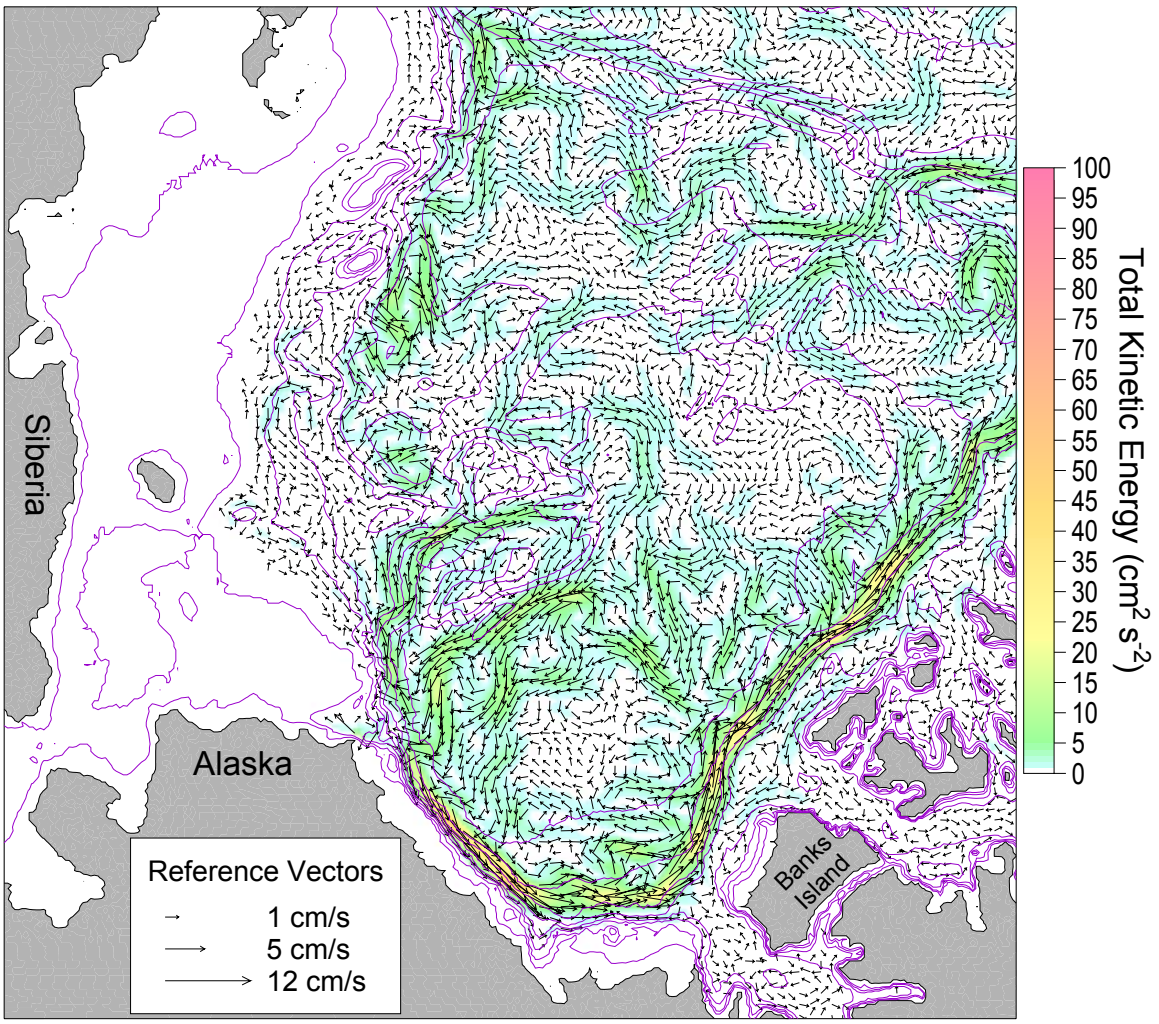

Figure 3.19 Decadal velocity difference between 2000-2001 and 1981-1982 in the halocline (54-149m). Every third vector in each direction is shown. Color shading represents total kinetic energy (cm^2/s^2) at every grid point. Total kinetic energy values between 0 and 1 cm^2/s^2 are not shaded.

A well-organized series of northeastward oriented difference vectors along the slope region extending from the Beaufort Sea past the entrances to the CAA and toward the Alpha Ridge indicates that the boundary flow along the slope region was stronger during 2000-2001 than 1981-1982. An organized series of southward oriented difference vectors along the Northwind Ridge exists. A review of the two-year mean currents in this region of the Northwind Ridge indicate that a northward flow along this region

existed during both these time periods but was much stronger during the 1981-1982 time period than during the 2000-2001 time period (see Figures 3.8 and 3.10). A region of northward flow from the Hanna Canyon into the Chukchi Plateau across the Northwind Abyssal Plain is indicative of the oppositely oriented flow that existed along this region during both time periods. Finally, difference vectors in the Makarov Basin indicate variable circulation in this region between these two time periods.

Analysis of velocity difference vectors in the Atlantic layer between 1991-1992 and 1981-1982 shows most variability is concentrated in the slope regions and in the Beaufort Sea towards the Alpha Ridge (Figure 3.20). Velocity difference vectors between these two time periods in the Atlantic layer indicate a weak cyclonic organization. This pattern is consistent with those at shallower depths indicating that boundary current flow along the slope regions was stronger in the Atlantic layer during the 1991-1992 than the 1981-1982 period.

Analysis of the mean velocity difference between the 2000-2001 and 1991-1992 time periods in the Atlantic layer again presents a pattern consistent with the upper layers (Figure 3.21). Prominent difference vectors are generally concentrated in the slope regions however there are fewer of them along the North Slope of Alaska and the Beaufort Sea. A distinct northwestward oriented series of difference vectors exists from the Chukchi Plateau to the Lomonosov ridge indicating the increased strength of the southeastward and eastward boundary current in the 1991-1992 period as compared to the 2000-2001 period. A

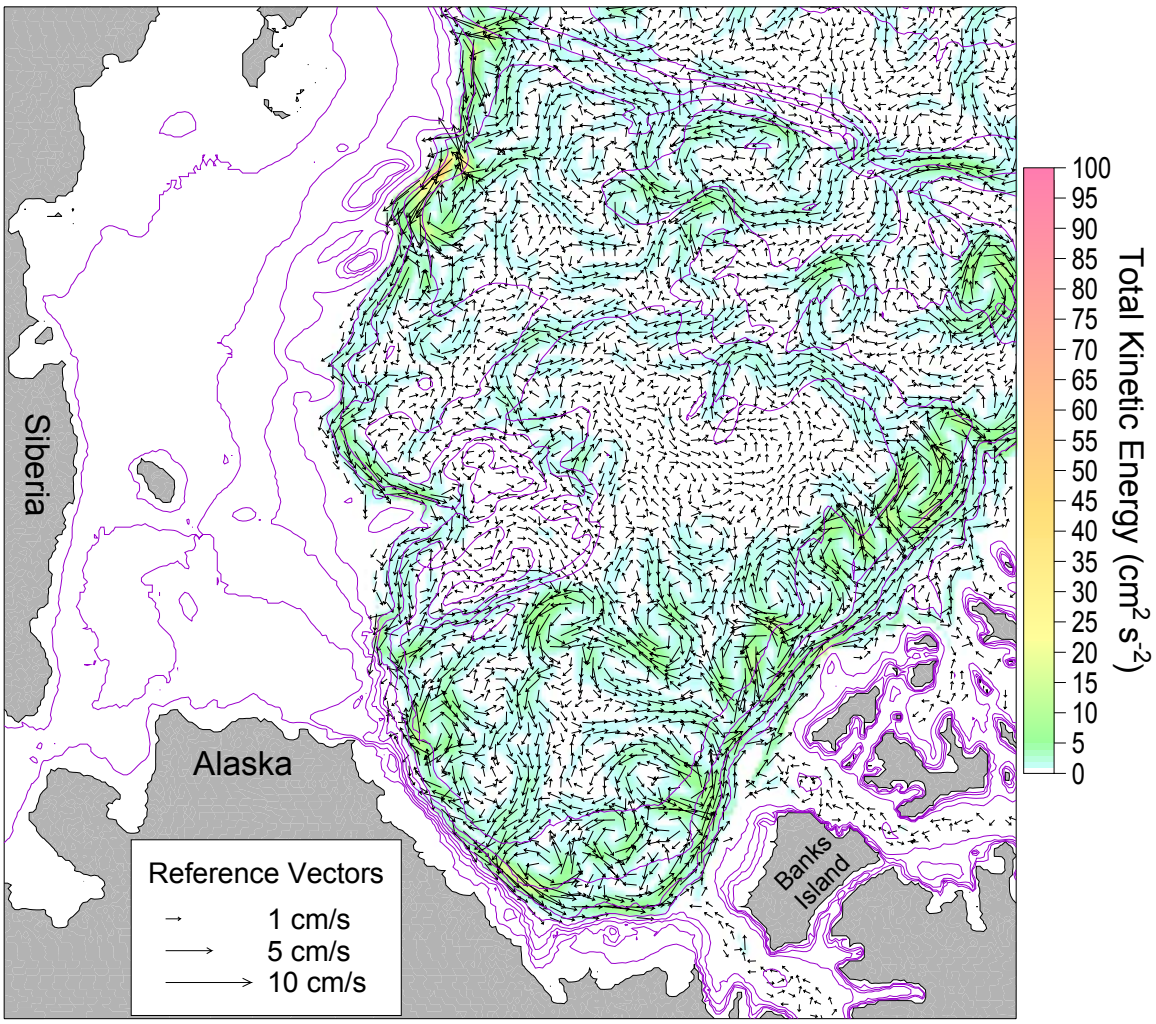

Figure 3.20 Decadal velocity difference between 1991-1992 and 1981-1982 in the Atlantic layer 268-850m). Every third vector in each direction is shown. Color shading represents total kinetic energy (cm^2/s^2) at every grid point. Total kinetic energy values between 0 and 1 cm^2/s^2 are not shaded.

narrow series of northward oriented difference vectors across the Northwind Abyssal Plain is indicative of flow in the opposite direction in this region during the 1991-1992-time period as compared to the 2000-2001-time period. A region of eddy-like patterns between the southern Beaufort Sea and the Alpha Ridge has replaced more organized difference along the boundary current here. Similar features exist east of the Northwind Ridge.

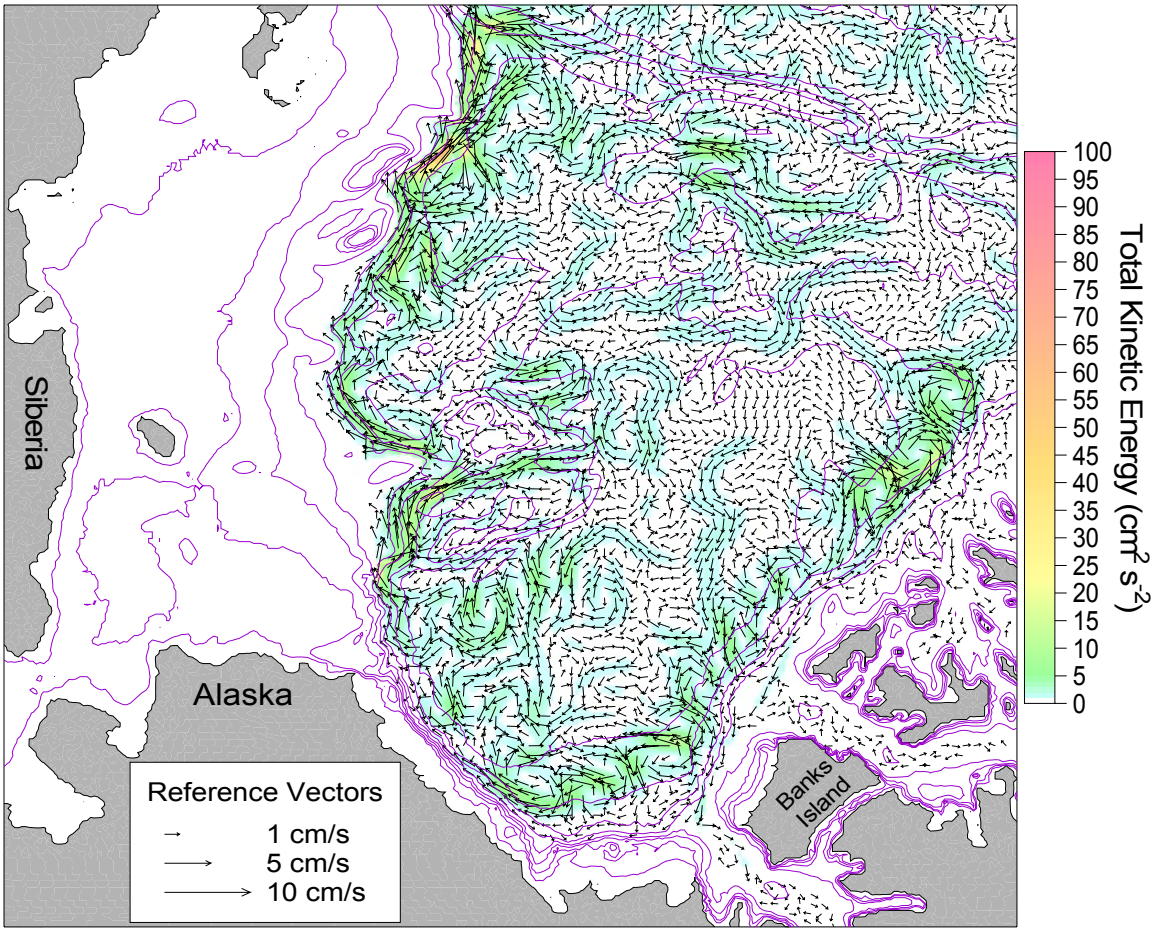

Figure 3.21 Decadal velocity difference between 2000-2001 and 1991-1992 in the Atlantic layer 268-850m). Every third vector in each direction is shown. Color shading represents total kinetic energy (cm^2/s^2) at every grid point. Total kinetic energy values between 0 and 1 cm^2/s^2 are not shaded.

The mean velocity differences between 2000-2001 and 1981-1982 are dispersed throughout the Canada Basin. A stronger organized section is concentrated in the southeastern Canada Basin and along the slopes adjacent to the entrances to the CAA (Figure 3.22). Differences exceed 25 cm^2/s^2 in this region. Unlike velocity differences between other time periods mostly eddy-like features are evident along the slope regions in the Makarov Basin. A narrow organized flow of difference vectors from the slope region off the Alaskan slope into the Northwind Abyssal Plain indicates that the flow along this pathway was

stronger in the 1981-1982-time period as compared to the 2000-2001-time period. A series of northeastward-oriented difference vectors flow along the slope from the Beaufort Sea to the Alpha Ridge indicate that the strength of the boundary current flow along the slope was greater during the 2000-2001 time period. A series of meanders or eddies in the Beaufort Sea indicates strong but unorganized variability that exists in this portion of the Atlantic layer.

B. CHUKCHI PLATEAU AND ADJACENT REGIONS

1. Volume Transport

The twenty-three (1979-2001) year mean depth-averaged velocity field (Figure 3.23) was computed to help determine cross-section locations in the model domain that would intersect the principal paths of property transport (see Figure 2.5). Velocity fields depicted in Figure 3.23 provide a qualitative indication that the majority of the boundary current flow crosses the Chukchi Plateau via the Chukchi Borderland Pass and Northwind Abyssal Plain.

Mean volume transports across selected sections in the Chukchi Plateau region (Figure 3.24) were computed from the vertical area integrals of the twenty-three year mean velocities normal to each section. Net, positive and negative volume transports were computed for three depth ranges: the entire water column, the Atlantic layer (268-850m), and the upper layer (0-220m). These transports are summarized in Tables 3.1, 3.2 and 3.3 respectively. Most analyses of circulation and volume transport will focus on the entire water column (Table 3.1). In the following

discussion, the arrows in Figures 3.24, 3.26 and 3.27 indicate the positive direction with respect to the sections.

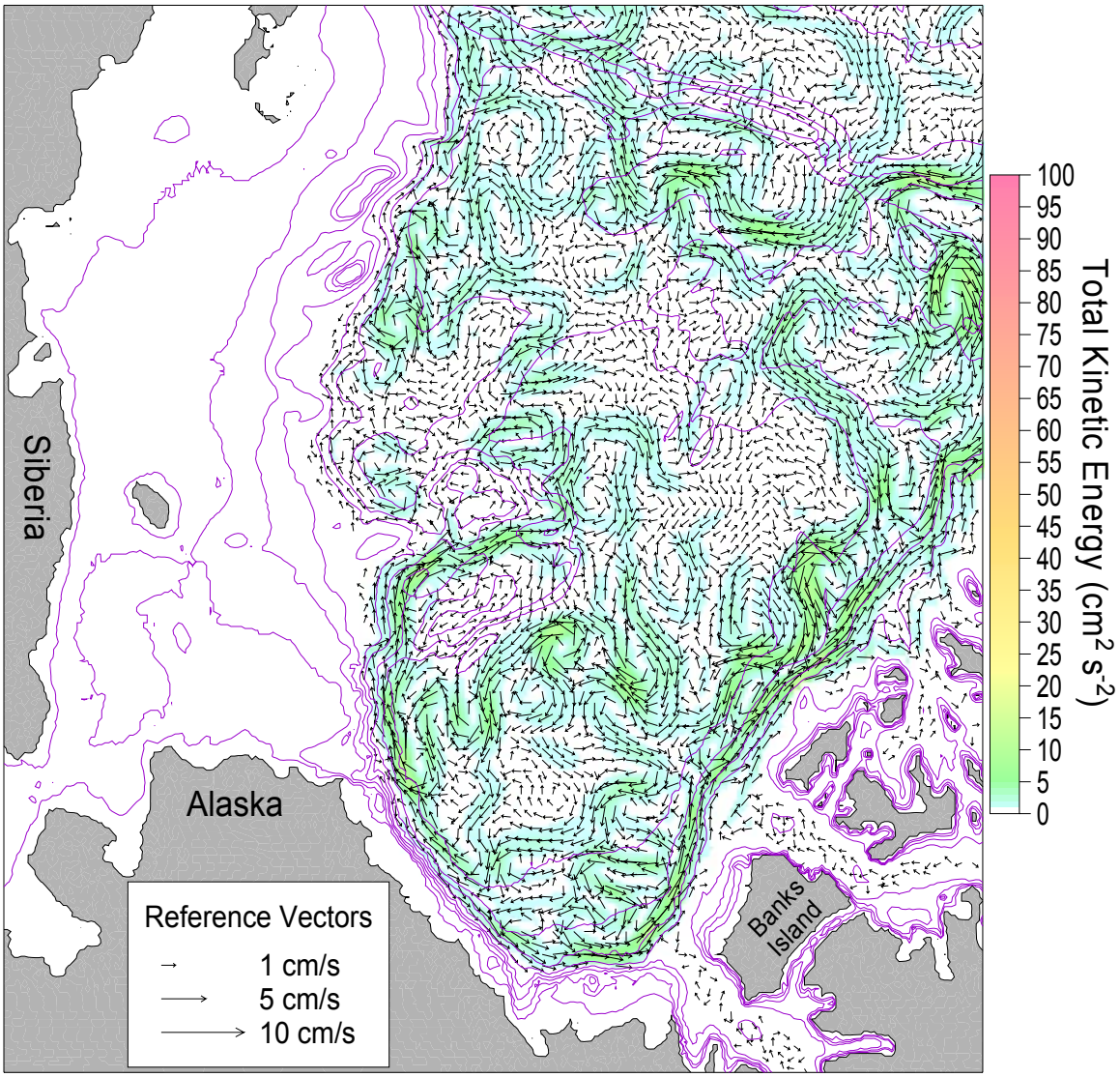

Figure 3.22 Decadal velocity difference between 2000-2001 and 1981-1982 in the Atlantic layer (268-850m). Every third vector is shown. Color shading represents total kinetic energy (cm^2/s^2) at every grid point. Total kinetic energy values between 0 and 1 cm^2/s^2 are not indicated.

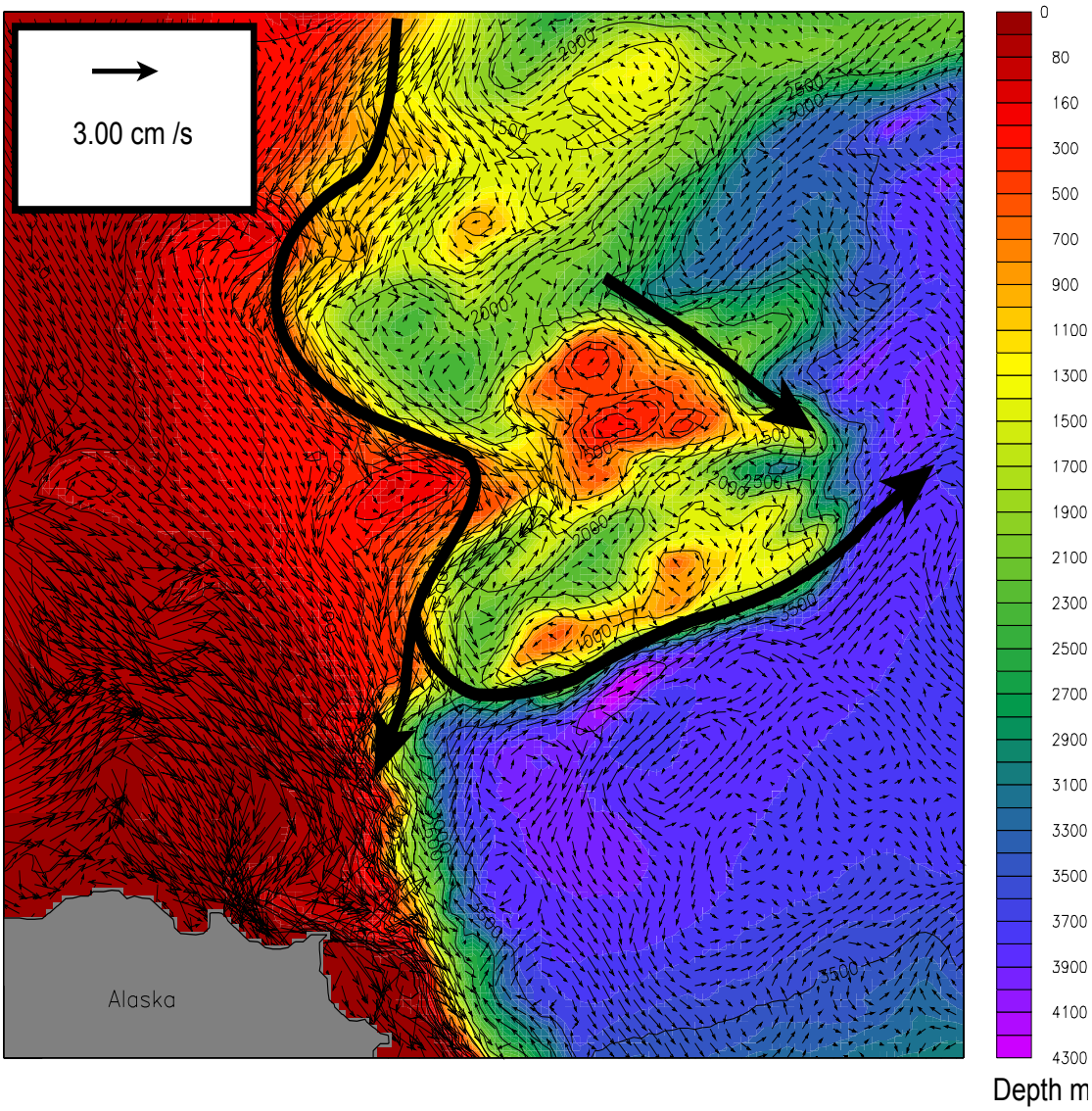

Figure 3.23 Twenty-three year mean, depth-averaged velocity fields. Every third vector is shown. Velocity vectors greater than 7 cm/s were truncated and the rest are shown using the square root function. The thick arrow is highlighting the prevalent pathway of the boundary flow through the Chukchi Borderland Pass and parallel to the Northwind Ridge.

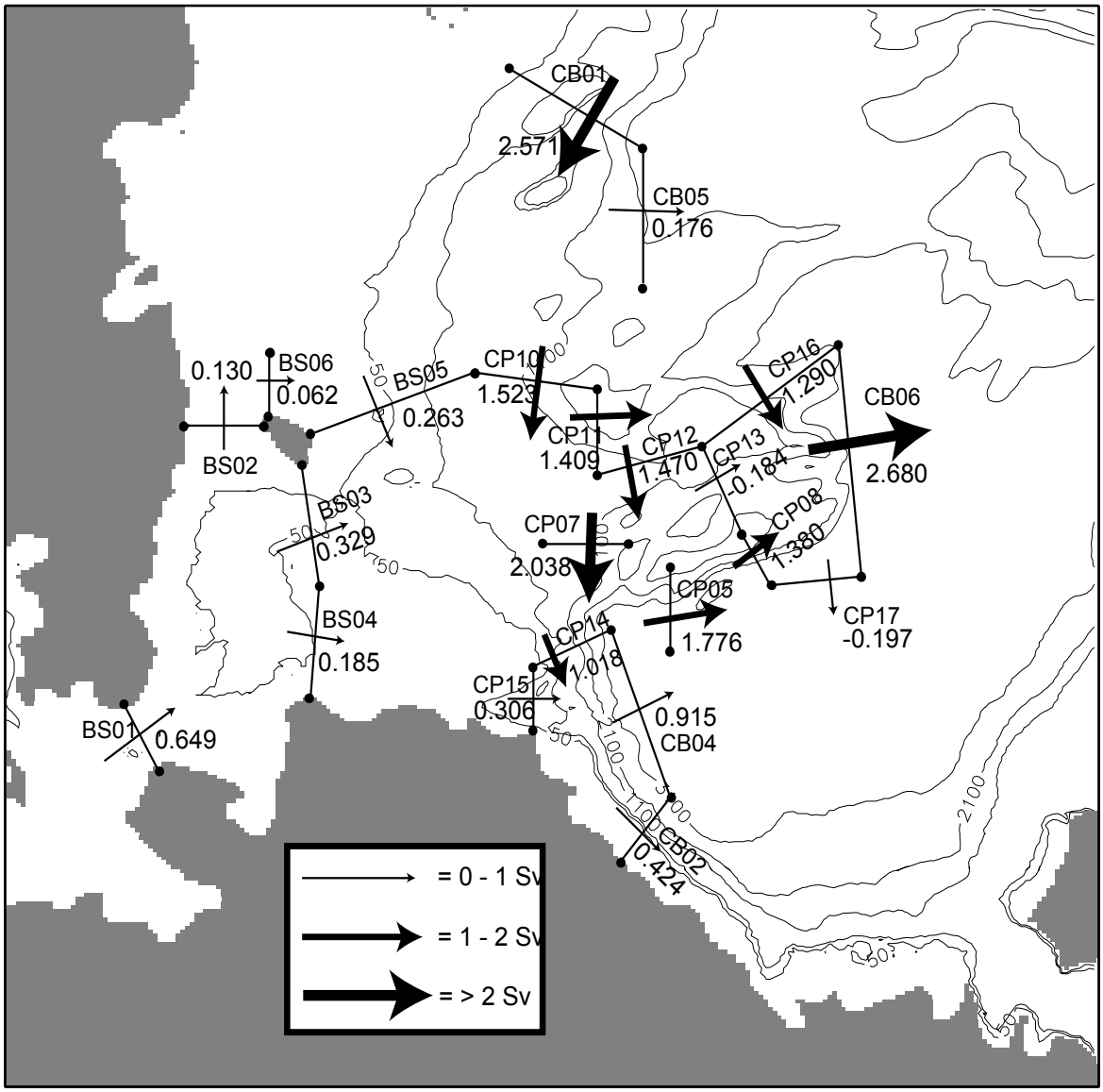

Figure 3.24 Twenty-three year (1979-2001) net mean volume transports (Sv) through the water column across sections established in the western Arctic calculated using monthly means averaged over a twenty-three year mean from 1979-2001. Arrows point in the direction of net positive flow.

Section	Net Vol	Vol Pos	Vol Neg	NetHeat	Heat Pos	Heat Neg	FW Net	FW Pos	FW Neg
CB01	2.571	2.991	-0.420	3.575	4.086	-0.511	11.675	11.260	0.415
CB02	0.424	1.258	-0.835	-2.429	-1.680	-0.749	41.472	39.988	1.483
CB04	0.915	4.095	-3.180	-0.725	2.792	-3.517	21.408	22.388	-0.980
CB05	0.176	1.485	-1.309	0.346	2.689	-2.342	0.542	-1.199	1.741
CB06	2.680	4.341	-1.661	-1.245	0.344	-1.589	5.591	-0.337	5.928
CP05	1.776	2.230	-0.454	0.926	1.550	-0.624	1.752	1.734	0.019
CP07	2.038	2.095	-0.057	2.332	2.382	-0.050	9.052	9.877	-0.824
CP08	1.380	1.847	-0.467	-0.717	-0.109	-0.608	2.115	1.283	0.832
CP10	1.523	2.129	-0.606	1.858	2.771	-0.913	7.762	8.122	-0.360
CP11	1.409	1.795	-0.386	1.969	2.487	-0.518	6.074	5.582	0.491
CP12	1.470	1.516	-0.047	2.012	1.928	0.084	4.417	6.620	-2.203
CP13	-0.184	0.420	-0.604	-0.868	0.407	-1.275	5.469	4.949	0.520
CP14	1.018	1.668	-0.650	-1.513	-0.885	-0.628	32.858	32.568	0.292
CP15	0.306	0.354	-0.048	-1.465	-1.729	0.264	25.137	28.918	-3.781
CP16	1.290	1.975	-0.684	2.758	3.318	-0.560	-2.883	-1.397	-1.486
CP17	-0.197	1.994	-2.191	2.349	1.572	0.776	-1.363	-3.812	2.449
BS01	0.649	0.725	-0.076	-0.330	-0.102	-0.228	45.092	50.584	-5.492
BS02	0.130	0.136	-0.006	-0.716	-0.742	0.027	10.384	11.112	-0.727
BS03	0.329	0.345	-0.016	-1.674	-1.742	0.067	23.607	25.019	-1.412
BS04	0.185	0.225	-0.040	0.130	0.196	-0.067	14.930	18.333	-3.402
BS05	0.263	0.288	-0.025	-1.161	-1.247	0.085	16.844	18.315	-1.471
BS06	0.062	0.066	-0.003	-0.331	-0.348	0.017	4.865	5.277	-0.412

Table 3.1 Twenty-three year mean volume transport (Sv), heat flux (TW) and freshwater flux (10^3 m^3/s) across defined cross sections for the full water column. Temperature is referenced to -0.1°C and salinity is referenced to 34.70 ppt. Positive values are in accordance with directions indicated in Figure 3.25.

An average of 2.991 Sverdrup (Sv) of water enters the study region from the Makarov Basin along the slope across section CB01 with an average 0.420 Sv in the opposite direction for a net southwestward transport flow of 2.571 Sv (Figure 3.24). A twenty-three year net mean volume transport of 0.176 Sv flows northward across section CB05 into the Makarov basin interior. Although the net northward transport is comparatively small it results from large opposite transports of 1.485 Sv to the north in the Makarov Basin and 1.309 Sv in the opposite direction. The majority of the volume that passes across section CB01 continues along the slope with net 1.523 Sv entering the Chukchi Plateau region across section CP10. After passing section CP10 the flow turns northeast and follows

topography with a net 1.409 Sv crossing section CP11. The main structure of the flow continues along the slope, turns immediately eastward and passes through the Chukchi Borderland Pass with 1.470 Sv flowing across section CP12.

The correlation coefficients of volume transport between cross section pairs CB01 and CP10, CB01 and CP11, and pair CP10 and CP11 are 0.637(24), 0.635(24) and 0.998(0) respectively. Correlations between volume transports across selected section pairs were conducted by comparing the twenty-three year time series of monthly means of each cross section. Values in parentheses that follow each correlation are the lag value associated with that correlation. Application of a thirteen-month low pass filter to the transports between these cross-section pairs increases correlations to 0.806(23), 0.807(23) and 0.998(0) respectively. This suggests that some additional volume exchange not accounted for in section CB01 contributes to the volume transport through the section CP10 and CP11. Correlation of cross section CP10 or CP11 with CP12 throughout the full water column are less at 0.551(0) and 0.530(0) respectively. A countercurrent is present in this region as shown in Figure 3.25. It is possible that this counter current and variability that it imposes is a factor contributing to the reduced correlation between cross sections CP10 or CP11 with CP12.

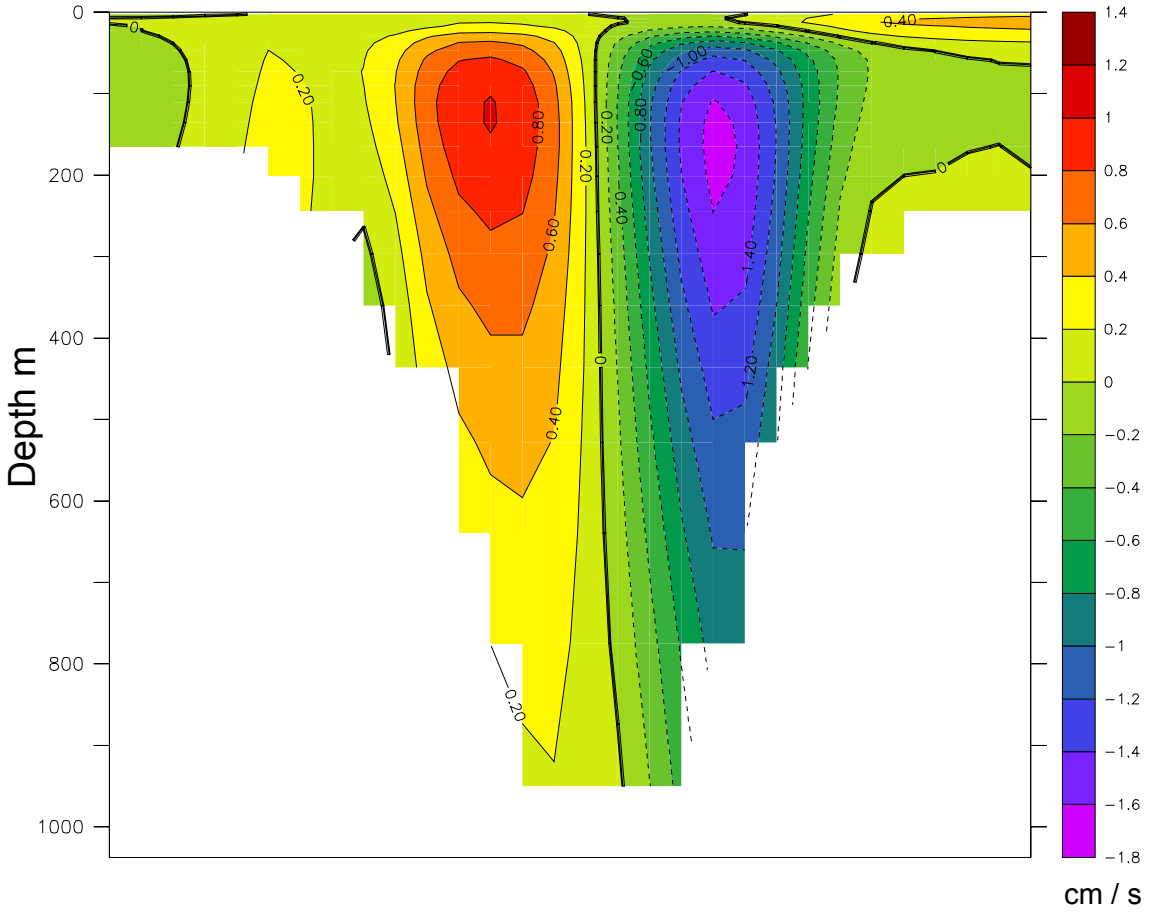

Figure 3.25 Twenty-three year mean velocity through section CP12. The intersection with cross section CP11 is on the left. Positive (negative) velocities are directed to the east (west).

After passing through section CP12 the majority of flow continues along the slope, centered roughly over the 1100 m isobath, and passes across the Northwind Abyssal Plain towards Hanna Canyon and section CP07. A net 2.038 Sv crosses section CP07 in the eastward direction. Correlations of volume transport across section CP07 with transports across sections immediately upstream yield correlation coefficients that are less than those associated with some upstream adjacent pairs. Correlation of cross sections CP11 and CP12 with cross section CP07 yield correlation coefficients of -0.599(-103), and 0.483(35) respectively. It is suspected that shelf and

upper slope waters from cross sections BS05, CP10 and CP12 contribute to volume transport across section CP07. After passing through cross section CP07 a portion of the flow continues through cross sections CP14 and CB02 with net transports of 1.018 Sv and 0.424 Sv, respectively. Past section CP07 a net northward flow of 1.776 Sv crosses section CP05 following the eastern flank of the Northwind Ridge CP05.

In addition to boundary flow that enters the Chukchi Plateau region across section CP10 a net eastward 1.290 Sv of water follows the northern end of the Chukchi Plateau across section CP16. The northern Chukchi Plateau region bounded by cross sections CP16, CB06, CP17, CP08 and CP13 receives a net 1.380 Sv and 0.197 Sv across sections CP08 and CP17, respectively. Transport out of this area includes a net 0.184 Sv southeastward across section CP13 and a net 2.680 Sv northward into the basin interior across section CB06.

The second largest source of water into the Canada Basin, in addition to Atlantic water from the northwest, is Pacific water. It enters the study region through the Bering Strait across section BS01 with a net transport of 0.649 Sv. This is in rough agreement with the estimate of an average 0.83 Sv obtained by observations from 1990-1994 by Roach et al. (1995). Pacific water inflow breaks into three general branches roughly flowing across sections BS03 and BS04 (see Figures 1.3 and 3.24). A net 0.130 Sv flows westward into the East Siberian Sea across section BS02 while a net 0.329 Sv and 0.185 Sv flow northward across sections BS03 and BS04 respectively. Roughly half (0.062 Sv) of the water passing BS02 immediately recirculates

along the northwest side of Wrangel Island across section BS06. The remaining half of the net flow across section BS02 probably recirculates outside section BS06 and crosses BS05 to the east. This recirculation combined with the 0.062 Sv across BS06 constitutes about 70% of the flow through BS05. The remaining 30% of transport across section BS05 originates in the Makarov Basin. The correlation coefficient for transports across sections BS02 and BS06 is 0.803(0). It increases to 0.882(0) using a thirteen-month low pass filter. A net of 0.263 Sv flows northeastward across section BS05. Correlations of flow across section BS01 with BS02, BS03, BS04 and BS06 is 0.742(0), 0.823(0), 0.819(0) and 0.687(0) respectively.

The area bounded by cross sections CP15, CP14, CB04 and CB02 east of Hanna Canyon includes much of the Shelf Basin Interaction (SBI) study region (Grebmeier et al., 1998). This area bounded by cross sections CP15, CP14, CB04 and CB02 will be referred to as the SBI study region through the remainder of this paper. Inflow into this region includes a net 0.306 Sv that flows northward across section CP15 and a net 1.018 Sv that flows eastward across sections CP14 for a total of 1.324 Sv entering the SBI region. Assuming all 0.649 Sv of Pacific water that crosses section BS01 recirculates in the direction of the SBI region, nearly half of the water that enters the SBI region is Pacific water. The correlation coefficient for flow between cross sections CP07 and CP14 is 0.852(0), and 0.884(1) after using a thirteen-month low pass filter. The correlation coefficient for flow between cross sections BS04 and CP15 is 0.839. Outflow from this region is via a net 0.915 Sv into the basin interior and a net 0.424 Sv

eastward along the slope across sections CB04 and CB02 respectively.

A net 1.165 Sv of Atlantic-derived water enters southeastward within the Atlantic layer (256-850 m) into the study region across section CB01 (Table 3.2). Transport patterns within the Atlantic layer are similar in direction to those through the entire water column (see Table 3.1) but magnitudes are less. After passing through cross section CB01 Atlantic water enters the Chukchi Plateau region across section CP10 and continues through cross sections CP11 and CP12. Net Atlantic layer volume transports across sections CP10, CP11 and CP12 are 0.713, 0.693 and 0.727 Sv, respectively. Correlations of transport across section CP10 with CP11 and CP12 in the Atlantic layer have coefficients 0.999(0) and 0.717(0), respectively. Correlations of transport across section CB01 with the transports at downstream cross sections CP10, CP11 and CP12 have coefficients of 0.675(0), 0.669(24) and 0.708(0), respectively. These correlation coefficients become 0.822(22), 0.834(23) and 0.691(2) respectively after applying a thirteen-month low pass filter to the transport time series.

A net 0.882 Sv of Atlantic water flows eastward across section CP07. A net 0.348 Sv (~35% of the full water column) continues eastward across section CP14 and a net transport of 0.555 Sv flows northward across section CP05. A net flow of 0.156 Sv exits this region northward across section CB04 and a net 0.138 Sv (~33% of the full water column) continues along the slope out of the SBI study region across section CB02.

Flow into the northern Chukchi Plateau region bounded by cross sections CP16, CB06, CP17, CP08 and CP13 via the Atlantic layer is through all cross sections except CB06. Net transports of 0.642 Sv, 0.221 Sv, 0.225 Sv and 0.173 Sv enters this region across sections CP16, CP17, CP08 and CP13 respectively. A net 0.510 Sv exits this region northward across section CB06 into the Canada Basin interior in the Atlantic layer. The apparent imbalance of inflow and outflow in Atlantic layer this region suggests a vertical transport, which is discussed in Chapter IV.

In the upper ocean (0-220 m) a net 0.980 Sv enters the study region flowing southeast across section CB01, with a net 0.048 Sv flowing northward across section CB05 (Table 3.3). The upper flow continues into the Chukchi Plateau, as described earlier, net transports of 0.666, 0.553, 0.568 and 0.752 Sv flow across sections CP10, CP11, CP12 and CP07 respectively. Past cross section CP07 a northward branch with a net 0.335 Sv flowing across section CP05 and the remainder flowing past the Hanna Canyon in the direction of cross section CP14. A net 0.791 Sv flows across section CP14 in the upper water column, which represents about 80% of the total net flow through CP14. A net 0.378 Sv (~40% of the full water column) flows northward out of the SBI study region into the Canada Basin interior across section CB04 and a net 0.676 Sv flows northeastward across section CB02 into the Beaufort Sea in the upper layer. This net transport of 0.676 Sv that exits the SBI region across section CB02 within the upper layer exceeds the net transport that exits this section through the entire water column (see Figure 3.24 and Table 3.1), suggesting a countercurrent below 220 m.

A net 0.163 Sv (~15% of the full water column) flows into the northern Chukchi Cap region across section CP16 in the upper ocean. Additional inflow to this region includes a net 0.237 Sv from the flow along the eastern Northwind Ridge across section CP08. Although the full water column exhibits a net southward flow across section CP13, in the upper ocean a net 0.034 Sv flows northward into the northern Chukchi Plateau. Almost no transport (net 0.001 Sv) exists across section CP17. In the upper ocean a net 0.428 Sv flows northward across section CB06 into the Canada Basin interior. This transport across section CB06 constitutes over 90% of the export out of the region enclosed by sections CP16, CB06, CP17, CP08, CP13 in the upper ocean.

2. Heat and Freshwater Transport

Freshwater and heat fluxes were calculated across all sections and results are summarized in Tables 3.1, 3.2 and 3.3 and shown in Figures 3.26 and 3.27. It is assumed that the majority of heat transport is contained within the model-defined Atlantic layer (268-850 m) therefore analysis will focus on the results in this layer (Table 3.2 and Figure 3.26) (Aagaard and Greisman, (1975), Rudels et al., (1994)). Heat flux is referenced to a temperature value of -0.1° Celsius.

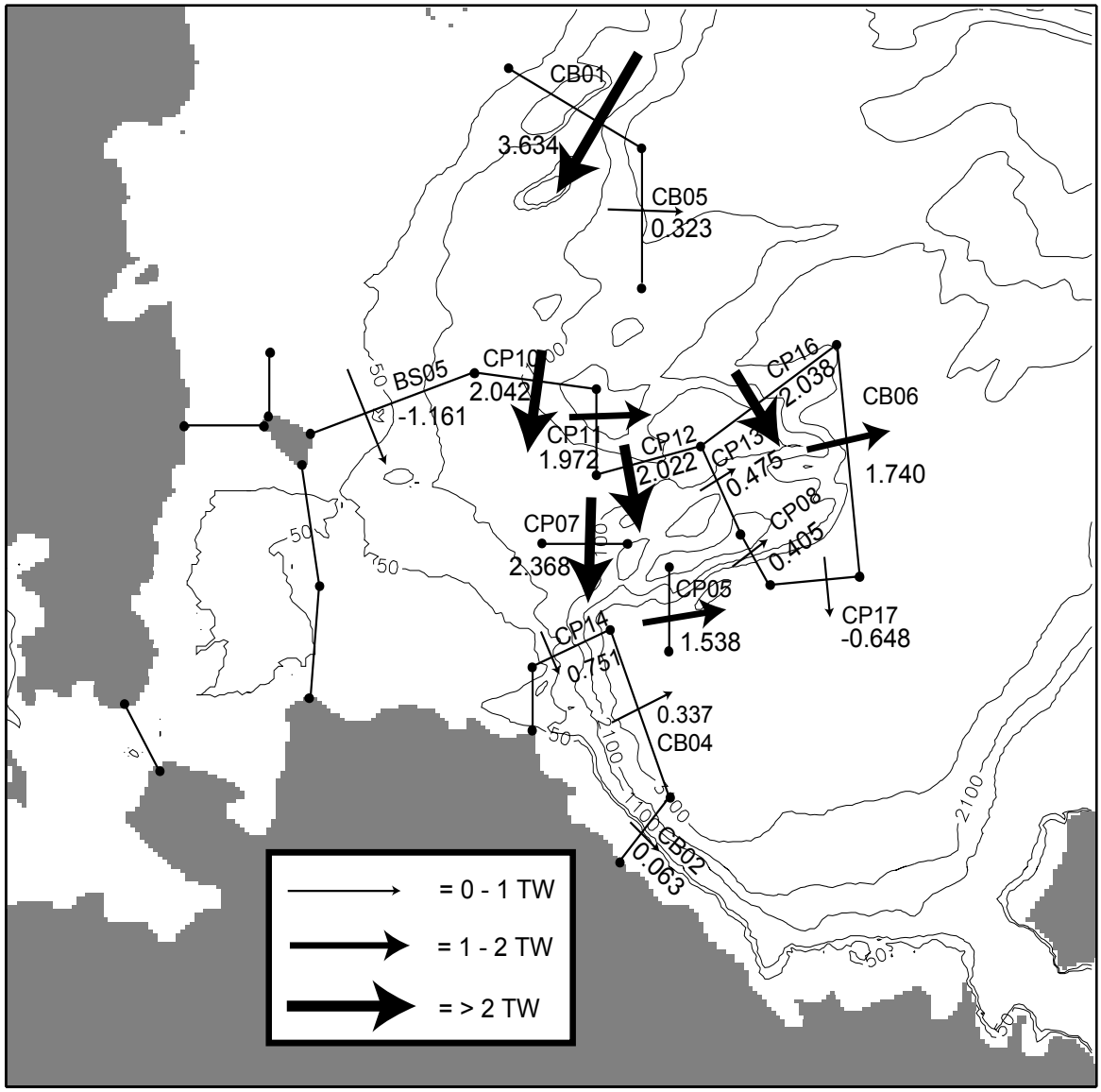

Figure 3.26 Average net heat flux (TW) through the Atlantic layer (268-850m) across sections established in the western Arctic calculated using monthly means averaged over a twenty-three year mean from 1979-2001. Temperature referenced to -0.1°C. Arrows point in the direction of net positive flow.

Section	Net Vol	Vol Pos	Vol Neg	Net Heat	Heat Pos	Heat Neg	Net FW	FW Pos	FW Neg
CB01	1.165	1.286	-0.121	3.634	4.002	-0.368	-3.713	-4.191	0.478
CB02	0.138	1.196	-1.057	0.063	2.962	-2.900	0.293	-2.597	2.891
CB04	0.156	1.224	-1.068	0.337	3.145	-2.808	-0.261	-3.097	2.836
CB05	0.086	0.636	-0.551	0.323	2.110	-1.787	-0.295	-2.611	2.317
CB06	0.510	1.011	-0.501	1.740	3.412	-1.672	-2.002	-4.108	2.105
CP05	0.555	0.692	-0.136	1.538	1.931	-0.393	-1.608	-2.026	0.418
CP07	0.882	0.896	-0.014	2.368	2.414	-0.046	-2.549	-2.591	0.043
CP08	0.225	0.313	-0.089	0.405	0.566	-0.162	0.117	0.095	0.021
CP10	0.713	0.925	-0.212	2.042	2.643	-0.601	-1.798	-2.496	0.698
CP11	0.693	0.807	-0.114	1.972	2.290	-0.318	-1.752	-2.143	0.391
CP12	0.727	0.736	-0.009	2.022	2.048	-0.026	-1.892	-1.917	0.025
CP13	0.173	0.328	-0.155	0.475	0.985	-0.510	-0.742	-1.289	0.546
CP14	0.348	0.499	-0.151	0.751	1.167	-0.416	-0.579	-0.976	0.397
CP15									
CP16	0.642	0.844	-0.202	2.038	2.681	-0.643	-2.644	-3.477	0.832
CP17	-0.221	0.396	-0.617	-0.648	1.432	-2.080	0.800	-1.521	2.321
BS01									
BS02									
BS03									
BS04									
BS05									
BS06									

Table 3.2 Twenty-three year mean volume transport (Sv), heat flux (TW) and freshwater flux (10^3 m^3/s) across defined cross sections in the Atlantic layer (268-850m). Temperature is referenced to -0.1°C and salinity is referenced to 34.70 ppt. Positive values are in accordance with directions indicated in Figure 3.27.

Atlantic-derived water that flows across section CB01 is a primary source of heat in the Atlantic layer of the Chukchi Plateau region. It contributes a southeastward flux of 4.002 TW across section CB01 with 0.368 TW recirculating in the opposite direction resulting in a net of 3.634 TW entering the study region across section CB01 in the Atlantic layer. The advection of heat in the Atlantic layer roughly follows volume transport circulation patterns of the entire water column. A net 2.042 TW crosses section CP10, which accounts for ~55% of the heat flux across section CB01. Beyond cross section CP10 a net 1.972 TW and 2.022 TW flux propagates across sections CP11 and CP12 respectively. A net flux of 2.368 TW crosses section CP07 in an eastward direction towards the SBI study

region. The higher positive net flux across section CP07 as compared to CP12 indicates contributions of heat that propagate from both cross sections CP10 and CP12.

Beyond cross-section CP07, greater heat flux is observed to advect northward across section CP05. A net 1.538 TW propagates northward across section CP05 while a lesser net of 0.751 TW propagates across section CP14. The increased northward heat flux across CP05 within the Atlantic layer is in qualitative agreement with the circulation in the Atlantic layer. Cross-section CP05 has a greater percentage of area across the Atlantic layer depth as compared to cross-section CP14. Cross-section CP14 bisects the steep continental slope and approximately half of the cross-sectional area is at depths shallower than the Atlantic layer.

The SBI study region is an area of high heat exchange despite low net exchange rates across sections. A heat flux of 1.167 TW enters the SBI region within the Atlantic layer through section CP14. The negative heat flux across section CP14 is -0.416 TW resulting in a net 0.751 TW entering the SBI region across section CP14. Positive heat flux of 3.145 TW propagates northward across section CB04 into the central basin. Negative heat flux of -2.808 TW directed southward across section CB04 results in a net heat flux northward into the basin interior across section CB04 of 0.337 TW. The eastward heat flux across section CB02 is 2.962 TW whereas the westward flux is 2.900 TW resulting in a small net eastward flux of 0.063 TW.

The northern end of the Chukchi Plateau bounded by cross sections CP16, CB06, CP17, CP08 and CP13 is an area of relatively high heat fluxes in the Atlantic layer. A

net heat flux of 2.038 TW enters this region across section CP16 and accounts for the majority of heat introduced into this area. Additional heat introduced into this region includes a net positive heat flux of 0.475 TW across section CP13 and a net 0.405 TW flux across section CP08 and a westward net flux of 0.648 TW across section CP17. A net 1.740 TW of heat propagates northward across section CB06, which identifies this region as a major heat source for the Canada basin interior. The export of 1.740 TW of heat out the area bounded by cross-sections CP16, CB06, CP17, CP08 and CP13 northward across section CB06 accounts only for just over half of the heat introduced into this region across the remaining four cross-sections. This suggests an additional heat loss out of the bounded region in the vertical direction.

Model hydrography shows that the majority of freshwater sources and transport is restricted to shallow depths therefore analysis of freshwater flux will focus on the upper layer depth (0-220 m) as summarized in Table 3.3 and Figure 3.27. Calculations of freshwater flux are referenced to 34.70 ppt. The depths of cross sections BS01 through BS06 and CP15 are less than 220 m, in these cases freshwater flux is analyzed across the entire depth as summarized in Table 3.1.

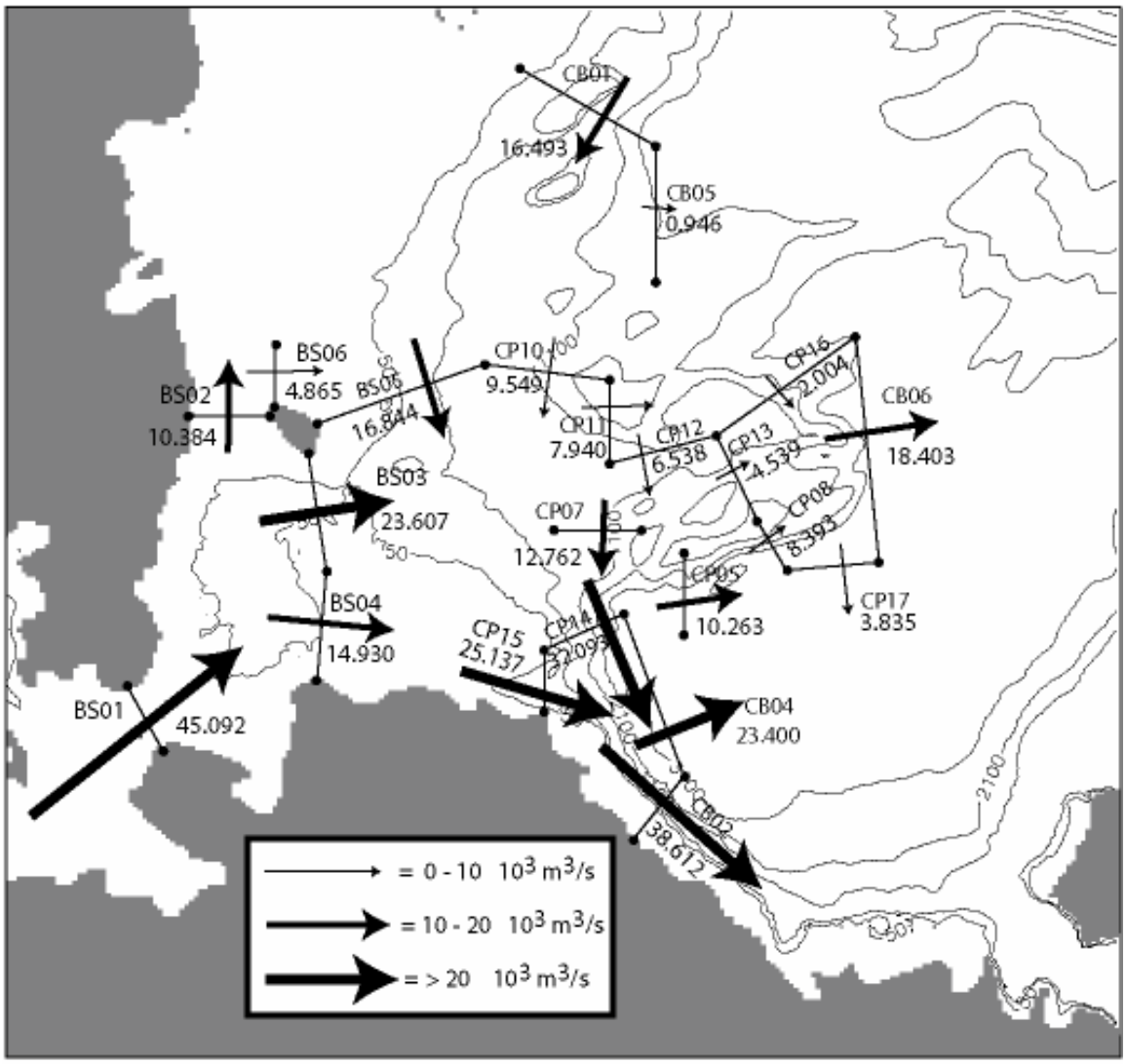

Figure 3.27 Average net freshwater flux (10^3 m^3/s) through the upper layer (0-220m) across sections established in the western Arctic calculated using monthly means averaged over a twenty-three year mean from 1979-2001. Salinity referenced to 34.70ppt. Arrows point in the direction of net positive flow.

Section	Net Vol	Vol Pos	Vol Neg	Net Heat	Heat Pos	Heat Neg	Net FW	FW Pos	FW Neg
CB01	0.980	1.029	-0.049	-1.047	-1.129	0.082	16.493	17.795	-1.302
CB02	0.676	0.736	-0.060	-2.629	-2.731	0.102	38.612	40.751	-2.139
CB04	0.378	0.835	-0.457	-1.490	-2.239	0.749	23.400	35.442	-12.042
CB05	0.048	0.236	-0.188	-0.062	-0.283	0.221	0.946	4.237	-3.292
CB06	0.428	0.537	-0.109	-1.252	-1.387	0.135	18.403	20.674	-2.271
CP05	0.335	0.390	-0.055	-0.612	-0.651	0.039	10.263	11.167	-0.904
CP07	0.752	0.766	-0.014	-0.086	-0.909	0.046	12.762	13.753	-0.991
CP08	0.237	0.296	-0.059	-0.559	-0.624	0.065	8.393	9.479	-1.086
CP10	0.666	0.769	-0.103	-0.580	-0.723	0.143	9.549	11.879	-2.329
CP11	0.553	0.600	-0.046	-0.458	-0.520	0.061	7.940	8.928	-0.988
CP12	0.568	0.600	-0.032	-0.392	-0.516	0.124	6.538	8.781	-2.243
CP13	-0.034	0.102	-0.136	0.269	-0.087	0.356	-4.539	1.491	-6.029
CP14	0.791	0.858	-0.067	-2.449	-2.571	0.122	32.093	34.394	-2.301
CP15									
CP16	0.163	0.274	-0.111	-0.132	-0.406	0.274	2.004	6.300	-4.296
CP17	-0.001	0.218	-0.219	-0.269	-0.563	0.294	3.835	9.077	-5.242
BS01									
BS02									
BS03									
BS04									
BS05									
BS06									

Table 3.3 Twenty-three year mean volume transport (Sv), heat flux (TW) and freshwater flux (10^3 m^3/s) across defined cross sections in the upper layer (0-220m). Temperature is referenced to -0.1°C and salinity is referenced to 34.70 ppt. Positive values are in accordance with directions indicated in figure 3.26.

The primary source of salt for this region is Atlantic-derived water that crosses section CB01 however; 16.493×10^3 m^3/s net positive flux of freshwater enters the study region across the upper layer of cross section CB01 as well. This freshwater possibly includes the eastern (i.e. runoff) from the shelves upstream of CB01. A net flux of 0.946×10^3 m^3/s propagates northward across section CB05. Net positive freshwater fluxes of 9.549×10^3 m^3/s, 7.940×10^3 m^3/s and 6.538×10^3 m^3/s propagate across sections CP10, CP11 and CP12 respectively. This propagation pathway is consistent with volume transport and heat flux. The lower values of positive net freshwater flux are indicative of the dominating role of salinity originating from Atlantic-derived water across section CB01 at this depth range.

The area in the northern Chukchi Plateau bounded by cross sections CP16, CB06 CP17, CP08 and CP13 receives a total influx of freshwater of 10.397×10^3 m^3/s from cross section CP16 (2.004×10^3 m^3/s) and CP08 (8.393×10^3 m^3/s). A net 18.403×10^3 m^3/s of freshwater exits the region northward across section CB06 providing a source of freshwater to the basin interior. A net 3.835×10^3 m^3/s of freshwater flux propagates eastward across section CP17 and a net negative flux of -4.539×10^3 m^3/s propagates northwestward across section CP13 that indicates 4.539×10^3 m^3/s of freshwater flux in the opposite direction. A freshwater flux of 16.380×10^3 m^3/s exiting across sections CP16, CB06 CP17, CP08 and CP13 in excess of the inward flux suggests that this area is a freshwater source for the upper ocean. The excess net heat within the Atlantic layer in this region could provide a mechanism to melt overlying sea ice, thereby providing an additional source of the freshwater. This notion will be addressed in Chapter IV.

The dominant source of fresh water for the region is Pacific water that enters the region through the Bering Strait. A net freshwater flux of 50.584×10^3 m^3/s passes through the Bering Strait northward across section BS01. A net 5.492×10^3 m^3/s of freshwater recirculates in the opposite direction, resulting in a net positive flux of 45.092×10^3 m^3/s of freshwater entering the Arctic in Pacific water across section BS01. Propagation of net positive freshwater flux is similar to volume transport patterns beyond BS01. A net positive westward freshwater flux of 10.384×10^3 m^3/s is present across section BS02 and northward net positive flux of freshwater of 4.865×10^3 m^3/s across section BS06. A net 23.607×10^3 m^3/s freshwater flux exists

in the northward direction across section BS03 and a net freshwater flux of 14.930×10^3 m^3/s exists across section BS04. A sum of freshwater flux across sections BS02, BS03 and BS04 exceeds the freshwater introduced across section BS01 by nearly 4×10^3 m^3/s, which indicates an additional source of freshwater, possibly due to net ice melt and runoff.

Net freshwater flux into the SBI study region includes 32.093×10^3 m^3/s and 25.137×10^3 m^3/s across sections CP14 and CP15 respectively. Assuming all freshwater that enters as Pacific water across the Bering Strait recirculates into the SBI region nearly 80% of the 57.23×10^3 m^3/s of freshwater that enters the SBI region in the upper layer originates as Pacific water. Net 23.400×10^3 m^3/s of freshwater exits the SBI region northward into the interior across section CB04. A net 38.612×10^3 m^3/s of freshwater exits the SBI region eastward across section CB02 in the upper layer. A surplus freshwater flux of nearly 5×10^3 m^3/s exits the SBI region in the upper layer across sections CB02 and CB04 as compared to freshwater entering the region across sections CP14 and CP15. This surplus again suggests the source of freshwater in the region likely consisting of ice melt and runoff.

THIS PAGE INTENTIONALLY LEFT BLANK

IV. DISCUSSION

The 1979-2001, twenty-three-year mean velocity fields present circulation patterns of the region that are generally cyclonic in nature (see Figures 3.1 - 3.3). In general the boundary flow is characterized by a narrow current (~150 km) throughout the Canada Basin that follows the slope bathymetry over the depth range of ~ 200-1100 m. This boundary current crosses the Chukchi Plateau and then turns southeastward towards the Hanna Canyon. Upon exiting the Northwind Abyssal Plain a portion of this boundary flow separates to the north and follows along the east side of the Northwind Ridge (see Figure 3.3).

The climatological mean circulation in the upper ocean (0-26 m) exhibits a cyclonic flow along the slope regions, the East Siberian Sea and the northern Chukchi Sea. Additionally there is a wide and generally northward-to-northeastward flow through much of the Canada Basin interior (see Figure 3.2). The most pronounced cyclonic boundary flow of the model mean circulation is in the halocline layer (54-149m) where TKE values commonly exceed 25 cm^2/s^2.

Comparatively less energy is contained in the Atlantic layer (268-850m) where most of the transport is restricted to cyclonic boundary flow. The flow is strongest in the Makarov Basin from the Lomonosov Ridge through the Chukchi Plateau via the Chukchi Borderland Pass and along the slope in the eastern Canada Basin off Banks Island to the Lomonosov Ridge. TKE values in the Atlantic layer exceed 25 cm^2/s^2 along the narrow boundary flow of the Makarov Basin and one region adjacent to the CAA over the Alpha

Ridge. Boundary flow in the Atlantic layer is significantly weakened in the southern Canada Basin and Beaufort Sea where TKE values are below 3 cm^2/s^2.

The variability over the 1979-2001 time period is evident by comparison of the circulation patterns among the three two-year average velocities (1981-1982, 1991-1992, 2000-2001) in the upper ocean (see Figures 3.5 - 3.7), the halocline (see Figures 3.8 - 3.10) and the Atlantic layer (see Figures 3.11 - 3.13). The three two-year averages that are considered present three distinguishable circulation patterns. The 1981-1982 and 2000-2001 time periods are somewhat similar, while the 1991-1992 time period exhibits greater energy and a stronger, more cyclonic flow in all areas of the Canada Basin particularly in the boundary flow and in the Atlantic layer (see Figures 3.5-3.13). The difference vectors (see Figures 3.14 through 3.22) illustrate the magnitude and orientation of the differences. This does not present a comprehensive analysis of the variability that took place between 1979 and 2001 in the western Arctic but does provide a framework for a general understanding of it.

Thompson and Wallace (1998) described an increase in the sea level pressure variability from the mid 1980's to early 1990's indicating a more cyclonic atmospheric regime in the Arctic. Using a simplified Arctic Ocean model Proshutinsky and Johnson (1997) identified two general oceanic circulation schemes, i.e. cyclonic and anticyclonic, in response to wind forcing from 1946 to 1993. Maslowski et al. (2000 and 2001) using a coupled ice-ocean model obtained similar responses of the upper ocean and sea-ice to cyclonic atmospheric forcing that

appeared in the late 1980's and then diminished approximately a decade later. Their results for the late 1990's suggested an opposite (i.e., anticyclonic) trend in the circulation of the sea ice and upper ocean. McLaughlin et al. (2002) discussed the anticyclonic and cyclonic regimes in the context of a coupled ocean atmosphere system based on observational data. The model intensity of the 1991-1992 circulation scheme presented here (see Figures 3.6, 3.9, 3.12) is greater than the intensity of the 1981-1982 circulation scheme (see Figures 3.5, 3.8, 3.11). This period of increased intensity is followed by a reduction in strength as reflected in the 2000-2001 two-year average (see Figures 3.14, 3.15, 3.16) which is in agreement with Maslowski et al. (2001). These depictions of the circulation intensity illustrate the oceanic response to forcing by a cyclonic atmospheric regime that appeared in the mid 1980's, peaked in intensity in the late 1980's and early 1990's and then diminished by the early 2000's.

The intensity of the mean circulation in the Atlantic layer in the 2000-2001 time period (see Figure 3.11) appears slightly weaker than the twenty-three year mean average in the Atlantic layer (see Figure 3.4). The boundary current that exceeds 3 cm^2/s^2 extends from the Makarov Basin to the Beaufort Sea in the later figure. Boundary flow of this strength does not extend beyond the Makarov Basin in the 2000-2001 time period in the Atlantic Layer. Intensity of both the 1981-1982 and 1991-1992 two-year averages (see Figures 3.11 and 3.12 respectively) appear greater than the twenty-three year circulation (see Figure 3.4). Boundary flow in excess of ~25 cm^2/s^2 extends along most of the perimeter of the Canada Basin during

these two time periods while it is absent in the Beaufort Sea in the twenty-three year mean. This suggests periods of significantly weaker flow between these three two-year time averaged periods.

The thirteen-month low pass correlation between the transports a cross sections CB01 and CP10 through the full water column has a coefficient of 0.806. This indicates that ~65% of the interannual transport variability at section CP10 is associated with interannual transport variations that have propagated across the Chukchi Plateau from section CB01 over the twenty-three year period from 1979 to 2001. The net northward flow across section CB05 is relatively small however the positive and negative exchange is high with 1.485 Sv flowing northward and 1.309 Sv returning southward across section CB05.

Assuming some exchanges take place in the north-south direction through the ungaged region between section CB01 and CP10, it is difficult to assess how much water that passes through section CB01 reached section CP10. The total combined volume transport through cross sections BS05 and CP10 is 1.786 Sv. If all the water crossing section BS02 to the west (0.13 Sv) recirculates to the east through BS05 than the remainder of 1.656 Sv, or ~69%, should be water that passed through section CB01. This would suggest that ~65% of CB01 volume transport passes sections CP10 and BS05 and separates from the slope towards the interior through the ungaged region between the eastern edge of section CB05 and the junction of CP10 and CP11. It is hypothesized that most or all of this flow converges along the northwestern region of the Chukchi Plateau and is captured across section CP12 and CP16. The net volume flux

of 1.29 Sv through section CP16 accounts for ~48% of the flux through CB06 (2.680 Sv) which is lost to the interior.

Before discussing the circulation over the Chukchi Plateau this project will focus first on the Pacific Water contribution to the region from the Bering Strait (~0.65 Sv through section BS01). The downstream separation of the flow measured across three sections in the Chukchi Sea can be summarized as follows. The flow of 0.185 Sv through section BS04 extending from Cape Lisburne on the Alaskan coast to Herald Shoal accounts for ~29% of the volume transport across BS01. The majority of Pacific Water turns westward north of the Bering Strait with ~50% (0.329 Sv) entering the Herald Canyon through section BS03 between Herald Shoal and Wrangel Island. The remainder of the Pacific Water continues further west through Long Strait (section BS02), which accounting for ~21% of the volume flux through BS01. It is argued that all the water passing section BS02 recirculates around Wrangel Island to cross section BS05. Also some of the water crossing section BS03 enters the southeastern region of Chukchi Plateau. The remaining portion of flow through BS03 merges with water from section BS04 to flow northeast into the sections CB14 and CB15. Cross sections BS01 through BS04 describe all Pacific water that enters the Arctic through the Bering Strait. An estimated 79% of the freshwater that enters the SBI study region is Pacific water that has entered the region through the Bering Strait.

A. BOUNDARY CURRENT THROUGH THE CHUKCHI PLATEAU

The model results of the mean circulation for the Canada Basin are in general agreement with published literature depicting circulation in the region (e.g.,

Aagaard (1989), Rudels et al. (1994) and Smethie et al. (2000)). However, the results presented as part of this thesis indicate that the boundary flow follows the bathymetry of the northern Chukchi Rise, which results in a meander. This finding sheds light on the boundary flow pathway inferred by Rudels et al. (1994) and Smethie et al. (2000) and provides a contribution to a body of research that has a comparatively limited observational database.

The moderately strong boundary flow meander across the Chukchi Plateau via the Chukchi Borderland Pass (TKE of ~15 cm^2/s^2) provides support to the inferred circulation pathway across the Chukchi Plateau proposed by Rudels et al. (1994). Rudels et al. (1994) proposed a direct eastward flow across the base of the Chukchi Plateau at its junction with the continental slope (see Figure 1.1). Model results support this general destination but identify a specific pathway of this flow in the form of a northeast-to-southeast meander along the northern slope of the Chukchi Rise and south of the Chukchi Cap through the Chukchi Borderland Pass (see Figures 3.4 and 3.23).

Smethie et al. (2000) detected properties characteristic of Atlantic water at SCICEX 96 station 68 adjacent to the Chukchi Rise and station 44 at the southern end of the Canada Basin (Figure 4.1). This formed the basis of their conclusion that the boundary flow propagates all around the Chukchi Plateau. The model results of this thesis indicate that the majority of Atlantic layer transport is maintained within the boundary current that passes through the Chukchi Plateau via the Chukchi Borderland Pass and continues eastward into the southern Canada Basin towards the Beaufort Sea. The net mean flow

across sections CP05 and CP08 are northward along the east side of the Northwind Ridge both in the Atlantic layer and in the entire water column. This is in the opposite direction of the flow as proposed by Smethie et al., (2000) (Tables 3.1 and 3.2, Figure 3.24).

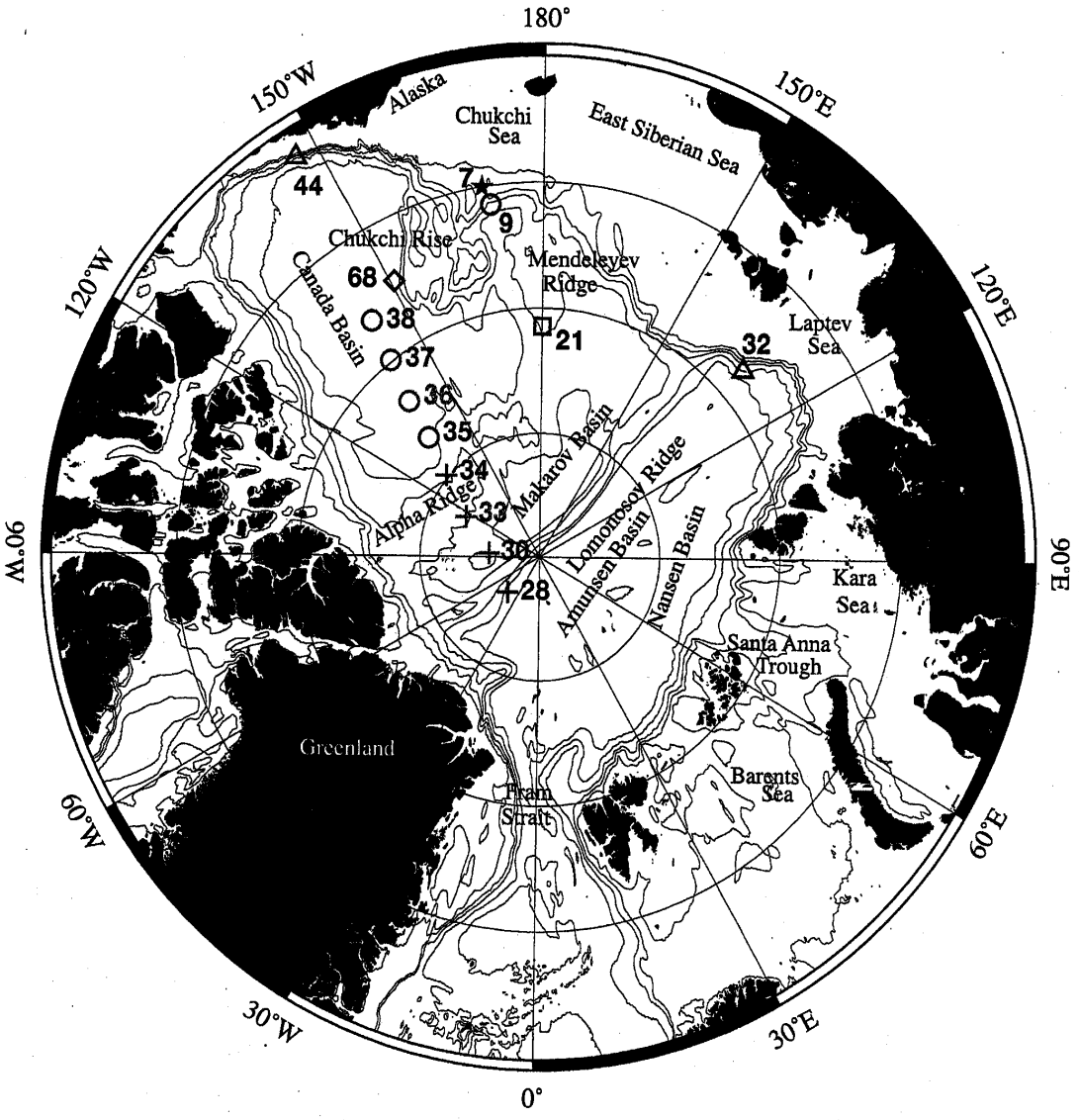

Figure 4.1 Locations of stations used in analysis by Smethie et al. (2000).

The pathway proposed by Smethie et al. (2000) indicates that the Atlantic water signature detected at SCICEX 96 station 68 would have originally branched off the boundary current to the north in the vicinity of the Arlis Plateau and propagated around the northern flanks of the Chukchi Plateau. Elements of model Atlantic layer flow appear to follow this pathway over the twenty-three year mean up to the approximate position of station 68 but in lesser amounts than the boundary flow that continues through the Chukchi Borderland Pass and across the Chukchi Abyssal Plain (see Figure 3.4). Model results suggest that it is likely the Atlantic water signature detected at SCICEX station 68 by Smethie et al. (2000) did not have to originally propagate from the north around the Chukchi Plateau. Instead these results suggest the Atlantic water passed through the Chukchi Borderland Pass, merged with the northward flow along the eastern side of the Northwind Ridge near the Hanna Canyon and approached station 68 from the south. The pattern proposed by Smethie et al. (2000) is partially evident in the 2000-2001 time period (see figures 3.10 and 3.13). However, flow parallel to the Northwind Ridge is northward in this time period, which is opposite the direction proposed by Smethie et al. (2000).

B. HEAT DISTRIBUTION AND ADVECTION

Swift et al. (1997) hypothesized that the Chukchi-Mendeleyev boundary region may be a source where waters spread from the slope regions into the central Canada Basin. The net northward transport across section CB05 of 0.176 Sv is small however, the positive northward transport of 1.485 Sv supports the suggestion made by Swift et al. (1997) that the Chukchi-Mendeleyev boundary region is a

source region for the injection of boundary waters into the basin interior. The positive northward heat flux of 2.689 TW and net heat flux of 0.346 TW northward across section CB05 identifies this region as a source of heat for the Canada Basin interior.

Smethie et al. (2000) stated that the SCICEX 96 data indicated Atlantic water is transported rapidly from the boundary to the interior of the Canada Basin but that the mechanism for this was undetermined. The positive, negative and net northward volume transport, heat and freshwater fluxes across sections CB05, CB06, and CB04 are summarized in Tables 3.1 - 3.3 and Figures 3.24, 3.26, and 3.27. The largest of the net volume transports and heat fluxes to the interior (2.680 Sv and 1.740 TW, respectively) are directed northward across section CB06. The largest net freshwater flux ($23.400 \times 10^3 m^3/s$) is directed northward across section CB04. These two locations of property transport are the most critical regions where shelf boundary waters are transported into the Canada Basin interior. Net volume transports within the Atlantic layer into the interior across sections CB05, CB06 and CB04 are 0.086 Sv (49%), 0.510 Sv (19%) and 0.156 Sv (17%) respectively. The values in parentheses reflect the ratio of Atlantic layer transport to full water column transport through the corresponding sections. The region surrounding section CB06 is an area of eddy generation with high positive and negative volume transport and heat flux across this section (see Tables 3.1 and 3.2).

Most of the sections on the Chukchi Shelf are above the depth range of the Atlantic layer except section BS05, which has a negative heat flux of 1.161 TW (i.e. a net flow

of water colder than the -0.1°C reference value in the positive direction). The total net heat available just upstream of the Chukchi Plateau is equal to ~2TW across section CP10, which is ~56% of the heat available at section CB01. In addition about 9% exits the boundary flow through CB05. Following the earlier discussion of volume transports this suggests that ~35% of water from section CB01 passes the gap between the eastern end of section CB05 and the junction of sections CP10 and CP11.

Considering that the net heat flux across section BS05 is in the southwestward direction all the heat that propagates eastward across section CP07 passes through either cross section CP10 or CP12. About 65% of the net eastward 2.368 TW crossing section CP07 turns northward through section CP05. Only a net 0.751 TW of heat (~32%) enters the SBI study region across section CP14.

Northward net upper layer volume transports across sections CP05 and CP08 are 0.335 Sv and 0.237 Sv, respectively (see Table 3.3). This northward, upper layer volume transport above the eastern side of the Northwind Ridge is consistent with the spreading pattern of shallow-water, temperature-maximum waters observed by Shimada et al. (2001) during the 1997 SHEBA experiment. The analysis of the dynamic height by Shimada et al. (2001) indicated that the expected northward baroclinic flow field is nearly parallel to the seafloor topography above the Northwind Ridge and the Chukchi Plateau. However, the results of heat flux in the upper layer in the model twenty-three year mean results are inconsistent with the temperature transport during 1997-98 as implied by Shimada et al. (2001). The net heat flux across sections CP05 and CP08 is

-0.612 TW and -0.580 TW respectively suggesting a net northward heat flux of water colder than -0.1°C in the upper layer. Because the analysis conducted by Shimada et al. (2001) focused on circulation and the advection of temperature in the upper 100 m during the 1997 SHEBA experiment, whereas the analysis of the upper layer in these model results covers the twenty-three year mean in the upper 220 m, direct comparison of results from these two studies is likely limited. In spite of the inconsistency between the heat transports proposed by Shimada et al. (2001) model results are consistent with the conclusion as proposed by Shimada et al. (2001) that seafloor topography in this region plays a crucially important role in upper ocean heat distribution. Additionally, the northward flow east of and parallel to the Northwind Ridge obtained in these model results is consistent with the advection pathways discussed by Shimada et al. (2001).

C. FRESHWATER DISTRIBUTION

The freshwater flux pattern in the study region is dominated by the contribution of freshwater made by Pacific water to the region. Comparing the contribution of fresh water to the region from cross section CB01 and from Pacific water that passes through the Bering Strait, over two and half times more freshwater is introduced into the region through the Bering Strait across section BS01 as compared to the upper 220 m of cross section CB01.

The large influx of freshwater from the Pacific Ocean through the Bering Strait and the pathway of net positive (i.e. northward) freshwater flux, as indicated in Figure 3.27, suggest that a significant portion of freshwater

found in the Canada Basin interior originates as Pacific water. A mean freshwater flux of 57.230×10^3 m^3/s enters the SBI study region across sections CP14 and CP15. Assuming that the entire freshwater flux of 45.092×10^3 m^3/s that crosses section BS01 eventually recirculates and merges with the general eastward flow in the region and enters the SBI region. Nearly 80% of the 57.230×10^3 m^3/s of the freshwater that enters the SBI study region in the upper 220 m is from Pacific water. Assuming proportionally that 80% of the net 23.400×10^3 m^3/s of freshwater flux that propagates northward across section CB04 is of Pacific origin then approximately 18×10^3 m^3/s of net freshwater flux that propagates across section CB04 into the basin interior is freshwater that entered the Arctic as Pacific water through the Bering Strait. This estimate is probably high because the amount of freshwater flux that exits the SBI study region across sections CB04 and CB02 exceeds the amount of influx across sections CP14 and CP15 by approximately 5×10^3 m^3/s in the upper 220 m suggesting that the additional freshwater is due to ice melt in the region. However, it is clear that the high amount of freshwater that is introduced into the western Arctic as Pacific water through the Bering Strait has a significant impact on the freshwater budget in the region and may be a more important source of freshwater in the interior Canada Basin than previously thought.

The 1997 SHEBA data analyzed by McPhee et al. (1998) indicated that the multi-year ice thickness was unexpectedly low and also identified an excess of freshwater in the SHEBA study region over the eastern Chukchi Plateau. An upward oceanic heat flux which was

much greater during 1997 than in the mid-70's suggests a mechanism that would provide the heat source to melt this ice. However, McPhee et al. (1998) indicated that ice melt alone cannot account for the increased amount of freshwater that was observed and therefore the source of freshwater found in the SHEBA study region was unclear.

These model results suggest two mechanisms to account for the freshwater surplus in the SHEBA study region discussed by Macdonald et al. (2002). First, freshwater generated by ice melt in the northern Chukchi Plateau region is the result of heat transported upward from the Atlantic layer. Secondly, advective pathways transport freshwater from the shelf regions to the interior, particularly freshwater that enters the region as Pacific water.

The amount of freshwater flux that exits the northern Chukchi Plateau across sections CP16, CB06 CP17, CP08 and CP13 in the upper ocean (0-220 m) exceeds the inward flux by 16.380×10^3 m^3/s. This suggests a freshwater source in this area. A net 2.97 TW enters the northern Chukchi Plateau region through the lateral cross sections in the Atlantic layer (268-850m) while only 1.740 TW exits across section CB06 suggesting vertical heat transport of 1.83 TW.

Upward transport of heat from the Atlantic layer could provide a mechanism to melt sea ice in this region that would provide a source of freshwater. These estimates indicate roughly 47 TW could be released upward across the horizontal area enclosed by sections CP16, CB06 CP17, CP08 and CP13 through vertical transport of water above the Atlantic layer ceiling at 0.1 cm/s and effect a temperature reduction of Atlantic layer water by $0.1^{\circ}C$. This 1.83 TW is

over twenty-five times smaller than this number, which could be satisfied by the upward motion over a smaller area, smaller velocity, over a smaller temperature difference, or a combination of the three. We note that the method employed to calculate flux, as a product of the mean velocity and the mean salinity or temperature could introduce inaccuracies that would account for some imbalance. However, it is assumed these inaccuracies are much smaller than variations in heat gain and loss from vertical transport.

The advection of ice previously formed elsewhere into this region, which subsequently melts, or the advection of ice melt water from other areas into the study region are mechanisms that have been suggested to account for this freshwater surplus. Macdonald et al. (2002) identified a surplus of ice melt water in the central Canada basin and a deficit in the shelf regions and verified that abundant amounts of fresh water runoff from the Mackenzie River were present in the interior ocean at the start of the SHEBA program. Macdonald et al. (2002) also observed runoff originating from either the Mackenzie or Yukon Rivers toward the eastern edge of the Northwind Ridge. These findings support the idea that shelf water was advected into the region. However, the advection mechanisms and details remain unclear.

The pattern of twenty-three year model mean circulation in the upper ocean from 0-26 m (see Figure 3.2), freshwater flux in the upper ocean from 0 - 220 m (see Table 3.3, Figure 3.27) and freshwater flux through the full water column (see Table 3.1) indicate a mechanism for transport of freshwater from the slope region towards

the Canada Basin interior. Twenty-three year mean circulation patterns in the upper ocean indicate an organized northward flow in the Canada Basin interior that would advect freshwater from the slope into the basin interior (see Figure 3.2). Net positive freshwater flux across section CB04 in the upper ocean denotes freshwater propagation from the slope region to the basin interior (Figure 3.27). Net northward flow across sections CP05, CP08, CB06 and CP17 provides an advective pathway that facilitates the transfer of freshwater from the slope region to the basin interior.

THIS PAGE INTENTIONALLY LEFT BLANK

V. CONCLUSIONS

The twenty-three year mean velocity fields of 1979-2001 present circulation patterns in the Canada Basin that are cyclonic in nature. This cyclonic signature varies in magnitude but is present in almost every time period and depth level analyzed. The most pronounced cyclonic boundary flow of the model mean circulation is in the halocline layer where total kinetic energy values commonly exceed 25 cm^2/s^2. Comparatively less energy is contained in the Atlantic layer where transport is primarily restricted to cyclonic boundary flow. The three two-year averages that are compared present distinguishable circulation patterns. The 1981-1982 and 2000-2001 time periods are somewhat similar while the 1991-1992 time period exhibits greater energy and a stronger, more cyclonic flow in all areas of the Canada Basin particularly in the boundary flow. TKE values commonly achieve values of 50 cm^2/s^2 in the 1991-1992 halocline layer. That cyclonic circulation in 1991-1992 is relatively more intense than cyclonic circulation in 2000-2001 is consistent with a cyclonic atmospheric regime that strengthened in the mid 1980's, peaked in the early 1990's and then diminished significantly by the early 2000's. This pattern agrees with the findings of Proshutinsky and Johnson (1997) and Maslowski et al. (2001).

These model results suggest an alternative circulation pathway of the boundary flow around the base of the Chukchi Plateau to that proposed by Smethie et al. (2000). Model results are more aligned with the general pathway of boundary flow over the Chukchi Plateau region as proposed

by Rudels et al. (1994). However, these results identify a northeast-to-southeast meander along the northern slope of the Chukchi Rise and south of the Chukchi Cap through the Chukchi Borderland Pass as the specific pathway of boundary flow across the Chukchi Plateau.

Net northward transport of properties into the interior across sections CB05, CB06 and CB04 identify these locations as regions where boundary water and their associated properties are transported into the Canada Basin interior. The net positive heat flux of 1.740 TW northward across section CB06 identifies this area as a major source of heat from the boundary current to the Canada Basin interior.

The analysis of model results suggests two mechanisms to account for the freshwater surplus, discussed by Macdonald et al. (2002), in the SHEBA study region. First, freshwater generated by ice melt in the northern Chukchi Plateau region is the result of heat transported upward from the Atlantic layer. Secondly, northward transport along the eastern side of the Northwind Ridge across section CP05 is an advective pathway that transports freshwater from the shelf regions to the interior.

Over two and half times more freshwater is introduced into the region through the Bering Strait than through the upper 220 m of cross section CB01. Roughly 80% of the freshwater that enters the SBI study region is from Pacific water that has entered the region through the Bering Strait. The high amount of freshwater that is introduced into the western Arctic as Pacific water may be a more important source of freshwater in the interior Canada Basin than previously thought.

VI. SUMMARY

The following analyses have been conducted to quantitatively and qualitatively investigate circulation in the western Arctic Ocean and its variability. First, the time-mean and interannually variable monthly velocity fields are analyzed from 1979-2001. Velocity output at three separate model defined depth intervals is averaged to describe the circulation in the upper ocean (0-26 m) (see Figure 3.2), within the halocline (54-149 m) (see Figure 3.3) and in the Atlantic layer (268-850 m) (see Figure 3.4). Second, two-year means of velocity fields are analyzed for the time periods 1981-1982, 1991-1992 and 2000-2001 for the upper ocean, halocline and Atlantic layer depth intervals (see Figures 3.5 through 3.13). Interdecadal velocity differences of two-year velocity means between the 1981-1982, 1991-1992 and 2000-2001 time period averages for the upper ocean, halocline and Atlantic layer are plotted (see Figures 3.14 through 3.22). Third, positive, negative and net volume transports and heat and freshwater fluxes through twenty-two cross sections in the western Arctic Ocean were calculated using monthly means from 1979-2001 in the entire water column, Atlantic layer (268-850 m) and the upper ocean layer (0-220 m) (see Tables 3.1, 3.2, 3.3 and Figures 3.24, 3.26, 3.27).

The twenty-three year mean (1979-2001) circulation in the Canada Basin is cyclonic in nature. One of the primary sources of inflow into the Canada Basin is Atlantic-derived water that enters the basin along the slope across the Lomonosov Ridge at the junction with the Eurasian continent. Another major source is Pacific water that

enters via the Bering Strait. River runoff and sea ice melt provide additional sources of freshwater. All these inputs into the Canada Basin are realistically accounted for in the model. Primary exit pathways from the Canada Basin are through the CAA and across the Canadian side of Lomonosov Ridge north of the Lincoln Sea into the Fram Strait.

The twenty-three year mean upper ocean circulation flows northeastward across much of the East Siberian Sea, merges with additional flow from the Bering Strait in the northern Chukchi Sea and contributes to a general northward-to-northeastward flow across the extent of the Canada Basin (see Figure 3.2). Mean boundary flow along the slope regions of the model-designated halocline maintains a generally cyclonic structure throughout the western Arctic (see Figure 3.3). Mean circulation in the Atlantic layer is characterized by a cyclonic boundary current flow along the slope regions throughout the Canada Basin with weak or no organized flow in the basin interior (see Figure 3.4).

The upper ocean circulation of the three two-year average time periods is similar to the twenty-three year mean climatological circulation (see Figures 3.5, 3.6, 3.7). The circulation pattern of the model-defined halocline layer for each of the three time averaged periods resembles the twenty-three year mean pattern with the 1991-1992 period exhibiting the strongest flow in all regions of the western Arctic (see Figures 3.8, 3.9, 3.10). Circulation in the Atlantic layer is characterized by a cyclonic boundary current flow along the slope regions throughout the Canada Basin with little or no organized

flow in the basin interior. The boundary current flow is weaker and less organized in the Atlantic layer in both the 1981-1982 and 2000-2001 time periods as compared to the 1991-1992-time period.

The model results of the mean circulation for the Canada Basin are in general agreement with published literature depicting circulation in the region. The majority of Atlantic layer transport is maintained within the boundary current that flows through the Chukchi Plateau via the Chukchi Borderland Pass and continues eastward into the southern Canada Basin towards the Beaufort Sea. Model results identify the northeast-to-southeast meander along the slope through the Chukchi Borderland Pass south of the Chukchi Cap and north of the Chukchi Rise as the specific pathway of this boundary flow.

These model results are inconsistent with the inferred circulation pathway of the boundary flow around the base of the Chukchi Plateau as proposed by Smethie et al. (2000). Also, these results suggest it is possible that the Atlantic water signature detected at SCICEX station 68 by Smethie et al. (2000) did not originally propagate from the north around the Chukchi Plateau but passed through the Chukchi Borderland Pass and merged with the northward flow along the eastern side of the Northwind Ridge in the vicinity of the Hanna Canyon.

Atlantic-derived water that flows within the Atlantic layer across section CB01 is a primary source of heat introduced into the Chukchi Plateau region. The propagation of heat in the Atlantic layer roughly follows volume transport circulation patterns in the entire water column. The dominant source of fresh water for the region

is Pacific water that enters the region through the Bering Strait. The high amount of freshwater that is introduced into the western Arctic as Pacific water through the Bering Strait may be a more important source of freshwater in the Canada Basin than previously thought.

The positive net northward volume transport and heat and freshwater fluxes across sections CB06 and CB04 identify these two locations as regions where boundary water and its associated properties are transported into the Canada Basin interior by direct flow, particularly across sections CB06 in the northern Chukchi Plateau region. Net positive freshwater flux across section CB04 in the upper ocean (0-220 m) indicates a direct mechanism (i.e. through local circulation) by which freshwater is introduced from the slope region to the basin interior (see Figure 3.27).

The additional upward heat flux of ~1.8 TW from the Atlantic layer in the northern Chukchi Plateau region enclosed by sections CP16, CB06, CP17, CP08 and CP13 is consistent with the results obtained by McPhee et al. (1998). This ~1.8 TW of upward heat flux is indicative of the additional oceanic heat flux observed by McPhee et al. (1998) during the SHEBA experiment and may provide a mechanism to melt more sea ice at the surface.

The northward flow across sections CP05, CP08, CB06 and CP17 defines an advective pathway that facilitates the transfer of freshwater from the Chukchi slope region to the basin interior and may account for some of the anomalously high amounts of freshwater mentioned by Macdonald et al. (2002).

A. RECOMMENDATIONS FOR FUTURE RESEARCH

Analyses of volume transports and property fluxes across additional cross-sections would afford greater certainty in conclusions regarding oceanography in the region. An additional cross-section from the eastern endpoint of cross-section CB05 to the junction of cross sections CP10 and CP11 would provide greater insight into any flow that branches off the eastward boundary current flowing downstream of section CB01. Additional cross-sections parallel to the Northwind Ridge in the vicinity of sections CP14 and CP17 would provide more conclusive information regarding recirculation in the region.

Segregation of flow into specified layers such as the surface layers for freshwater transport and the Atlantic layer for heat and salinity transport does not account for potential vertical transport. The imbalances between inward vs. outward heat and freshwater fluxes near the northern end of the Chukchi Plateau enclosed by cross sections CP16, CB06, CP17, CP08 and CP13 indicate that vertical transport may need greater consideration. An analysis of vertical volume and fluxes across selected horizontal sections may provide new interesting results. Incorporation of tides to better account for tidal mixing is encouraged.

Continued research partnerships with the U.S. Navy that allow scientists to take advantage of unique navy platforms and equipment are encouraged. The data obtained in the SCICEX cruises presented the scientific community a valuable opportunity to collect data that would otherwise have been impossible to obtain. The work by Smethie et al.

(2000) illustrates the tremendous dividends gained from cooperation between the military and scientific community.

The constant effort towards greater model resolution is an endeavor that always is supported. While the 1/12th degree resolution model that provided these results is extremely useful, this model is considered "eddy permitting" as eddy-like features with characteristic length scales smaller than ~37 km cannot truly be resolved. Improvements that will allow the resolution of smaller eddies will achieve a significant milestone in mesoscale oceanographic modeling and offer the opportunity to address outstanding questions regarding absolute energy levels and eddy activity as a possible mechanism for volume and property transport from a modeling standpoint.

Continued comparisons of results from the 1/12th degree model to observations would be a valuable exercise. A number of recent research projects in the region present data that will be useful for comparison. The SBI initiative, Chukchi Borderlands project and the ONR sponsored ice camp (ICEX03) in April of 2003, which this author participated in, are all expected to provide useful data for model comparison.

LIST OF REFERENCES

Aagaard, K., A Synthesis of the Arctic Ocean Circulation, in *Reun. Cons. Int. Explor. Mer.*, edited by P.-V. Rapp, pp. 11-22, 1989.

Aagaard, K., and E. C. Carmack, The Arctic Ocean and Climate: A Perspective, in *The Polar Oceans and Their Role in Shaping the Global Environment: The Nansen Centennial Volume*, edited by O.M. Johannesen, R. D. Muench, and J. E. Overland, pp. 5-20, American Geophysical Union, Washington, D.C., 1994.

Aagaard, K., and P. Greisman, Towards new mass and heat budgets for the Arctic Ocean, *J. Geophys. Res., 80*, 3821-3827, 1975.

Antonov, J. I., S. Levitus, T. P. Boyer, M. E. Conkright, T. D. O'Brien, and C. Stephens: World Ocean Atlas 1998 Vol. 1: Temperature of the Atlantic Ocean, *NOAA Atlas NESDIS* 27, *U.S. Government Printing Office*, Washington, D.C, 1998.

Boyer, T. P., S. Levitus, J. I. Antonov, M. E. Conkright, T. D. O'Brien, and C. Stephens: World Ocean Atlas 1998 Vol. 4: Salinity of the Atlantic Ocean, *NOAA Atlas NESDIS* 30, *U.S. Government Printing Office*, Washington, D.C, 1998.

Brass, G. W., Ed., 2002, Arctic Ocean Climate Change, U.S. Arctic Research Commission Special Publication No. 02-1, Arlington, VA, p. 14.

Coachman, L. K., and K. Aagaard, Transports through the Bering Strait: Annual and interannual variability, *J. Geophys. Res., 93,* 15535-15539, 1988

Dickson, R. R., J. Meincke, S. A. Malmberg, and A. J. Lee, The "Great Salinity Anomaly" in the northern North Atlantic 1968-1982, *Progr. Oceanogr., 20*, 103-151, 1988.

Dickson, R. R., I. Yashayaev, J. Meincke, B. Turrell, S. Dye, J. Holfort, Rapid Freshening of the Deep North Atlantic Ocean Over the Past Four Decades, in *Nature*, pp. 832-836, 2002.

Dukowicz, J. K., and R. D. Smith, Implicit free-surface method for the Bryan-Cox-Semtner ocean model, *J. Geophys. Res., 99* (C4), 7991-8014, 1994.

Environmental Working Group (EWG): Joint U.S.-Russian Atlas of the Arctic Ocean for the Winter Period [CD-ROM], *Natl. Snow and Ice Data Cent.*, Boulder, Colorado, 1997.

Environmental Working Group (EWG): Joint U.S.-Russian Atlas of the Arctic Ocean for the Summer Period [CD-ROM], *Natl. Snow and Ice Data Cent.*, Boulder, Colorado, 1998.

Gibson, J. K., P. Kallberg, S. Uppala, A. Hernandez, A. Nomura, E. Serrano, ERA-15 Description (Version 2-January 1999), ECMWF Re-Analysis Project Report Series, European Centre for Medium-Range Weather Forecasts, 1999.

Grebmeier, J. M., T. E. Whitledge, L. A. Codispoti, K. H. Dunton, J. J. Walsh, T. J. Weingartner, and P. A. Wheeler, 1998, Arctic System Science Ocean-Atmosphere-Ice Interactions Western Arctic Shelf-Basin Interactions Science Plan, ARCSS/OAII Report Number 7, Old Dominion University, Norfolk, VA, 65 pgs.

Johnson, M. A., A. Y. Proshutinsky, and I. V. Polyakov, Atmospheric Patterns Forcing Two Regimes of Arctic Circulation: A Return to Anticyclonic Conditions? *Geophys. Res. Lett., 26* (11), 1621-1624, 1999.

Killworth, P. D., D. Stainforth, D. J. Webb, and S. M. Patterson, The Development of a Free Surface Bryan-Cox-Semtner Ocean Model, *J. Phys. Oceanogr., 21*, 1333-1348, 1991.

Macdonald, R. W., F. A. McLaughlin, E. C. Carmack, Fresh Water and Its Sources During the SHEBA Drift in the Canada Basin of the Arctic Ocean, *Deep-Sea Research*, 49, 1769-1785, 2002.

Marble, D. C., Simulated Annual and Seasonal Arctic Ocean and Sea-Ice Varability from a High Resolution, Coupled Ice-Ocean Model, Ph.D. dissertation, Naval Postgraduate School, Monterey, 2001.

Maslowski, W., B. Newton, P. Schlosser, A. J. Semtner, and D. Martinson, Modeling Recent Climate Variability in the Arctic Ocean, *Geophys. Res. Lett., 27* (22), 3743-3746, 2000.

Maslowski, W., D. C. Marble, W. Walczowski and A. J. Semtner, On Large Scale Shifts in the Arctic Ocean and Sea Ice Conditions During 1979-1998, *Annals Glac.*, 33, 545-550, 2001.

Maslowski, and W. Walczowski, Circulation of the Baltic Sea and Its Connection to the Pan-Arctic Region-A Large Scale and High-Resolution Modeling Approach, *Boreal Environment Res.*, 7, 319-325, 2002.

Maslowski, W., D. Marble, W. Walczowski, U. Schauer, J.L. Clement, and A.J. Semtner, On Climatological Volume, Heat and Salt Transports Through the Barents Sea and Fram Strait from a Pan-Arctic Coupled Ice-Ocean Model Simulation, *J. Geophys. Res., conditionally accepted,* 2003.

Maykut, G., A., Energy Exchange Over Young Sea Ice in the Central Arctic, *J. Geophys. Res., 83* (C7), 3646-3658, 1978.

McClean, J., W. Maslowski, and M. Maltrud: Towards a Coupled Environmental Prediction System, Computational Science (Eds: Alexandrov, Dongorra, and Tan), Lecture Notes in Computer Science 2073 Springer-Verlag, pp. 1098-1107, 2001.

McLaughlin, F., E. Carmack, R. Macdonald, A.J. Weaver, J. Smith, The Canada Basin, 1989-1995: Upstream Events and Far-Field Effects of the Barents Sea, *J. Geophys. Res., 107* (C7), 19-1 - 19-20, 2002.

McPhee, M. G., T. P. Stanton, J. H. Morison, and D. G. Martinson, Freshening of the Upper Ocean in the Arctic: Is Perennial Sea Ice Disappearing?, *Geophys. Res. Lett., 25* (10), 1729-1732, 1998.

Mesinger, F., A. Arakawa, Numerical Methods Used in Atmospheric Models, p. 64, WMO-ICSU Joint Organizing Committee, 1976.

Pfirman, S. L., D. Bauch, and T. Gammelsrod, The Northern Barents Sea: Water Volume Distribution and Modification, in *The Polar Oceans and Their Role in Shaping the Global Environment: The Nansen Centennial Volume*, edited by O.M. Johannesen, R.D. Muench, and J.E. Overland, pp. 77-94, American Geophysical Union, 1994.

Pickart, R. S., Shelfbreak Circulation in the Alaskan Beaufort Sea: Mean Structure and Variability, *J. Geophys. Res.*, submitted, April, 2003.

Preller, R. H., P. G. Posey, W. Maslowski, D. Stark, T. C. Pham, Navy Sea Ice Predition Systems, *Oceanography.*, 15, (1), 44-56, 2002.

Proshutinsky, A., and M. Johnson, Two Circulation Regimes of the Wind-Driven Arctic Ocean, *J. Geophys. Res.*, 102, 12493-12514, 1997.

Proshutinsky, A., and R. H. Bourke and F. A. McLaughlin, The Role of the Beaufort Gyre in Arctic Climate Variability: Seasonal to Decadal Climate Scales, *J. Geophys. Res.*, *29*, 15-1 - 15-4, 2002.

Roach, A. T., K. Aagaard, C. H. Pease, S. A. Salo, T. J. Weingartner, P. V., and M. Kulakov, Direct Measurements of Transport and water Properties Through the Bering Strait, *J. Geophys. Res.*, *100* (C9), 18433-18457, 1995.

Rothrock, D. A., Y. Yu, and G. A. Maykut, Thinning of the Arctic Sea-Ice Cover, *Geophys. Res. Lett.*, *26*, 3469-3472, 1999.

Rothrock, D. A., J. Zhang, and Y. Yu, The Arctic Ice Thickness Anomaly of the 1990s: A consistent View from Observations and Models, *J. Geophys. Res.*, *108* (C3), 28-1 - 28-10, 2003.

Rudels, B., E. P. Jones, L. G. Anderson, and G. Kattner, On the Intermediate Depth Waters of the Arctic Ocean, in *The Polar Oceans and Their Role in Shaping the Global Environment: The Nansen Centennial Volume*, edited by O. M. Johannesen, R. D. Muench, and J.E. Overland, pp. 33-46, American Geophysical Union, Washington, D.C, 1994.

Semtner, A. J., and R. M. Chervin, Ocean Circulation from a Global Eddy-Resolving Model, *J. Geophys. Res.*, *97*, 5493-5550, 1992.

Semtner, A. J., Modeling Ocean Circulation, *Science*, 269, 1379-1385, 1995.

Shimada, K., E. C. Carmack, K. Hatakeyama and T. Takizawa, Varieties of Shallow Temperature Maximum Waters in the Western Canadian Basin of the Arctic Ocean, *Geophys. Res. Lett.*, *28*, 3441-3444, 2001.

Smethie, W. M., P. Schlosser, and G. Bonisch, Renewal and Circulation of Intermediate Waters in the Canadian Basin Observed on the SCICEX '96 Cruise, *J. Geophys. Res.*, *105* (C1), 1105-1121, 2000.

Smith, D. M., Recent Increase in the Length of the Melt Season of Perennial Arctic Sea Ice, *Geophys. Res. Lett.*, *25*, 655-658, 1998.

Steele, M., and T. Boyd, Retreat of the Cold Halocline Layer in the Arctic Ocean, *J. Geophys. Res., 103* (C5), 10,419-10,435, 1998.

Steele, M., R. Morley, and W. Ermold, Polar Science Center Hydrographic Climatology (PHC) A Global Ocean Hydrography with a High Quality Arctic Ocean, *J. Clim.*, 14(9), 2079-2087, 2000.

Swift, J. H., E. P. Jones, K. Aagaard, E. C. Carmack, M. Hingstrom, R. W. MacDonald, F. A. McLaughlin, and R. G. Perkin, Waters of the Makarov and Canada Basins, *Deep Sea Res, Part II,* 44 (8), 1503-1529, 1997.

Thompson, D. W., and J. M. Wallace, The Arctic Oscillation Signature in the Wintertime Geopotential Height and Temperature Fields, *Geophys. Res. Lett.*, *25*, 1297-1300, 1998.

Thompson, D. W., J. M. Wallace and G.C. Hegerl, Annular Modes in the Extratropical Circulation Part II: Trends, *J. of Climate*, 13 (5), 1018-1036, 2000.

Woodgate, R. A., K. Aagaard, R. D. Muench, J. Gunn, G. Bjork, B. Rudels, A. T. Roach, and U. Schauer, The Arctic Ocean Boundary Current Along the Eurasian Slope and the Adjacent Lomonosov Ridge: Water Volume Properties, Transports, and Transformations from Moored Instruments, *Deep Sea Res*, *Part I*, 48, 1757-1792, 2001.

Wijffels, S. E., R. W. Schmitt, H. L. Bryden, and A. Stigebrandt, Transport of Freshwater by the Oceans, *J. Phys. Oceanogr., 22*, 155-162, 1992.

THIS PAGE INTENTIONALLY LEFT BLANK

INITIAL DISTRIBUTION LIST

1. Defense Technical Information Center
   Ft. Belvoir, Virginia

2. Dudley Knox Library
   Naval Postgraduate School
   Monterey, California

3. Mary Batteen
   Department of Oceanography
   Naval Postgraduate School
   Monterey, California

4. Tim Stanton
   Department of Oceanography
   Naval Postgraduate School
   Monterey, California

5. Rost Parsons
   Naval Oceanographic Office
   Bay St. Louis, Mississippi

6. Kelly Taylor
   National Ice Center
   Washington, DC